

**Odetics**

An adventure in American creativity

NASA-CR-194752

Rel Date 5-10-92  
SBIR - 07.07-5000

**FINAL REPORT**

**ADVANCED OBJECT COLOR IDENTIFIER SYSTEM**

**VOLUME II OF II**

**PHASE II SBIR**

**CONTRACT NAS13-339**

7N-74-CR

1-3341

P-103

**PREPARED FOR:**

**NATIONAL AERONAUTICS AND SPACE ADMINISTRATION  
JOHN STENNIS SPACE CENTER  
ATTN: HUGH CARR/HA31  
CONTRACT NAS13-339  
NSTL, MS 39529**

**SUBMITTED BY:**

**ODETICS, INC.  
AI CENTER  
1515 S. MANCHESTER AVENUE  
ANAHEIM, CA 92802**

**JULY 30, 1990**

**SBIR RIGHTS NOTICE**

THIS SBIR DATA IS FURNISHED WITH SBIR RIGHTS UNDER NASA CONTRACT NO. NAS13-339. FOR A PERIOD OF 2 YEARS AFTER ACCEPTANCE OF ALL ITEMS

USE T	(NASA-CR-194752) ADVANCED OBJECT	N94-71332	DT BE
DISCLA	COLOR IDENTIFIER SYSTEM, VOLUME 2		FOR
PROCU	Final Report (Odetics) 103 p		F THE
CONTR		Unclas	AND
DISCLA			BE BY
SUPPO			THE
GOVER		29/74 0198341	CRIZE
OTHER			, BUT
IS REI			ILITY
FOR U			OTICE
SHALL			OR IN
PART.			

**INTENSITY DEPENDENT SPATIAL SUMMATION  
(THE IDS ALGORITHM)**

# Intensity-dependent spatial summation

Tom N. Cornsweet and John I. Yellott, Jr.

Cognitive Science Group, University of California, Irvine, California 92717

Received November 13, 1984; accepted April 16, 1985

Psychophysical evidence indicates that, in the human retina, the size of the spatial-summation area decreases as illuminance increases. Such a relationship would be beneficial for the detection of spatial contrast in the presence of photon noise. We analyze an image-processing mechanism in which the area of a strictly positive point-spread function varies inversely with local illuminance while its volume remains constant. In addition to its expected effect of improving spatial resolution as illuminance increases, this mechanism also yields center-surround antagonism and all other manifestations of bandpass filtering and accounts for Ricco's law and Weber's law—including the failures of both laws as a function of test conditions. The relationship between this mechanism and lateral inhibition is analyzed.

## 1. INTRODUCTION

Many psychophysical and physiological experiments can be interpreted as showing that light falling upon any one point of the retina creates an excitatory effect at neighboring points and that this lateral excitation combines additively with the direct excitation produced by light itself.<sup>1</sup> Psychophysical evidence also indicates that the extent of lateral excitation—the size of the spatial-summation area—increases as retinal illuminance decreases.<sup>2,3</sup>

One obvious and undesirable consequence of spatial summation is, in effect, to blur the neural image, and so it is natural to look for compensatory benefits of the process. A plausible suggestion is that intensity-dependent spatial summation is an adaptive response to the intrinsic noisiness of light. If the effective flux density in an image is  $I$  (absorbed photons/unit time/unit area), then both the mean and the variance of the actual quantum catch per unit time over an area  $A$  equal  $IA$ . This statistical relationship imposes a fundamental constraint on spatial contrast detection.

Suppose that a change in illuminance from  $I$  to  $I + cI$  is to be detected with an error rate of the order of 0.001 and that the visual system is a perfect detector limited only by quantal fluctuations. Then the effects of the incident quanta must be summed over an area  $A$  large enough that<sup>4</sup>

$$IA > 10/c^2.$$

Thus, to detect a 100% contrast change ( $c = 1$ ) lasting one time unit,  $IA$ , the total number of quanta whose effects are summed during one time unit must be greater than 10. To detect a contrast of 1% requires that  $IA > 100,000$ .

Individual human photoreceptors collect quanta over areas of the order of  $10^{-5}$  mm<sup>2</sup> and integrate their quantum catch over temporal durations of the order of 0.1 sec. Taking absolute threshold to be 100 quanta/0.1 sec at the cornea, spread over a retinal area of the order of  $10^{-3}$  mm<sup>2</sup>, and assuming that 10% of corneal quanta are effectively absorbed by photopigment,  $I$  at the absolute threshold of human vision is of the order of  $10^4$  (quanta/0.1 sec)/mm<sup>2</sup>. Therefore the value of  $IA$  for an individual receptor at absolute threshold is only about 1/100th of that needed to detect 100% contrast reliably and about  $10^{-6}$  that needed to detect 1% contrast. Thus, if no spatial summation occurred, a 100% contrast could be de-

tected only when retinal illuminance reached 100 times the absolute threshold level (a statement that is self-contradictory, since the absolute threshold is a contrast detection), and 1% contrast could not be detected until the illuminance was of the order of  $10^6$  times absolute threshold (that is, around 1 cd/m<sup>2</sup>). Spatial summation can thus be seen as a device for pooling the retinal quantum catch over areas larger than a single receptor, allowing reliable contrast detection at scotopic and mesopic light levels. And the fact that the summation area becomes smaller as illuminance increases can be interpreted as an adjustment that tends to keep the summation area  $A$  as small as possible at each light level  $I$ , subject to a requirement of the form  $IA > 10/c^2$ , thereby minimizing needless reductions in spatial resolution.

This noise-compensation interpretation of spatial summation is well known, especially through the seminal work of Rose.<sup>5</sup> However, it does not seem to be widely recognized that an adaptive spatial-summation mechanism can automatically create effects resembling a number of well-known visual phenomena not generally associated with photon noise, including edge enhancement (Mach bands) and other band-pass-filter effects usually attributed to lateral inhibition. We have analyzed a model visual system based on the following assumption: Each point in the retinal image gives rise to a nonnegative point-spread function whose height is directly proportional to image intensity at that point and whose volume remains constant—so that the area covered by the point spread varies inversely with local image intensity. The output image is the sum of the point-spread functions generated around each input point. We refer to this operation as "intensity-dependent spatial summation."

This simple operation proves to have a surprising number of immediate consequences that resemble important features of human vision. It creates Mach bands at edges, sombrero-shaped impulse responses, and a low-frequency falloff in the spatial contrast-sensitivity function. [In fact, when the point-spread function is Gaussian, it yields the same contrast-sensitivity function (CSF) as a linear lateral inhibitory model whose point-spread function is the negative Laplacian of a Gaussian, as in the theory of Marr and Hildreth.<sup>6</sup>] In addition, the same assumption implies Weber's law (including its failures as a function of light intensity and target size) and Ricco's law (including the fact that the area of perfect spatial

summation shrinks as the background light level increases) and causes visual acuity (the high-frequency cutoff of the CSF) to increase as the square root of mean luminance.<sup>7</sup> These consequences are robust under changes in the exact shape of the point-spread function (i.e., square, triangular, Gaussian, etc.) and depend only on the fundamental assumption that the area under that function is inversely proportional to local image intensity.

Finally, it is noteworthy that this spatial-summation mechanism mimics not only the main effects usually attributed to lateral inhibition, such as Mach bands, but also the apparent dependence of lateral inhibition itself on the mean luminance level. For example, the response to small spots has a distinct sombrero form only when the spot is superimposed upon a relatively high-intensity background. When background intensity is low the "negative" brim of the sombrero becomes vanishingly small, as though lateral inhibition failed at low light levels—a result that has been reported for retinal ganglion cells<sup>8,9</sup> and that is also found in psychophysical measurements of spatial contrast sensitivity.<sup>10,11</sup> Here, however, there is never any inhibition—all the model's consequences are due to changes in the width of a nonnegative point-spread function. A similar realistic dependence on background intensity also appears in the model's response to other stimulus configurations commonly used in psychophysical experiments. For example, the background intensity level beyond which detectability of a target obeys Weber's law shifts upward as the area of the target decreases.<sup>12</sup>

### Organization

In this paper we describe the basic mathematical properties of image processing by intensity-dependent spatial summation. Our purpose is to introduce a theoretical tool that may prove useful in visual system modeling and also in image-processing technology. In Section 2 we define the simplest intensity-dependent spatial summation (IDS) operator and derive some general results used repeatedly later on. In Sections 3 and 4 we describe the effects of applying this IDS operator to images commonly used in psychophysical measurements of spatial contrast sensitivity, such as edges, spots, and gratings. By and large, these effects are qualitatively in agreement with the results of psychophysical experiments, but we point out some significant differences and comment on their implications. We also note similarities between the consequences of IDS processing and physiological results frequently cited as demonstrations of lateral inhibition in the retina. In Section 5 we discuss the relationship between IDS operators and linear operators commonly employed in visual theory and the potential value of IDS operators in artificial image processing. In Section 5 we also describe a generalized IDS operator that retains the basic properties of the model introduced in Section 2 and allows a better fit to psychophysical data.

Although IDS is in a sense motivated by photon-noise considerations, this paper focuses on its consequences for deterministic input images, for which analytic results can be obtained relatively easily. That is not so for Poisson noisy images, which apparently must be approached by simulation methods and properly form the subject for another paper.

## 2. THE INTENSITY-DEPENDENT SPATIAL-SUMMATION MODEL

Figure 1 illustrates the basic ideas of the IDS model. A two-dimensional input image (here, a sharp edge) is recorded by an array of photoreceptors, and they feed into a summation network that performs the IDS operation. That operation consists of two stages. First, each receptor gives rise to a nonnegative point-spread function whose center height is directly proportional to the intensity of the input image at that receptor and whose volume is constant—so that its area (that is, the volume divided by the center height) is inversely proportional to the input intensity. Second, these point-spread functions are added together to create the output image. That image is then read out over an array of output channels—one for each receptor location.

In this section we define the general class of IDS operators, give an example based on Gaussian point-spread functions, and derive some useful technical results. In Section 3 we work out the response properties of IDS models for a variety of one-dimensional input images, and in Section 4 we do the same for two-dimensional inputs. Whenever possible we derive the general properties that characterize the model's responses independent of the exact shape of the point-spread function. Then in every case we give the specific form of the response for the special case of a Gaussian point-spread function and illustrate the profile of that response graphically.

For mathematical convenience, our analytic treatment assumes that the photoreceptors are infinitely small relative to the size of the input and the output images. That is, we deal with the continuous case, in the same spirit as theories that model retinal processing by a convolution of continuous retinal images with continuous impulse responses. This continuous approximation to the discrete nature of actual retinas and man-made image processors provides realistic results up to input image intensity levels that would cause the point-spread function to become narrower than a single receptor or a single pixel.

### Notation and Assumptions

$I(x, y)$  denotes the input image intensity at point  $(x, y)$ ;  $O(p, q)$  denotes the output image intensity at point  $(p, q)$  when the input image is  $I(x, y)$ . ( $p$  and  $q$  refer, respectively, to the  $x$  and the  $y$  coordinates in the output image plane.) When the input image is obvious, we occasionally denote the output image simply as  $O(p, q)$ .

The basic idea of the model is that each input point  $(x, y)$  contributes a nonnegative point-spread value to every output point  $(p, q)$ , the size of the contribution depending on the input intensity value  $I(x, y)$  and the distance from  $(x, y)$  to  $(p, q)$ . Thus we need to specify a spread function of the general form  $S[(x, y), (p, q), I]$  that gives the contribution from  $(x, y)$  to  $(p, q)$  when the input intensity at  $(x, y)$  is  $I$ . We assume first that

- (1)  $S$  is nonnegative.
- (2)  $S$  is spatially homogeneous and circularly symmetric. (That is,  $S$  can be written as a function of two real variables in the form  $S[(x - p)^2 + (y - q)^2, I]$ .)

Next we formalize the fundamental assumption that the

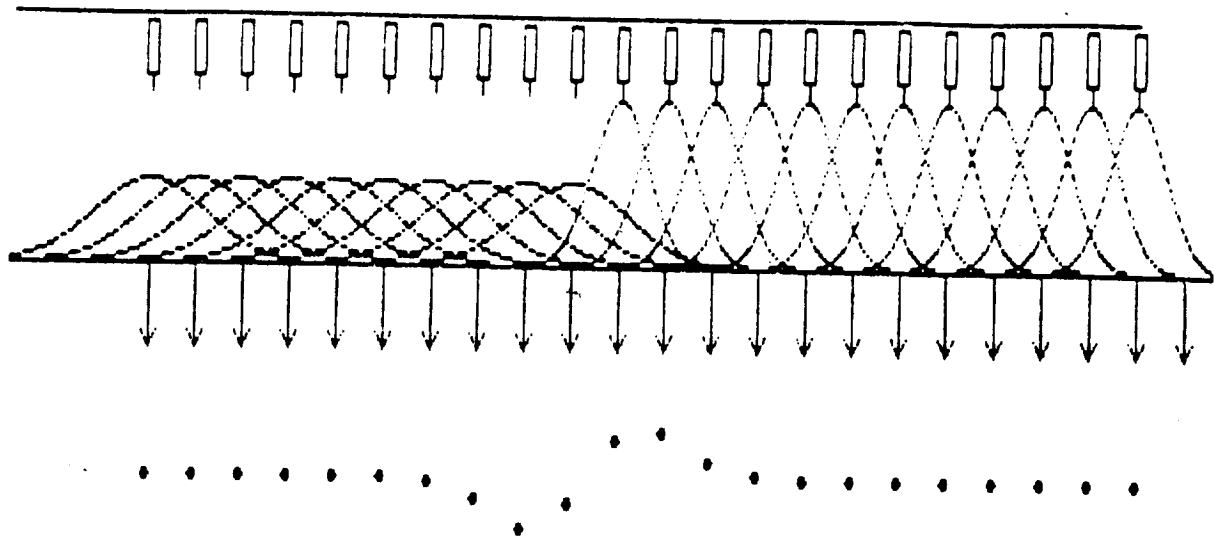


Fig. 1. Schematic diagram of the IDS model. From top to bottom: input image profile (here, a sharp edge); photoreceptors; photoreceptor point-spread functions (for the Gaussian case of the model); output channels (arrows); output image profile (dots).

area covered by the point-spread function around each input point varies inversely with the input intensity at that point. To accomplish this we assume that the center height  $S(0, I)$  is directly proportional to the input intensity  $I$ , while the volume under  $S$  remains constant for all nonzero values of  $I$ :

$$(3) \quad S[(x-p)^2 + (y-q)^2, I] = I \times S[I \times [(x-p)^2 + (y-q)^2], 1].$$

For any spread function  $S$ , integrating the right-hand side of assumption (3) over  $p, q$  yields a constant value  $V_s$  that is independent of  $I$ , while the height at the center [i.e.,  $S(0, I)$ ] equals  $I \times S(0, 1)$ . So the equivalent area under the point-spread function around any input point (volume divided by center height) is  $1/I$  times the constant  $V_s/S(0, 1)$ . The choice of the volume constant  $V_s$  is arbitrary; it simply sets the value of the model's baseline response to uniform-field inputs, as is shown below in Theorem 1. We take this to be unity.

(4) The integral of  $S[(x-p)^2 + (y-q)^2, I]$  over the  $p, q$  plane equals 1.0.

Given assumption (4), the remaining constant  $1/S[0, 1]$  equals the equivalent area of the point-spread function when the input intensity  $I = 1$ . This parameter determines the numerical values of the point-spread areas for all input intensities and needs to be chosen appropriately to fit the model to psychophysical data. We make no specific assumption here about its value since that will depend on the units used to measure retinal area and light intensity.

In view of assumption (3), the point spread  $S$  is really a function of a single variable, so we can suppress the redundant intensity variable and express the fundamental assumption of the model as follows.

The point spread from input point  $(x, y)$  to output point  $(p, q)$  is

$$I(x, y) \times S[I(x, y) \times [(x-p)^2 + (y-q)^2]],$$

where  $I(x, y)$  is the input image intensity at  $(x, y)$  and  $S$  is a nonnegative real function for which

$$\int_{-\infty}^{\infty} \int_{-\infty}^{\infty} S(p^2 + q^2) dp dq = 1.$$

Different cases of the model can then be created by different choices of the basic spread function  $S$ , i.e.,  $S$  may be Gaussian (as in the example below), square, exponential, etc. However, as we shall see, the exact choice makes little difference.

Note that the functional form of the spread function remains constant as  $I(x, y)$  varies. For any input intensity  $I$  the point spread takes the form  $I \times S(Ir^2)$ , where  $S$  is a fixed function and  $r$  is distance from the input point. Thus the effect of the input intensity at each point is simply to rescale the spread function, leaving its basic form unchanged. As will be seen below in Theorem 3 and subsequently, this is an important feature of the model.

Finally, we assume that the output image is the sum of the point-spread functions:

$$(5) \quad O[I(x, y)](p, q) = \int_{-\infty}^{\infty} \int_{-\infty}^{\infty} I(x, y) \times S[I(x, y) \times [(x-p)^2 + (y-q)^2]] dx dy.$$

Assumption (5) entirely captures the notion of an IDS operator.

#### Example: The Gaussian Case

Suppose that  $S$  is the Gaussian function

$$S(x^2 + y^2) = (1/2\pi) \times \exp[(-1/2) \times (x^2 + y^2)]$$

corresponding to the joint probability density function (pdf) of two independent normal random variables, each with mean zero and variance one. Then the point spread around an input point  $(x, y)$  with intensity  $I(x, y)$  is

$$[I(x, y)/2\pi] \times \exp[(-1/2) \times I(x, y) \times [(x-p)^2 + (y-q)^2]],$$

i.e., a bivariate normal density function, centered at that point, corresponding to the joint pdf of two normal random variables, each having variance  $1/I$ . Figure 2 illustrates this point-spread function for several values of  $I$ . We use this example

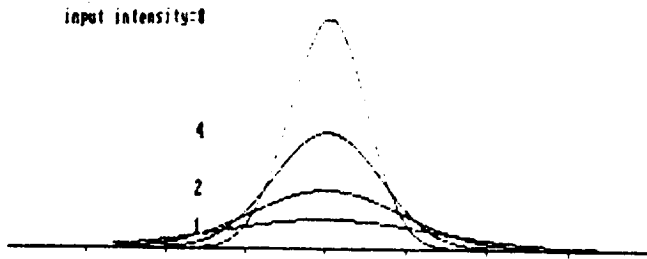


Fig. 2. Point-spread functions of the Gaussian case of the IDS model shown for four input intensities.

throughout to illustrate the model. Mathematically it is uniquely convenient because the Gaussian is the only circularly symmetric function that is also separable. However, as was noted earlier, the effects of IDS are largely independent of the exact shape of the spread function. To demonstrate this, our theorems are proved for arbitrary spread functions that satisfy assumptions (1)–(4).

This Gaussian version of the model has a point spread whose effective width is  $6/\sqrt{I}$ . Assuming a photoreceptor width of  $1/150$ -deg visual angle ( $2\ \mu\text{m}$ ), the point spread would shrink to a single receptor when  $I$  becomes greater than 800,000. We have confined our examples to  $I$  values less than 10,000 to keep the results of our continuous analysis realistic. In the figures below, the spatial units are degrees. The graphs show output image profiles over a retinal distance of  $\pm 2$  deg, plotted at 150 points/deg.

### Preliminary Results

An easy way to see that the model is nonlinear is to note the following.

#### Theorem 1

The output to any nonzero uniform field is the uniform field 1.0. [That is, when  $I(x, y) \equiv I > 0$ ,  $O(p, q) \equiv 1$ .]

#### Proof

Put  $I(x, y) = I$  in assumption (5) and make the change of variable  $u = (x - p)\sqrt{I}$ ,  $v = (y - q)\sqrt{I}$ . (Note: The output to a zero-intensity uniform field is again a zero-intensity field. Thus it might seem that there is a discontinuity in the uniform-field response. In practice this is not so, because any real input image is limited in spatial extent, whereas Theorem 1 assumes a truly infinite uniform field. For uniform-field inputs of any finite size, the response can be made as near zero as desired by making the input intensity sufficiently low.)

The physical meaning of Theorem 1 can be understood in the following way. Because the volume under the spread function at each point is constant and independent of the input intensity, the total output of the system is independent of its input—the effect of any input image is not to change the total amount of output but only to change its spatial distribution. Since a spatially uniform input image must generate a uniform output image, it follows that the output amplitudes corresponding to all uniform input images must be identical.

The next theorem simply documents a property built in by assumption (2): The IDS model is invariant under translations and rotations.

#### Theorem 2

If the input image is translated or rotated by any amount, the output image is unchanged except for translation or rotation by the same amount.

#### Proof

For translation: To represent a translation of the output to image  $I(x, y)$  [i.e.,  $O[I(x, y)](p - j, q - k)$ ] put  $p = p - j$ ,  $q = q - k$  in assumption (5) and make the change of variable  $u = x + j$ ,  $v = y + k$ . This yields

$$\iint I(u - j, v - k) \times S[I(u - j, v - k)] \times [(u - p)^2 + (v - q)^2] du dv,$$

which is the output for the translated input image  $I(x - j, y - k)$ . (Note: To simplify notation we omit the limits of integration in this expression and those below. Unless otherwise noted, these can always be assumed to be the entire plane.)

For rotation: To represent a rotation of the output to  $I(x, y)$  by a counterclockwise angle  $\theta$  we substitute  $p \cos \theta + q \sin \theta$  for  $p$  and  $q \cos \theta - p \sin \theta$  for  $q$  in assumption (5) and make the change of variable  $x = u \cos \theta + v \sin \theta$ ,  $y = v \cos \theta - u \sin \theta$ . Expanding the squared terms, we get

$$\begin{aligned} &\iint I(u \cos \theta + v \sin \theta, v \cos \theta - u \sin \theta) \\ &\times S[I(u \cos \theta + v \sin \theta, v \cos \theta - u \sin \theta)] \\ &\times [(u - p)^2 + (v - q)^2] du dv, \end{aligned}$$

which is the output for the rotated input image  $I(x \cos \theta + y \sin \theta, y \cos \theta - x \sin \theta)$ .

The final theorem of this section describes the effect of multiplying all the input image intensities by a common factor—i.e., the effect of changing the input image from  $I(x, y)$  to  $c \times I(x, y)$ , as would happen with the retinal image of a real scene if the illumination falling upon that scene changed. This simple theorem is really the mathematical heart of the model: From it we can prove that Weber's law holds at edges, that Ricco's law holds for spots on a dark background, and that visual acuity increases in proportion to the square root of the mean luminance level—all regardless of the specific form of the point-spread function.

#### Theorem 3 (Scaling Theorem)

For every positive constant  $c$  and every input image  $I(x, y)$

$$O[cI(x, y)](p, q) = O[I(x/\sqrt{c}, y/\sqrt{c})](p\sqrt{c}, q\sqrt{c}). \quad (1)$$

In words, this means that the effect of multiplying all the intensities in the input image by a constant  $c$  is the same as first expanding the original image spatially by a factor  $\sqrt{c}$  along both axes, then applying the summation operator in assumption (5) to that image, and finally shrinking the output image back to the original size. Thus, for example, each spatial frequency  $f$  in the image  $cI(x, y)$  is treated like frequency  $f/\sqrt{c}$  in the image  $I(x, y)$ .

#### Proof

The right-hand side of Eq. (1) is

$$\begin{aligned} &\iint I(x/\sqrt{c}, y/\sqrt{c}) S[I(x/\sqrt{c}, y/\sqrt{c})] \\ &\times [(x - p\sqrt{c})^2 + (y - q\sqrt{c})^2] dx dy. \end{aligned}$$

Making the change of variable  $u = x/\sqrt{c}$ ,  $v = y/\sqrt{c}$ , we obtain

$$\iint cI(u, v) \times S[cI(u, v) \times [(u - p)^2 + (v - q)^2]] du dv,$$

which is the left-hand side of Eq. (1).

### 3. RESPONSES TO ONE-DIMENSIONAL PATTERNS: EDGES, BARS, AND GRATINGS

Suppose that the input image is intrinsically one dimensional, i.e.,  $I(x, y) = I(x)$ . (Because of Theorem 2, it is sufficient to consider only vertical one-dimensional inputs.) Making this substitution in assumption (5), we have

$$O[I(x)](p, q) = \int \sqrt{I(x)} \int \sqrt{I(x)} S[(x - p)\sqrt{I(x)}]^2 + [(y - q)\sqrt{I(x)}]^2] dy dx.$$

Now in the inner integral (over  $y$ ) we make the change of variable  $v = (y - q)\sqrt{I(x)}$  to obtain

$$O[I(x)](p) = \int_{-\infty}^{\infty} \sqrt{I(x)} \$[(x - p)\sqrt{I(x)}] dx, \quad (2)$$

where  $\$$  is the line-spread function corresponding to  $S$ , given by

$$\$(x) = \int_{-\infty}^{\infty} S(x^2 + y^2) dy. \quad (3)$$

It is easily seen that  $\$$  is always nonnegative, symmetric about the origin, and integrates to 1. In the Gaussian example we have

$$\$(x) = \int_{-\infty}^{\infty} (1/2\pi) \exp[(-1/2)(x^2 + y^2)] dy \\ = (1/\sqrt{2\pi}) \exp[(-1/2)x^2],$$

so the line spread around a line with intensity  $I$  is a normal pdf centered on the line, with variance  $1/I$ . Thus for the Gaussian case the response to one-dimensional patterns is given by

$$O[I(x)](p) = \int_{-\infty}^{\infty} [\sqrt{I(x)}/\sqrt{2\pi}] \\ \times \exp[(-1/2)I(x)(x - p)^2] dx. \quad (4)$$

#### Step Response

Suppose that  $I(x)$  is an edge of the form  $I(x) = I$  for  $x \leq 0$ ,  $I(x) = I + D$  for  $x > 0$  (that is, a step). Then, for the Gaussian case, Eq. (4) yields the response

$$O(p) = N[x(I + D)^{1/2}] + N[-x\sqrt{I}], \quad (5)$$

where  $N$  is the cumulative normal distribution function:

$$N[z] = \int_{-\infty}^z (1/\sqrt{2\pi}) \exp[(-1/2)x^2] dx.$$

Figure 3 shows the Gaussian-model step response [i.e., Eq. (5)] for a number of edges. These edges differ in illuminance (that is,  $I$ ), but the ratio of the lighter to the darker side is the same for all—i.e., the ratio  $(I + D)/I$ , and consequently the Weber fraction  $D/I$ , is a constant. (Here  $D/I = 10$ .) It can be seen that the response displays Mach bands symmetrically located on either side of the step. At the step itself the response is always 1.0

To understand intuitively how Mach bands can be created

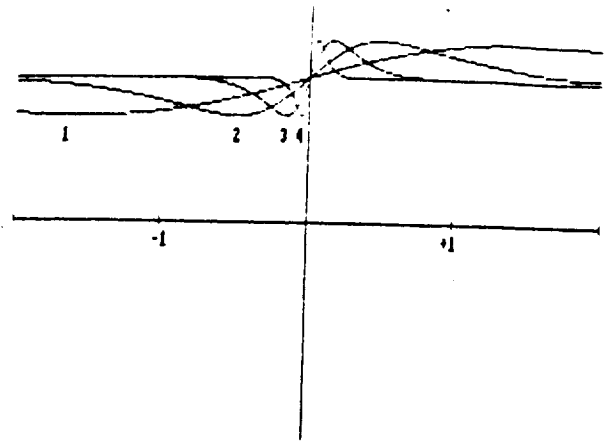


Fig. 3. Edge-response profiles. The input image was a step at zero from intensity  $I$  to  $I + D$ .  $I/D = 10$  in all cases. Curve 1,  $I = 0.1$ ; curve 2,  $I = 1$ ; curve 3,  $I = 10$ ; curve 4,  $I = 100$ .

by a purely positive point-spread mechanism (i.e., without lateral inhibition) it may be helpful to reexamine Fig. 1, bearing in mind that the output at each point is the sum of the spread functions above that point. As the edge is approached from the left (i.e., from the low-intensity side), the output decreases below the baseline level because there is less spread excitation coming from receptors on the right-hand side of the edge, which have narrower spread functions. Conversely, as the edge is approached from the high-intensity side, the output rises above the baseline level because of the extra excitation contributed by receptors on the low-intensity side, which have wider spread functions.

A second important feature of the response profiles in Fig. 3 is that the effect of increasing  $I$  is to move the peak and the trough of the Mach bands closer to the edge itself, but their amplitudes remain the same. This is a consequence of the fact that the input edges here all have the same Weber fraction  $D/I$ . Analysis of Eq. (5) shows that the peak of the positive-going Mach band occurs at  $P_{\max} = [(1/D)\log(1 + D/I)]^{1/2}$ , and its value there is

$$O(P_{\max}) = N[(1 + I/D)\log(1 + D/I)]^{1/2} \\ + N[-(I/D)\log(1 + D/I)]^{1/2},$$

which is a function only of the ratio  $D/I$ . The trough of the negative-going Mach band occurs at  $P_{\min} = -P_{\max}$ , and the output value there is  $1 - [O(P_{\max}) - 1]$  (i.e., the peak is as far above the baseline response 1.0 as the trough is below it.) Thus the peak and trough values of the step response depend only on the Weber fraction  $D/I$ . Assuming a downstream detector mechanism that registers a perturbation in an otherwise uniform field when the output value at any point differs from the baseline 1.0 response by more than some threshold value, it follows that the Gaussian version of the model implies Weber's law for edge detection.

This result is not unique to the Gaussian case of the IDS model. Instead it holds for all cases [i.e., for all choices of the point-spread function  $S$  that satisfy assumptions (1)–(4)]. The following theorem shows why.

#### Theorem 4

Suppose that  $I(x, y)$  is a straight edge separating a uniform field of intensity  $I$  from a field of intensity  $I + wI$ . Then the

maximum and minimum values of the output to  $I(x, y)$  are independent of  $I$  and depend only on the Weber fraction  $w$ .

#### Proof

Because of Theorem 2 it is sufficient to consider only vertical edges of the form  $I(x, y) = I(x) = I$  (for  $x > 0$ );  $= I + wI$  (for  $x \leq 0$ ). Suppose that  $V(x)$  is a vertical edge image defined by  $V(x) = 1$  for  $x < 0$ ;  $= 1 + w$  for  $x \geq 0$ . Assume that the maximum value of the output  $O[V(x)](p)$  occurs at  $p = P_{\max}$  and that the minimum value occurs at  $p = P_{\min}$ . Let  $I(x) = I$  for  $x < 0$  and  $I + wI$  for  $x \geq 0$ . Then  $I(x) = I \times V(x)$ , and so from Theorem 3 we have

$$\begin{aligned} O[I(x)](p) &= O[I \times V(x)](p) \\ &= O[V(x/\sqrt{I})](p\sqrt{I}) = O[V(x)](p\sqrt{I}). \end{aligned}$$

[The last equality holds because here  $V(x/\sqrt{I}) = V(x)$ .] The maximum value of the last expression in this line occurs at  $p\sqrt{I} = P_{\max}$  and its minimum at  $p\sqrt{I} = P_{\min}$ , and so the maximum (minimum) output to  $I(x)$  occurs at  $p = P_{\max}/\sqrt{I}$  ( $p = P_{\min}/\sqrt{I}$ ) and has the same value there that the output to  $V(x)$  has at  $P_{\max}$  ( $P_{\min}$ ).

Two other features of the Gaussian-case step response can also be shown to be common to all IDS models: the fact that the output value at the step itself is always 1.0 and the fact that the locations of the peak and trough of the response move closer to the step as the baseline input-intensity level  $I$  increases. (The latter is true under the conditions that prevailed in Fig. 3, i.e., the edge separates fields of intensities  $I$  and  $I + D$ , and the Weber fraction  $D/I$  remains constant while  $I$  changes.)

To prove the first point, suppose that the input image is a vertical edge of the form  $I(x, y) = I$  for  $x \leq 0$  and  $I + D$  for  $x > 0$ . We are concerned with the value of the output image  $O(p, q)$  along the vertical axis  $p = 0$ , and since it is sufficient to consider only a single point, we pick the origin [i.e., the point  $(p, q) = (0, 0)$ ]. Then, from assumption (5), the output for an arbitrary spread function  $S$  is

$$\begin{aligned} O(0, 0) &= \int_{-\infty}^{\infty} \int_{-\infty}^0 I \times S[I(x^2 + y^2)] dx dy \\ &\quad + \int_{-\infty}^{\infty} \int_0^{\infty} (I + D) \times S[(I + D)(x^2 + y^2)] dx dy. \end{aligned}$$

We know that  $I \times S[I(x^2 + y^2)]$  is a circularly symmetric function whose integral over the entire  $x, y$  plane is 1.0, and the first integral in the expression above integrates this function over the half-plane  $x \leq 0$ , so its value must be 0.5. The same argument applies to the second integral, and consequently the entire expression equals 1.0.

Now to show that the distance from the edge to the locations of the maximum and minimum output values decreases as  $I$  increases, we can use the fact, shown in the proof of Theorem 4, that if  $P_{\max}$  is the location of the maximum when the edge separates fields of intensities  $I$  and  $I + w$ , then the maximum occurs at  $p = P_{\max}/\sqrt{I}$  when the fields are  $I$  and  $I(1 + w)$ . So the distance between the location of the maximum and the edge itself varies inversely with  $\sqrt{I}$ . The same result for the minimum follows from the same argument.

The main result of this section is that for all IDS models, the step response always satisfies Weber's law. The same is also true of the response to bars and spots with sharp edges, provided that they are large—meaning large enough that there

is no interaction between the responses to their two opposite edges. The next subsection should clarify this point.

#### Bar Response

Again, because of Theorem 2, it is sufficient to consider only vertical bars. Suppose that  $I(x, y) = I(x) = I$  (a positive constant) for  $|x| > W/2$ ;  $I(x) = I + D$  for  $|x| \leq W/2$  (so the input is a bar of width  $W$  and intensity  $D$  superimposed upon a uniform field of intensity  $I$ ). Then the output for the Gaussian model is

$$\begin{aligned} O(p) &= N[\sqrt{I} \times (p - W/2)] + N[-\sqrt{I} \times (p + W/2)] \\ &\quad + N[(I + D)^{1/2} \times (W/2 - p)] \\ &\quad - N[-(I + D)^{1/2} \times (W/2 + p)]. \end{aligned} \quad (6)$$

The form of the bar response depends on the bar width  $W$  and the background intensity  $I$ . Figure 4 illustrates the width effect: A narrow bar on a fairly intense background produces a response whose profile is sombrero shaped, quite like the line-spread function of a linear lateral-inhibitory model based on a difference of Gaussians or the negative Laplacian of a Gaussian. A wide bar of the same intensity on the same background produces Mach bands at both edges, and inside the edges the response returns to the baseline response value, just as would be expected from a linear model whose modulation transfer function (MTF) vanishes at the origin. The peak and trough amplitudes of the Mach bands in this case

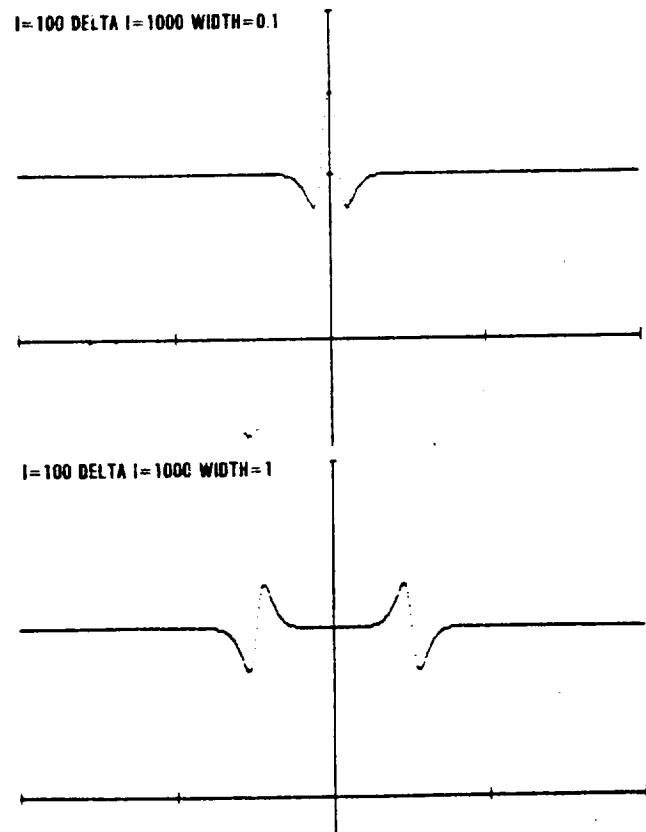


Fig. 4. Bar-response profiles for a narrow bar (top) and a wide bar (bottom) on a high-intensity background. Background intensity,  $I$ ; bar intensity,  $I + \Delta I$ . Bar widths are as indicated in the figure. Tick marks on the abscissa indicate a width of 1.0.



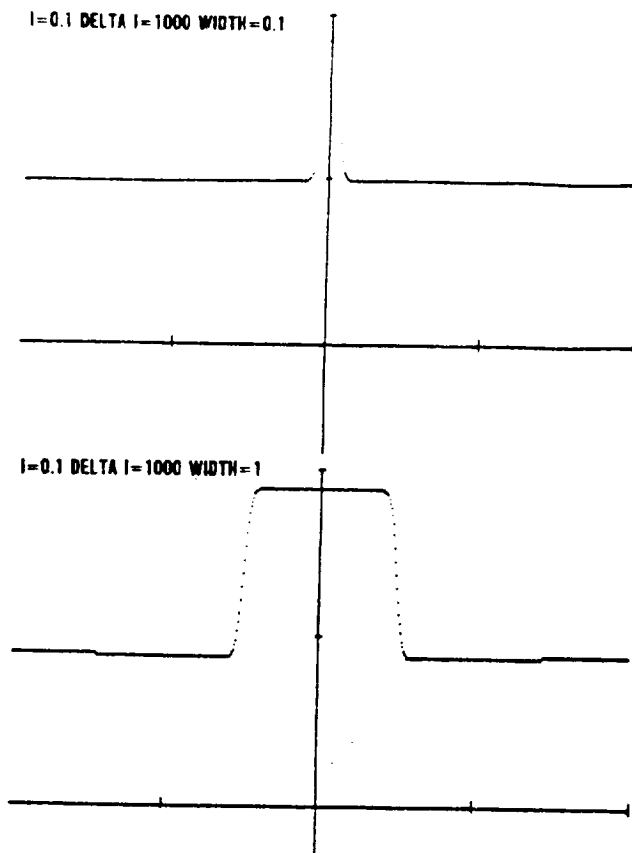


Fig. 5. Response profiles for the same bars as in Fig. 4 when the background has low intensity.

depend only on the Weber fraction  $D/I$ , so the detectability of wide bars should obey Weber's law.

Figure 5 shows output profiles for the same narrow and wide bars, but now superimposed upon a low-intensity background. The top panel illustrates how in this case the inhibitory lobes of the response to the narrow bar disappear (or, more precisely, become so broad and attenuated as to be unnoticeable), and only the central excitatory portion of the response is evident. Thus "lateral inhibition" apparently fails when the background intensity is low—the receptive fields lose what appear to be their antagonistic surrounds and seem now to consist only of positive centers.

The bottom panel of Fig. 5 shows that the response to a wide bar also changes dramatically when the background intensity changes from high to low. Instead of a pair of narrow positive and negative Mach bands at both edges separated by an internal region of baseline-level output, the response now appears to be uniformly high within the bar, and outside each edge there is a broad negative Mach band. (If this bar were made much wider, the response inside its edges would eventually return to the baseline value, so that each edge would exhibit both positive and negative Mach bands. In general, the response profile for any target depends on its size relative to the background illuminance level.) From the standpoint of a classical receptive-field analysis it might appear that large receptive-field units retain their antagonistic surrounds at low light levels, whereas small units lose them—perhaps because of insufficient quantum catches in the regions feeding the smaller units. In an IDS system all these effects are due to

intensity-dependent changes in the area of positive spatial summation.

### Sinusoidal Grating Response

Suppose that the input is a sinusoidal grating of the form  $I(x, y) = I(x) = L(1 + k \cos 2\pi f x)$ :  $L$  is the mean intensity level,  $k$  is the grating contrast, and  $f$  is its spatial frequency. Because our operator is nonlinear we know that it must produce some harmonic distortion. Figure 6 shows the Gaussian-model response to high- (90%) and low- (20%) contrast sinusoidal grating inputs. At high contrast levels distortion is apparent: It takes the form of a spurious second harmonic that creates noticeable dimples at the peaks of the response. For low contrast levels, however, the output closely approximates a pure sine wave. Appendix A shows that for the Gaussian model the output to a low-contrast sinusoidal grating of the form  $I(x) = 1 + k \cos 2\pi f x$  is approximately

$$O(p) = 1 + [2\pi^2 f^2 \exp(-2\pi^2 f^2)] k \cos 2\pi f p. \quad (7)$$

The approximation given by Eq. (7) is obtained by solving Eq. (4) for  $I(x) = 1 + k \cos 2\pi f x$  under the assumption that  $k^2 = 0$ . Consequently it is quite accurate for input contrasts on the order of 10% or less.

For low-contrast sinusoidal grating inputs, then, the outputs of the model are effectively sinusoidal, and it makes sense to speak of its MTF—i.e., the ratio of output contrast to input contrast as a function of input frequency. Let  $G(f, L)$  denote the MTF for mean input level  $L$ . Equation (7) shows that

$$G(f, 1) = 2\pi^2 f^2 \exp(-2\pi^2 f^2). \quad (8)$$

To obtain the general form of the MTF we use the scaling theorem:

$$\begin{aligned} O[L(1 + k \cos 2\pi f x)](p) &= O[1 + k \cos 2\pi f x / \sqrt{L}](p\sqrt{L}) \\ &= 1 + [2\pi^2 (f/\sqrt{L})^2 \exp(-2\pi^2 (f/\sqrt{L})^2)] k \cos 2\pi f p. \end{aligned}$$

So the MTF is

$$G(f, L) = 2\pi^2 (f/\sqrt{L})^2 \exp[-2\pi^2 (f/\sqrt{L})^2]. \quad (9)$$

Figure 7 shows this MTF for a range of mean intensity levels, plotted in the conventional way on log-log coordinates. In this plot the MTF shifts bodily to the right as  $L$  increases: Its peak (the best frequency) occurs at  $f = (1/\pi\sqrt{2}) \times \sqrt{L}$ , and visual acuity (defined as the highest frequency for which the MTF exceeds any fixed threshold) increases directly as  $\sqrt{L}$ .

Both the bandpass characteristics of the MTF and its bodily shift with changes in mean luminance (when the frequency

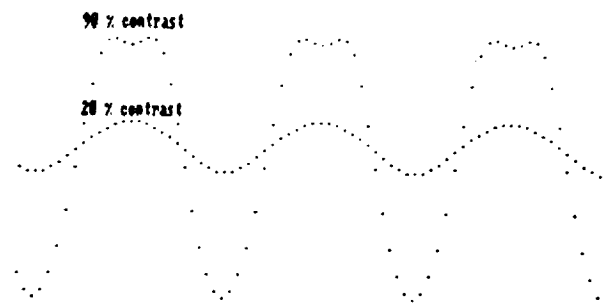


Fig. 6. Sinusoidal grating response profiles for high-contrast (90%) and low-contrast (20%) gratings.

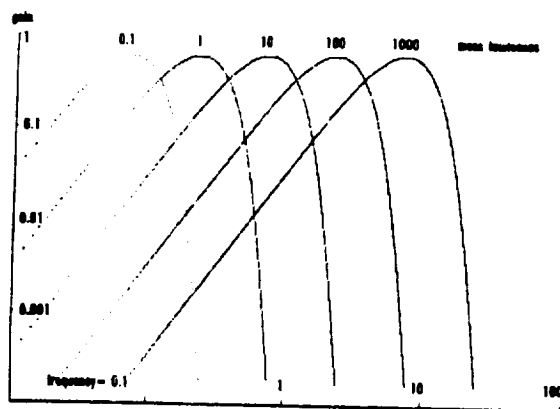


Fig. 7. MTF's of the Gaussian IDS model for various input mean luminance levels.

axis is logarithmic) are general properties of IDS models, independent of the exact form of the spread function  $S$ . Bandpass properties follow from the fact that very low frequencies will act like uniform fields and be driven to the baseline-response level, and very high frequencies will be attenuated by the basic point-spread operation. Bodily shifts with mean luminance follow from the scaling theorem, as is shown by the following.

#### Theorem 5

Suppose that for some range of contrast values the output to a sinusoidal input of the form  $I(x) = 1 + k \cos 2\pi f x$  is another sinusoid of the form  $O(p) = 1 + G(f) k \cos 2\pi f p$ . Then for any mean intensity level  $L$  the output to the sinusoidal input  $L(1 + k \cos 2\pi f x)$  is  $1 + G(f/\sqrt{L}) k \cos 2\pi f p$ . [In other words, the MTF at mean intensity  $L$  is  $G(f/\sqrt{L})$ .]

#### Proof

From Theorem 3

$$\begin{aligned} O[L(1 + k \cos 2\pi f x)](p) &= O[1 + k \cos 2\pi f(x/\sqrt{L})](p\sqrt{L}) \\ &= 1 + G(f/\sqrt{L}) k \cos 2\pi(f/\sqrt{L})(p\sqrt{L}) \\ &= 1 + G(f/\sqrt{L}) k \cos 2\pi f p. \end{aligned}$$

Consequently all IDS operators cause the peak frequency of the MTF, and also any high-frequency cutoff (visual acuity), to increase proportionally with the square root of the mean luminance level. These increases continue up to luminance levels at which saturation begins to occur, i.e., the point-spread area shrinks to the size of a single receptor.

Psychophysical evidence indicates that the peak frequency and the high-frequency cutoff of the human spatial CSF show similar increases with mean retinal illuminance below the photopic range, though in general the changes are smaller than those expected from an IDS model. A plot of log visual acuity versus log retinal illuminance based on the data of Schlaer<sup>7</sup> is quite well fitted by a straight line with slope 3/8 (instead of 1/2) up to about 5 Td, after which acuity levels off rapidly. The spatial CSF's of Van Ness and Bouman<sup>10</sup> show a peak frequency that increases by 0.8 log unit (instead of 1) as mean illuminance increases from 0.09 to 9 Td. Raising mean illuminance beyond this point produces smaller changes in the CSF peak, and above 90 Td it appears that the entire CSF becomes independent of the mean luminance level.

Another difference between the behavior of IDS models and

psychophysical data is that human CSF's generally show a decrease in sensitivity at the peak frequency as mean luminance decreases,<sup>10,11</sup> whereas the IDS model MTF maintains a constant gain at its peak frequency.

Discrepancies between IDS-model predictions and psychophysical data obtained at photopic luminance levels are to be expected in view of the model's automatic saturation property. It is interesting to note that the signal-detectability argument given in Section 1 implies that reliable detection of contrasts of the order of 0.1–1% covering an area the size of a single photoreceptor requires a quantum catch of the order of  $10^6$ – $10^8$  times absolute threshold, or approximately 10–1000 Td. Over the range 10–1000 Td, then, the visual system loses its need for spatial summation, and so the disappearance of an IDS mechanism through saturation would not be disadvantageous. In this connection it is worth recalling that rod saturation occurs in the same range.<sup>13</sup>

Discrepancies below the photopic range call for a different sort of reconciliation. One approach is to weaken the IDS model's assumption that the point-spread area varies inversely with quantum catch. In Section 5 we develop a generalized IDS model in which that area varies as a power function of the input intensity. This allows the model to predict visual acuity and peak-frequency changes with mean luminance more in line with empirical results. A second approach is to take into account the time required for a point-spread effect to disperse across the retina. When plausible assumptions about this are combined with the actual temporal conditions prevailing during CSF measurements, preliminary analysis indicates that the IDS model yields a rise in peak-frequency sensitivity with increasing mean luminance comparable with that exhibited by human CSF's.

The exact shape of the MTF of an IDS model depends on the form of its point-spread function, and so it is an interesting coincidence that for the Gaussian case the MTF [Eq. (9)] turns out to be the same one produced by Marr and Hildreth's linear DEL<sup>2</sup>-G model of early visual processing.<sup>6</sup> In that model the image is convolved with the Laplacian of the Gaussian function  $-(1/\sigma^2 2\pi) \exp[-(1/2)(x^2 + y^2)/\sigma^2]$ , i.e., with the sombrero-shaped point-spread function

$$(1/\sqrt{\pi})^2 (1/\sigma^2)^2 [1 - (x^2 + y^2)/2\sigma^2] \exp[-(1/2)(x^2 + y^2)/\sigma^2].$$

The Fourier transform of that point-spread function is

$$4\pi^2(u^2 + v^2) \exp[-2\pi^2\sigma^2(u^2 + v^2)],$$

and so its MTF for one-dimensional sinusoidal gratings is

$$4\pi^2 f^2 \exp(-2\pi^2 \sigma^2 f^2).$$

It follows that the Gaussian IDS model cannot be distinguished from a single channel DEL<sup>2</sup>-G model by experiments that simply determine the shape of the CSF at any fixed mean luminance level. [Such experiments generally involve small contrast values, in the range 10% or less, so that the approximation in Eq. (9) is valid. For high contrast values the non-linearity of the IDS model would become an important factor and could allow an experimental discrimination between the models.] Marr and Hildreth<sup>6</sup> show that a DEL<sup>2</sup>-G filter is essentially indistinguishable from a difference-of-Gaussians filter of the sort used by Wilson and Bergen,<sup>14</sup> and so the same is true of single-channel linear models based on that filter.

#### 4. RESPONSES TO TWO-DIMENSIONAL PATTERNS

##### Ricco's Law and Weber's Law

Ricco's law states that the detectability of a spot of light depends only on the product of its area and intensity. Experimentally, in human vision, this holds for spots up to a certain critical size—a size that decreases as the background intensity increases.<sup>2,3</sup> We show here that the IDS model implies that Ricco's law holds for spots of all sizes on a background field of zero intensity—in the sense that the peak value of the output to such an input is the same for all spots of the same shape that have the same product of area times intensity. On nonzero backgrounds it causes Ricco's law to hold (in the same sense) for spots up to a critical area that decreases as the background intensity increases. (The experimental fact that

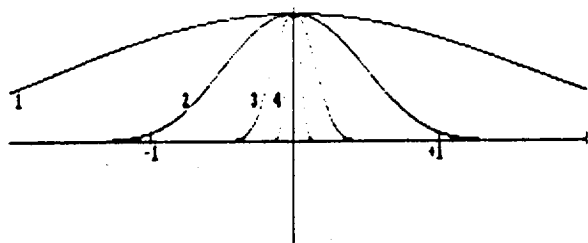


Fig. 8. Response profiles for square spots on a dark background. Spot area ( $A$ ) times intensity ( $I$ ) was held constant at 10. Curve 1,  $I = 1$ ,  $A = 10$ ; curve 2,  $I = 10$ ,  $A = 1$ ; curve 3,  $I = 100$ ,  $A = 0.1$ ; curve 4,  $I = 1000$ ,  $A = 0.01$ .

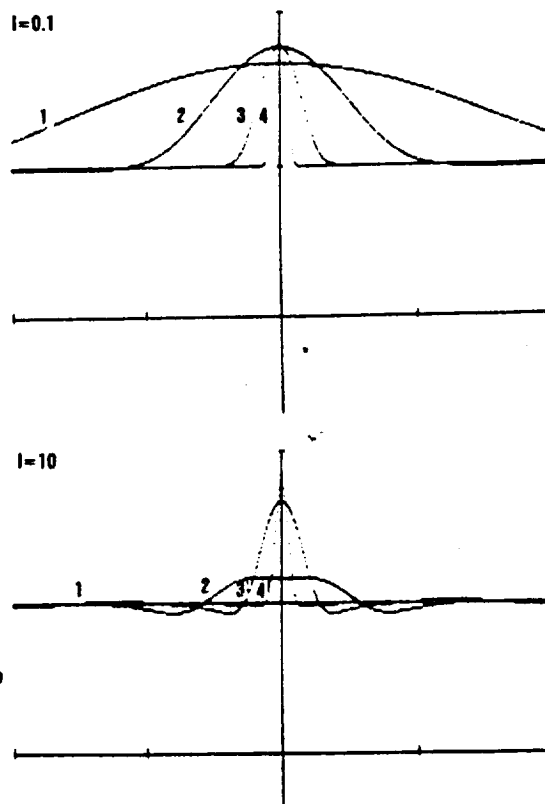
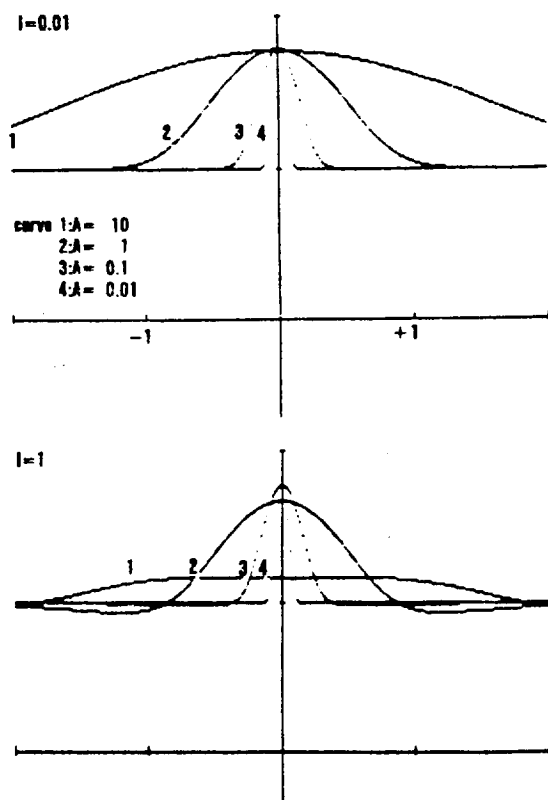


Fig. 9. Response profiles for square spots on nonzero backgrounds of various intensities. The input images were squares of intensity  $I + D$  surrounded by backgrounds of intensity  $I$ . The spot area ( $A$ ) times its incremental intensity ( $D$ ) was held constant ( $D \times A = 10$ ), and responses were computed for  $A = 0.01, 0.1, 1$ , and  $10$ . Upper left, background intensity  $I = 0.01$ ; upper right,  $I = 0.1$ ; lower left,  $I = 1$ ; lower right,  $I = 10$ .

Ricco's law holds for only a limited range of areas even on a nominally dark background does not necessarily contradict the model, since the activity in real visual systems does not fall to zero in darkness.) The IDS model also predicts the types of configurational effect reported by Sakitt,<sup>15</sup> who found that two separated spots lying within Ricco's area do not yield perfect summation but instead require more total quanta for detection than a single spot in the same area.

Figure 8 shows the profiles of the Gaussian IDS-model response to square spots of various sizes on a zero background. The input image here was  $I(x, y) = I$  for  $|x| \leq W/2, |y| \leq W/2$ ,  $I(x, y) = 0$  elsewhere (so the spot area was  $W^2$ ). The output equation in this case is

$$O(p, q) = \{N[(W/2 - p)\sqrt{T}] - N[-(W/2 + p)\sqrt{T}]\} \times \{N[(W/2 - q)\sqrt{T}] - N[-(W/2 + q)\sqrt{T}]\}. \quad (10)$$

In this figure all spots have a (area  $\times$  intensity) value of 10. The response profiles shown here run along the horizontal axis through the center of the squares. It can be seen that the peak output value is the same for all inputs. This is a general property of IDS models.

##### Theorem 6

The peak value of the output to uniform patches of light on a zero-intensity background is the same for all patches of the same shape that have the same product (area  $\times$  intensity).

##### Proof

For convenience we prove the theorem for square spots, but the form of the proof applies to any shape. Suppose that  $I'(x,$

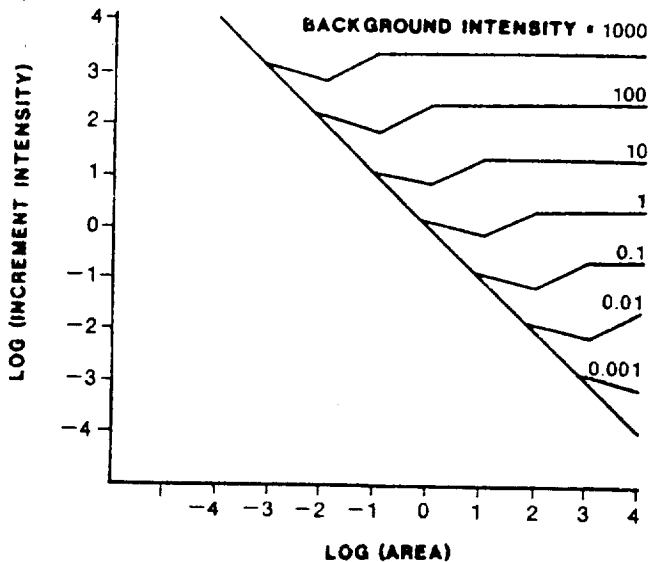


Fig. 10. Increment threshold as a function of test spot area for background fields of various intensities. The input images were square spots of area  $A$  and intensity  $I + D$  surrounded by uniform background fields of intensity  $I$ . Each curve shows, in log-log coordinates, the value of  $D$  required to produce a peak response of 1.15 as  $A$  increases over eight log units. Background intensities range from  $I = 1000$  (top curve) to  $I = 0.001$  (bottom curve). The diagonal straight line represents Ricco's law; each curve follows this line up to some area value and then departs from it as shown.

$y)$  is a square spot of width  $W$  and intensity  $I$  on a dark background, i.e.,  $I'(x, y) = I$  for  $|x| \leq W/2, |y| \leq W/2$ ; and  $I'(x, y) = 0$  elsewhere. And suppose that  $I(x, y)$  is another square with intensity  $cI$  and width  $W/\sqrt{c}$ , so that (area  $\times$  intensity) is  $I \times W^2$  for both. Then  $I(x, y) = cI'(x\sqrt{c}, y\sqrt{c})$ , and so from Theorem 3

$$\begin{aligned} O[I(x, y)](p, q) &= O(cI'(x\sqrt{c}, y\sqrt{c}))(p, q) \\ &= O[I'(x, y)](p\sqrt{c}, q\sqrt{c}). \end{aligned}$$

Consequently, if the peak output to  $I'(x, y)$  occurs at  $(p', q')$ , the peak output to  $I(x, y)$  occurs at  $(p'/\sqrt{c}, q'/\sqrt{c})$  and has the same value as the peak output to  $I'(x, y)$ .

For nonzero backgrounds, the IDS model implies that Ricco's law holds as an approximation for small spots: Up to a certain spot size the peak output value remains constant out to several decimal places (e.g., 3) for all spots (of the same shape) that have the same value of (area  $\times$  intensity). The higher the background intensity, the smaller the critical area beyond which Ricco's law begins to fail.

Figure 9 shows the profiles of the Gaussian-model responses to square spots of various sizes on various backgrounds. Spot (area  $\times$  intensity) was held constant at 10. On the lowest-intensity background (0.01) the peak-response value remains constant for areas ranging from 0.01 to 10. When the background intensity is increased to 0.1 the peak-response value is still constant for areas up to 1.0 but drops below the constant value for the largest spot (area = 10). For a background intensity of 1, only the two smallest spots preserve a constant peak output, and, finally, at the highest background intensity (10) Ricco's law fails for all but the smallest spot. (At this background intensity, Ricco's law would hold only for spots with areas  $\leq 0.01$ .)

The equation for the Gaussian-model response to square spots of intensity  $I + D$  on backgrounds of intensity  $I$  is

$$\begin{aligned} O(p, q) &= 1 + \{[N[A(W/2 - p)] - N[-A(W/2 + p)]] \\ &\quad \times [N[B(W/2 - q)] - N[-B(W/2 + q)]] \\ &\quad - \{[N[B(W/2 - p)] - N[-B(W/2 + p)]] \\ &\quad \times [N[A(W/2 - q)] - N[-A(W/2 + q)]]\}, \quad (11) \end{aligned}$$

where  $A = (I + D)^{1/2}$ ,  $B = \sqrt{I}$ , and  $W$  is the spot width.

Figure 10 summarizes the Ricco law behavior of the model. It shows, for a range of background intensities, the spot intensity needed to produce a constant peak response as a function of spot area. (The spots here were squares, and the peak-response value at threshold was taken to be 1.15. That value was chosen for convenience: It is the peak response to a square of unit area when  $D = 1$  and  $I = 0.1$ . The choice of threshold value is irrelevant here; other values yield curve families that look like those in Fig. 10.) For all background levels the constant-response curve runs for some distance along a line of slope  $-1$ , indicating obedience to Ricco's law, and then departs from this line when the spot area reaches a critical value. After a brief further decline with further increases in area (Piper's law), the curves increase a bit and then level out to constant values. For spot areas in that final range the peak response occurs as a Mach band at their edges and is governed by Weber's law.

#### Increment-Threshold versus Background-Intensity Curves

The last point is made more explicit by Figs. 11 and 12. Figure 11 replots three of the curves from Fig. 10 in the form of standard increment-threshold versus background-intensity (TVI) curves. It can be seen that these TVI curves evolve through three stages. When background intensity is low the curve is flat, as though threshold were limited by dark light (though here there is none). Next there is a transitional stage in which the TVI curve increases with a slope that is first somewhat less than one and then somewhat greater. Finally, when background intensity is sufficiently high, the TVI curve

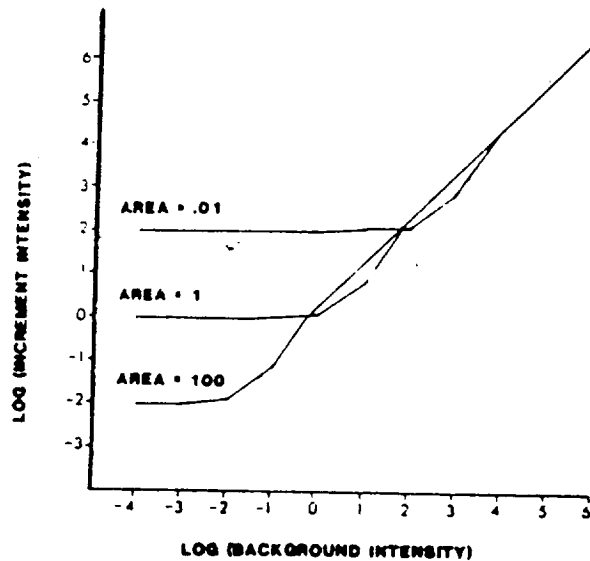


Fig. 11. TVI curves for test spots of different areas. These are replots of data from Fig. 10. Each curve shows the incremental intensity  $D$  required to produce a fixed peak-response value when the input is a square spot of area  $A$  and intensity  $I + D$ , surrounded by a background of intensity  $I$ . The three curves shown are for  $A = 0.01$ ,  $A = 1$ , and  $A = 100$ . As background intensity increases, all curves eventually terminate in a diagonal straight line corresponding to Weber's law.

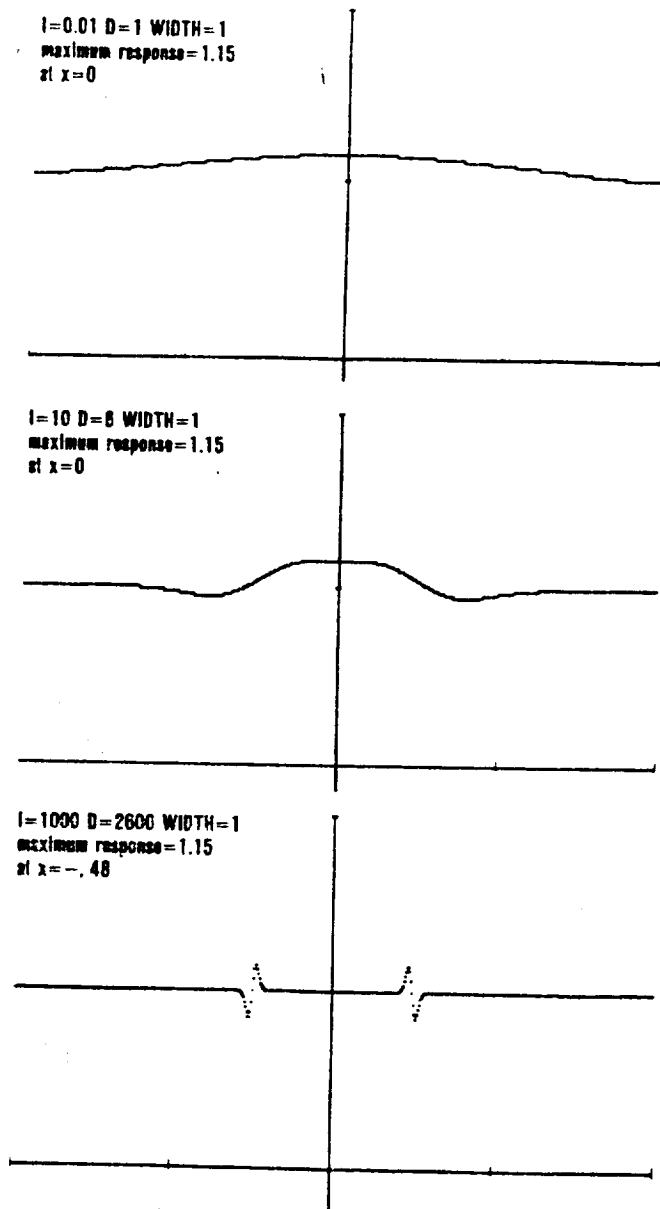


Fig. 12. Response profiles at threshold for a spot of fixed area on backgrounds of various intensities. Each curve shows the profile of the response to a square test spot of area  $A = 1$  and intensity  $I + D$  surrounded by a uniform background of intensity  $I$ . The increment value  $D$  in each case is that required to produce a peak output value of 1.15. Top profile, background intensity  $I = 0.01$ ; middle,  $I = 10$ ; bottom,  $I = 1000$ .

attains a slope of one (Weber's law) and retains it for all higher backgrounds. The background-intensity values corresponding to these three ranges depend on the size of the test spot: The larger the spot, the sooner its TVI curve begins to follow Weber's law.

These TVI curves are in good qualitative agreement with standard psychophysical results,<sup>13</sup> except that in the Weber's law region our curves all run together, whereas in practice one expects to find a slightly smaller threshold value of the Weber fraction for larger test spots.<sup>16</sup> This can be understood in terms of the fact that larger spots have longer perimeters, which should increase their relative detectability once the edge response becomes the dominant factor. We have not sought to model such an effect, since to do so realistically would in-

roduce issues of noise and probability summation beyond the scope of this paper.

Figure 12 shows how the shape of the threshold-value response profile changes as background intensity increases. These profiles are for a test spot of area 1.0. On low-intensity backgrounds (in the zero-slope portion of the TVI curve) the response is simply a broad shallow bump, peaking in the center of the test spot. Here threshold is determined by the increment intensity required to make this central peak exceed the threshold criterion. In the next background-intensity range (corresponding to the transitional-slope portion of the TVI curve) the response profile at threshold has a sombrero shape, with apparent inhibitory regions surrounding a central positive bump. Here threshold is still determined by the response value at the center of the spot. Finally, on a high-intensity background, the response profile consists entirely of Mach bands at the edges of the test spot, and threshold is determined by their peak values. Those peaks follow Weber's law, as was shown earlier in Section 3, and this is the Weber region of the TVI curve.

### Shape of the Impulse Response

Figure 13 illustrates, for small spots, a point made earlier for thin bars: At moderate to high background intensities, the IDS model produces a sombrero-shaped impulse response (center-surround antagonism), but when the same spot lies on a low-intensity background, the depression of surrounding activity becomes negligible, and the response appears to be

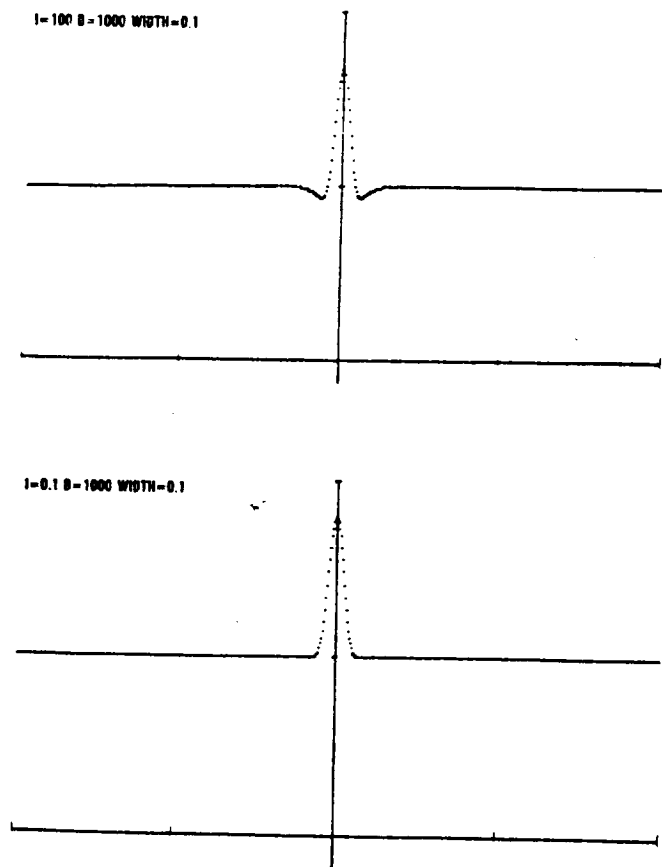


Fig. 13. Response profiles for a small square spot of fixed incremental intensity ( $D = 1000$ ) superimposed upon a high-intensity (top curve,  $I = 100$ ) or a low-intensity (bottom curve,  $I = 0.1$ ) background. Spot width, 0.1.

purely positive—as though lateral inhibition had failed at low light levels. Mammalian retinal ganglion cells have been reported to behave in this fashion.<sup>8,9</sup> That fact has generally been interpreted in terms of a loss of the inhibitory contribution from the antagonistic-surround portion of the cell's receptive field. We see here that the same effect also occurs naturally in a system involving no inhibition.

The cause of this apparent loss of lateral inhibition on low-intensity backgrounds is that when the background level is low, the width of the point-spread function in the background region is large, and consequently the value of the response at points near the test spot is the sum of many small contributions coming from a large portion of the field. The high-intensity test spot reduces the amount of spread coming from receptors directly beneath it, but these are relatively few in number, and consequently their overall point-spread contribution to the response at nearby points is negligible to begin with. Thus, when it is removed, there is only a negligible reduction in the response level. When the background intensity is high, however, the point-spread function is narrow, and the response level at points near the test spot is the sum of spread values contributed by a relatively small number of closely neighboring points. In this case the loss of the spread values formerly contributed by points beneath the test spot causes a substantial reduction in the response level at points adjacent to that spot. Thus the same test spot creates appreciable "lateral inhibition" at nearby points when it is superimposed upon a high-intensity background and no apparent inhibition when the background is low.

### Configurational Effects

At any given background intensity, Ricco's area can be defined as the area of the largest spot for which Ricco's law holds. If Ricco's law were the result of summation within the central region of a classical receptive field, one might expect all targets smaller than Ricco's area to be equally detectable if they have the same value of the product (area  $\times$  intensity). Sakitt found, however, that Ricco's law is violated within Ricco's area when the target is a pair of spatially separated spots rather than a single continuous one.<sup>15</sup> Her experiment showed that two spots that deliver a fixed total number of quanta within Ricco's area may be undetectable even though the same number of quanta are detectable when imaged in the form of a single spot. Moreover, she showed that her results could not be reconciled with the idea of spatial summation over a fixed-size receptive field even if one allows for the possibility that receptors have different weights depending on their positions within the field.

For the IDS model these configurational effects pose no difficulty. It predicts what Sakitt found: The peak response to two spatially separated spots, each of area  $A$  and intensity/unit area  $D$ , is less than the peak response to one spot of area  $A$  and intensity  $2D$ , even though they lie entirely inside an area that would yield apparently perfect spatial summation when tested with larger continuous spots. Figure 14 illustrates this effect.

The top panel shows the response profile for a single square spot of intensity  $I + D$  surrounded by a background of intensity  $I$ .  $I$  here is 0.1, and Fig. 9 shows that at this background intensity the width of Ricco's area is 1.0. The spot whose response profile is shown here has a width of 0.1, and its (area  $\times$  intensity) value is 10. (That is,  $D$  is 1000.) The

peak-response value for this spot is 1.78. The bottom panel shows the response profile for a pair of square spots, each of width 0.1, whose edges are separated by a gap of 0.05. The background intensity is again  $I = 0.1$ , and each spot has an intensity  $D = 500$ , so the combined (area  $\times$  intensity) value for the two spots is 10. Thus this pair of spots falls well within the area of perfect spatial summation for this background intensity and have the same total (area  $\times$  intensity) value as the single spot. However, the peak-response value for the pair is only 1.55.

This behavior can be understood qualitatively in the same way as the IDS model's creation of Mach bands at edges. Here the single spot's response contains a substantial contribution coming from receptors lying under the background portion of the input image. The responses to the separated squares gain a smaller contribution from spreading, because each square has a high intensity and consequently creates a narrower spread function in the receptors beneath it than they would produce if the low-intensity background were present. Thus each square reduces the point spread that its receptors would have contributed to the output of its neighbor.

The following expression is the output image equation for the Gaussian case of the IDS model when the input image is

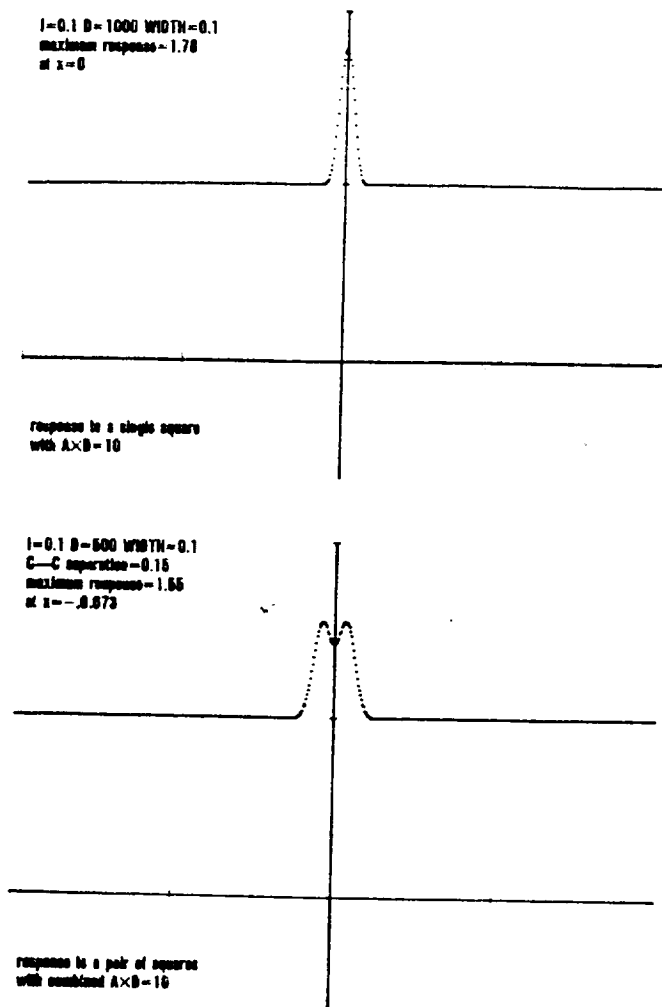


Fig. 14. Configurational effects within Ricco's area. The top curve is the response profile for a single square spot with (area  $\times$  intensity) = 10. The bottom curve is the response profile for a pair of square spots whose combined (area  $\times$  intensity) value was also 10.

a pair of squares of intensity  $I + D$ , width  $W$ , and center-center separation  $S$ , surrounded by a uniform background of intensity  $I$ . It assumes that the squares are both centered on the  $x$  axis. The curve in the bottom panel of Fig. 14 is a plot of the profile of this output function along the  $p$  axis (i.e., the horizontal axis of the output image).

$$\begin{aligned} O[p, q] = & 1 + \{N[A(W/2 - q)] - N[A(-W/2 - q)]\} \\ & \times \{N[A(S/2 + W/2 - p)] - N[A(S/2 - W/2 - p)]\} \\ & + \{N[A(W/2 - q)] - N[A(-W/2 - q)]\} \\ & \times \{N[A(-S/2 + W/2 - p)] - N[A(-S/2 - W/2 - p)]\} \\ & - \{N[B(W/2 - q)] - N[B(-W/2 - q)]\} \\ & \times \{N[B(S/2 + W/2 - p)] - N[B(S/2 - W/2 - p)]\} \\ & - \{N[B(W/2 - q)] - N[B(-W/2 - q)]\} \\ & \times \{N[B(-S/2 + W/2 - p)] - N[B(-S/2 - W/2 - p)]\}, \end{aligned} \quad (12)$$

where  $A = (I + D)^{1/2}$  and  $B = \sqrt{I}$ .

## 5. DISCUSSION

### Intensity-Dependent Spatial Summation as a Psychophysical Model

For a model based on a single assumption, the IDS model gives a surprisingly complete first-approximation description of human spatial vision for retinal illuminances ranging from absolute threshold up to around 10 Td. It predicts the two major effects usually associated with spatial summation: the dependence of Ricco's area on background luminance and the fact that visual acuity increases approximately as the square root of mean luminance. And, unexpectedly, it also predicts two major effects that are not usually thought of as related to spatial summation—or, indeed, to each other: Mach bands and Weber's law. Those two effects are typically explained in terms of mechanisms quite different from the one embodied in the IDS model: lateral inhibition for Mach bands and nonlinear transduction for Weber's law. Here we examine the relationship between those familiar concepts and the IDS mechanism. We also describe a way in which the IDS model can be modified to produce a closer fit to psychophysical data and point out a connection between IDS processing and brightness constancy.

### Mach Bands and Constant-Volume Models

Mach bands are generally attributed to a neural process of lateral inhibition that can be modeled by convolving the retinal image with a sombrero-shaped point-spread function whose negative brim represents the inhibition.<sup>17</sup> We will refer to this as the standard linear lateral inhibitory (LLI) model. Within the framework of linear systems theory, lateral inhibition is the only possible explanation of Mach bands, since Mach bands correspond to a high-pass filter effect and in a shift-invariant linear model such an effect can be produced only by a point-spread function containing negative lobes. However, we have seen that the IDS model, which is nonlinear, creates Mach bands with a purely positive point-spread function.

Thus the IDS model represents a new principle for generating edge enhancement, namely, edge enhancement will be produced by any model in which each photoreceptor creates a point-spread function whose volume is the same for all input

intensities. Recall that the fundamental assumption of the IDS model is that the height of the receptor output function varies directly with input intensity but its volume remains constant. As a consequence, the effect of an image on the system is not to change its total output but rather to redistribute that output in space. It follows that, when the input is a uniform field, the output must also be uniform and that output level will be the same regardless of the input level—this is the intuitive proof that was given for Theorem 1 in Section 2. In other words, the sensitivity of the IDS model to uniform fields is zero.

Put another way, the IDS model has zero sensitivity at spatial frequency zero. And by extension it is clear that the same is true of any model in which the volume under the receptor output function remains constant across all input intensities. Furthermore, if the model responds at all, its sensitivity will rise from zero as frequency increases, so that it will act like a high-pass filter. And that, in turn, is what is generally meant by edge enhancement: Low frequencies are attenuated more than high frequencies, so that in the image itself large uniform areas are attenuated more than edges. It follows that all constant-volume models will produce edge enhancement.

An example of a constant-volume model different from the IDS model is illustrated in Fig. 15. Here the receptor point-spread function is the sum of two functions: a Gaussian whose variance remains constant and whose height is directly proportional to the input intensity  $I$ , added to another Gaussian whose variance also remains constant but whose height varies as  $(c - I)$ , so that the total volume under the spread function (i.e., the volume under the sum of the two Gaussians) is always equal to  $c$  regardless of the input intensity  $I$ . Because the volume is constant, this model will attenuate low frequencies and produce Mach bands. [Note that if  $c$  is positive the composite spread function will be entirely positive when the input level  $I$  is low and then will assume a sombrero shape at higher input levels, when  $(c - I)$  becomes negative.]

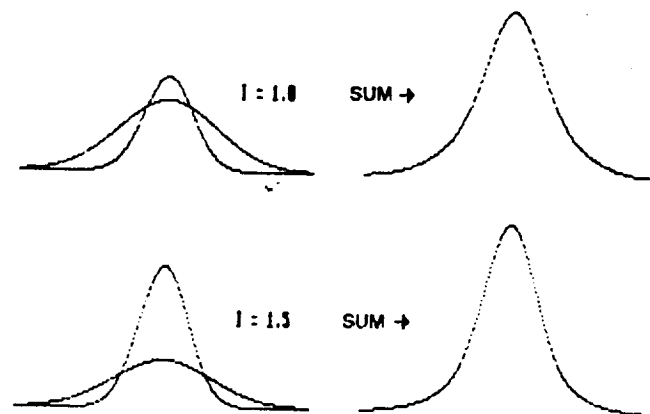


Fig. 15. Component curves for the point-spread function of a constant-volume model that differs from both the IDS model and the LLI model. Here the point spread is the sum of two functions, one whose height increases proportionally with the input intensity  $I$  [here, a Gaussian of the form  $I \times G_1(x, y)$ , where  $G_1$  has a fixed standard deviation  $\sigma_1$ ] and another whose height varies as  $c - I$ , where  $c$  is a positive constant [here,  $(c - I) \times G_2(x, y)$ , where  $G_2$  has fixed standard deviation  $\sigma_2$  and  $\sigma_2 > \sigma_1$ ]. Component curves for two values of  $I$  are shown on the left, and the corresponding composite point-spread functions are shown on the right.

In general, this constant-volume model is nonlinear since superposition fails: The output to a uniform field with intensity  $2I$  (i.e.,  $c$ ) is not twice the output to a field with intensity  $I$  (also  $c$ ). However, when  $c$  equals zero the model is linear—in fact, it is the standard LLI model. Thus that model falls in the intersection between two distinct classes of model for edge enhancement: It is simultaneously a constant-volume model and a linear model with negative lobes in its impulse response. Since no linear model can be a constant-volume model unless the volume under its impulse response is zero (and consequently the value of its MTF is zero at the origin), it follows that the only linear models that can produce edge enhancement with complete dc suppression are also constant-volume models.

We see then that the edge-enhancement properties of the standard LLI model need not necessarily be attributed to inhibition *per se*. Instead, they could equally well be said to follow from the fact that it, like the IDS model, is a constant-volume model.

### Weber's Law and a Generalized Intensity-Dependent Spatial-Summation Model

Weber's law is often attributed to an early nonlinear transformation in the visual system that causes the neural response to an input of intensity  $I$  to be approximately proportional to  $\log I$ . This very old idea is not really satisfactory because it does not explain why Weber's law fails at low luminances, and, more critically, even when buttressed with the concept of dark light, it still cannot explain why the range of background luminances for which Weber's law holds exactly should depend on the size of the test spot. The IDS model accounts for Weber's law and its failures on a totally different principle. Here the height of the receptor response varies linearly with the input intensity, and Weber's law arises as an edge effect that is due to spatial summation—an effect that begins to become significant only at a critical level of background luminance, which increases as the size of the test spot decreases. A natural question here is: What specific feature of the IDS model causes Weber's law to occur at all?

The answer cannot be the constant-volume assumption *per se*, since that assumption is shared by the standard LLI model, which does not imply Weber's law. And for the same reason, it cannot be the assumption that the height of the receptor spread function is directly proportional to the input intensity. In fact, the key to the model's Weber-law behavior is the constant-shape assumption, i.e., the assumption that the form of the spread function when the input intensity is  $I$  is  $I \times S(Ir^2)$ , where  $r$  is distance from the receptor. This assumption keeps the volume under the spread function constant by causing the equivalent area (volume/center height) to vary inversely with  $I$ . But closer analysis shows that this specific area-intensity relationship is not necessary for Weber's law. In fact, if the spread function takes the form  $I^n \times S(I^n r^2)$ , where  $n$  is any nonzero exponent, and all the other assumptions of the IDS model remain the same, the resulting model still implies Weber's law, though now the area under the spread function varies inversely with  $I^n$  instead of simply  $I$ . Thus the critical feature is really the fact that the model causes the spread function to change with intensity by rescaling the  $x$  and  $y$  coordinates of the retinal plane by factors that exactly undo the change in its height, thereby leaving its volume constant.

To prove that the generalized IDS model mentioned in the last paragraph implies Weber's law, recall that the key to our proof that all IDS models imply Weber's law, regardless of the form of the basic spread function (Theorem 4 in Section 3) was the scaling theorem (Theorem 3). Suppose now that we alter assumption (3) of Section 2 so that the spread to output point  $(p, q)$  from input point  $(x, y)$  with input intensity  $I(x, y)$  is

$$(3A) \quad [I(x, y)]^n S\{[I(x, y)]^n [(x-p)^2 + (y-q)^2]\},$$

where  $S$  is any spread function satisfying assumptions (1)–(4) of Section 2. And suppose that the output image is still the sum of the spread functions, i.e., assumption (5) now becomes

$$(5A) \quad O[I(x, y)](p, q) = \iint [I(x, y)]^n \times S\{[I(x, y)]^n [(x-p)^2 + (y-q)^2]\} dy dx.$$

Then Theorem 3 can be generalized as shown below.

### Theorem 3A (Generalized Scaling Theorem)

For every positive constant  $c$  and every input image  $I(x, y)$

$$O[cI(x, y)](p, q) = O[I(x/\sqrt{c}^n, y/\sqrt{c}^n)](p\sqrt{c}^n, q\sqrt{c}^n). \quad (13)$$

### Proof

As in the proof of Theorem 3, we express the right-hand side of Eq. (13) in terms of the integral in assumption (5A) and make the change of variable  $u = x/(\sqrt{c}^n)$ ,  $v = y/(\sqrt{c}^n)$ . The result is the left-hand side of Eq. (13) expressed in integral form.

From Theorem 3A it is easy to prove that Theorem 4 still holds for this generalized IDS model, i.e., the maximum and the minimum values of the output on the high and the low sides of an edge still depend only on the ratio between the input intensities on the two sides. In other words, the generalized IDS model in which the point-spread area varies inversely with  $I^n$  still implies Weber's law in the same way as the original model.

In fact all the theorems proved for the original model still hold for this generalization, since their proofs in every case depended only on the scaling theorem. The only difference is that, wherever the original theorems and proofs mention the mean luminance level  $L$ , one needs to substitute  $L^n$  in the general case. Thus Theorem 5, which showed that visual acuity increases as  $\sqrt{L}$ , can be immediately generalized to show that acuity in this model increases as  $\sqrt{L}^n$ . As noted in Section 3,  $n$  values less than 1.0 are more in line with psychophysical acuity measurements (e.g.,  $n = 0.75$  for the data of Schlaer<sup>7</sup>). This is also true of measurements of the size of Ricco's area as a function of background luminance: Barlow's<sup>2</sup> results obtained at 6.5-deg eccentricity require a  $n$  of the order of 0.2, and the foveal data of Glezer<sup>3</sup> are fitted by  $n = 0.5$ .

### Discounting the Illuminant: Weber's Law and Brightness Constancy

Most objects in natural scenes emit no light of their own but simply reflect light from the sun or some artificial source. Normally the reflectances of objects remain constant over time, but their illumination may vary by factors as large as  $10^{10}$ , so the irradiance of their optical images can vary by the



same factor. After IDS processing the peak and trough amplitudes of the Mach bands at edges depend only on the ratio between the input image intensities on the two sides (Fig. 3). This ratio depends only on the reflectances of an object and its background and is independent of scene illumination. The shapes and the positions of these peaks and troughs, however, depend on the absolute input intensities and thus on illumination: Both become narrower and move closer to the edge itself as illumination increases. For any object-background combination, then, there is some illumination level beyond which the Mach bands generated on opposite sides of the object no longer overlap one another. At this level and all higher ones, the output image of the object consists of an edge-enhanced border whose peak and trough amplitudes depend on the reflectance ratio across its edges and whose interior has the baseline output value (1.0 for the IDS operators defined in Section 2). Of course this critical illumination level is lower the larger the object. Assuming that an object can be detected when the peak of its edge response differs from the baseline response value by more than some criterion amount, it follows that in an IDS system the detectability of any object will follow Weber's law once the illumination level gets high enough.

If the apparent brightness of an object is unaffected by its illumination and depends only on its reflectance and that of its background, as is roughly true in human vision, one speaks of brightness constancy. In the human visual system, the apparent brightness of the interiors of large objects of uniform luminance must be based on an extrapolation from their edges, since the retinal images of the interiors are effectively stabilized images and consequently cannot contribute to their visibility.<sup>18</sup> If an extrapolation mechanism based its assignment of interior brightnesses on the peak and trough values of the Mach bands at the edges of objects and received its input from an IDS operator, it too would exhibit brightness constancy for all objects beyond a certain size.

### Intensity-Dependent Spatial Summation as an Image-Processing Algorithm

Intensity-dependent spatial summation seems potentially useful as a first-stage image-processing operation for applications involving the same type of boundary conditions faced by the retina—applications in which the inputs are Poisson noisy images whose mean intensity levels [(quanta/pixel)/frame] can vary substantially from scene to scene (e.g., because of changes in illumination) and also within a single image (e.g., because of shadows). These conditions occur naturally for television pictures of real scenes illuminated by the sun.

### Automatic Gain Control

The illumination falling upon natural scenes can vary over the course of a day by as much as  $10^{10}$ . No recording medium can readily accommodate such an enormous dynamic range. There are two fundamental objections to the usual solutions to this problem, such as the use of filters or amplifier gain changes. First, they are insensitive to local variations in scene illumination, e.g., owing to shadows: The effective luminance of the entire scene is reduced by a common factor, which can reduce the signal level in shadowed areas down into the range of the system noise. This is symptomatic of the second objection, which is more general. Spatial contrast detection is in principle limited by photon noise at all illumination

levels; contrast sensitivity can always be improved by increasing the quantum catch. Thus any gain-control mechanism that simply enforces a fixed quantum catch, as the use of an iris or a filter does, is bound to become increasingly inefficient as the illumination level rises.

The IDS mechanism automatically compresses all input intensities into a output range extending from zero up to around twice the value of the constant point-spread volume (i.e., 0–2 when that volume is taken to be 1.0, as it was arbitrarily in the IDS model of Section 2.) In doing this it makes efficient use of every photon: As the image plane illuminance increases, the extra photons serve to decrease the size of the spatial-summation area, improving spatial resolution while maintaining a fixed reliability of contrast detection. And this effect occurs locally within a single image, so that in every region the size of the summation area is matched to the illumination falling upon objects in that portion of the scene.

### Noise Smoothing and High-Frequency Attenuation

In noise smoothing by local averaging, the size of the summation area is usually held constant throughout any single image. The effect is simply low-pass linear filtering. This is a sensible way of suppressing photon noise, provided that the mean intensity level is known in advance (so that the summation area can be set inversely proportional to it) and that there is not much variation around the mean level within any single image. If the last condition cannot be guaranteed, either summation over a fixed area loses potentially resolvable high frequencies in the high-intensity regions of the image (because the summation area is too large for the mean luminance level in those regions), or else the low-intensity parts of the image become needlessly noisy (because the summation area is too small for the mean luminance level there), or both effects occur at once in different parts of the image.

The IDS operation, on the other hand, acts like a spatial filter whose high-frequency cutoff is always adjusted to match the prevailing light level (Fig. 7). In effect, it selects for attenuation the spatial frequencies that are so high, relative to the mean quantum catch/pixel, that they could not be reliably discriminated from photon noise. Thus the mean luminance level does not have to be known in advance, because the IDS mechanism adjusts to it automatically. And since this process occurs locally, different parts of the same image can have different mean intensity levels without requiring the mechanism to compromise on a single high-frequency cutoff. Instead, each region's cutoff frequency is automatically matched to its local mean intensity level. Thus, if the input is an image of a natural scene illuminated by the sun and some parts of the scene are in shadow, all parts of the output image will simultaneously tend to contain the maximum amount of high-frequency information justified by their local mean luminance levels.

### Edge Enhancement

Edge enhancement is usually accomplished by convolving the input image with a more or less sombrero-shaped point-spread function consisting of a positive central region and a negative surround. For Poisson noisy optical images, this bandpass-filtering operation has no effect on the signal-to-noise ratio: If the input image takes the form  $I \times r(x, y)$ , where  $I$  is scene illumination and  $r(x, y)$  is the reflectance distribution over a scene, after convolution the mean to standard deviation ratio

at each point is still proportional to  $\sqrt{I}$ . If the volume of the point-spread function is zero, as it usually is, uniform regions in the input image at any intensity  $I$  are converted into bandpass-filtered Gaussian noise with mean zero and variance  $I$  at every point. This noise is the background against which objects must be detected. For any value of  $I$ , the size of the sombrero must be adjusted to ensure an adequate signal-to-noise ratio at the Mach bands produced at edges, since those are the only places where most objects will be visible. In general, the critical size varies inversely with  $I$ , and, if the filter is poorly matched to the actual value of  $I$  in a given scene, the result will be either a needless loss of high-frequency information (when the sombrero is wider than necessary) or edges that cannot be discriminated from noise (when the sombrero is too small). If  $I$  varies greatly within a scene, the filter cannot be appropriate for all regions simultaneously, and one defect or the other is inevitable, just as with linear noise-smoothing filters.

An IDS operator acts like a bandpass filter whose frequency range automatically changes to match the prevailing mean-luminance level, both from scene to scene and also locally within scenes. Consequently, the parameter of an IDS filter (i.e., the width of its point-spread function) needs to be adjusted only for a single luminance level, and the filter will then adapt to all other levels (up to its saturation point), maintaining essentially the same size edge response at all levels for constant-contrast edges (because of the Weber-law property discussed above) and increasing spatial resolution as scene illumination increases. It can be shown that, for the Gaussian case, the IDS response to Poisson noisy uniform fields has a constant mean and variance for all values of  $I \geq 0.01$ . Consequently, the background noise against which objects are detected does not increase with scene illumination, and the detectability of edges (and thus of large targets) should remain constant as illumination increases, while resolution improves.

## 6. SUMMARY

We have analyzed a nonlinear model of retinal image processing, the IDS model, based on a single assumption: The height of the point-spread function varies directly with illuminance, whereas its volume remains constant, so that the area under the spread function around each photoreceptor is inversely proportional to the illuminance at that receptor. This assumption allows reliable spatial contrast discrimination in the face of photon noise while simultaneously maximizing spatial resolution. It proves to have the following consequences:

- (1) *Bandpass Filtering.* The input image is effectively bandpass filtered, producing Mach bands at edges and an apparent center-surround antagonism in the response to small spots. In general, the model mimics effects normally attributed to lateral inhibition. This mimicry includes the fact that the appearance of lateral-inhibitory effects depends on illumination: At low background intensity levels, responses to small test spots exhibit no noticeable surround antagonism.
- (2) *Ricco's Law.* For spatially continuous targets smaller than a critical size, the peak response value depends only on the product of target area times intensity. Thus detection of such targets should obey Ricco's law. The size of the crit-

ical area (that is, the size of Ricco's area) varies inversely with the background illuminance.

- (3) *Configurational Violations of Ricco's Law.* Within Ricco's area (that is, the area of apparent perfect spatial summation as determined with spatially continuous targets), Ricco's law fails for noncontinuous targets: A single spot produces a larger peak response than two separated spots that have the same combined area  $\times$  intensity product.

- (4) *Del<sup>2</sup>-G MTF.* The response to low-contrast sinusoidal gratings closely approximates a sinusoid, allowing one to define a MTF. For the Gaussian case of the IDS model, the MTF at any fixed mean luminance level has the same form implied by a LLJ model based on the negative Laplacian of a Gaussian.

- (5) *Visual Acuity Improves with Illumination.* The MTF varies with illuminance in such a way that any high-frequency cutoff increases as the square root of the mean luminance level (for the simplest version of the model). This implies that visual acuity should vary in the same way.

- (6) *Weber's Law Succeeds or Fails Depending on Target Size and Background Intensity.* The response to edges separating large uniform fields obeys Weber's law: The peak and trough values of the Mach bands at edges depend only on the ratio between the input image intensities on the two sides of the edge. When a target of fixed size is superimposed upon background fields of increasing intensity, its response profile evolves through three stages: first a simple bump, then a sombrero, and, finally, a pair of Mach bands at both edges with a baseline-response level between. The smaller the target is, the higher is the background level required to reach this final stage. Once it is reached, the detectability of the target satisfies Weber's law for all higher background luminance levels. In general, the model implies threshold versus background intensity curves whose shapes closely resemble those found in psychophysical experiments.

- (7) *Brightness Constancy.* Assuming that the brightness of a target depends on the size of its edge response, the Weber property implies that sufficiently large targets will exhibit brightness constancy; i.e., their brightnesses will be independent of the scene illumination and depend instead only on their reflectances relative to that of the background.

## APPENDIX A: DERIVATION OF THE RESPONSE TO LOW-CONTRAST SINUSOIDAL GRATINGS

We derive here the approximation given in Eq. (7). Suppose that the input is a vertical sinusoidal grating of the form  $I(x) = 1 + k \cos 2\pi x/\lambda$ . Then from Eq. (4) the output profile along the horizontal axis is exactly

$$O(p) = \int_{-\infty}^{\infty} [(1 + k \cos 2\pi x/\lambda)^{1/2} / \sqrt{(2\pi)}] \times \exp[(-1/2)(1 + k \cos 2\pi x/\lambda)(x - p)^2] dx.$$

For arbitrary values of  $k$  this integral seems quite intractable. However, when  $k$  is small enough that  $k^2$  can be treated as zero, it can be solved as follows. First, write  $1 + k \cos 2\pi x/\lambda$  as

$$[1 + (k/2)\cos 2\pi x/\lambda]^2 - (k^2/4)\cos^2 2\pi x/\lambda.$$

Dropping the second term, we have

$$(1 + k \cos 2\pi/x) \approx 1 + (k/2) \cos 2\pi/x,$$

and substituting this approximation into the output equation yields

$$O(p) \approx \int_{-\infty}^{\infty} [(1 + j \cos 2\pi/x)/\sqrt{(2\pi)}] \\ \times \exp[(-1/2)(x - p)^2] \\ \times \exp[(-j)(\cos 2\pi/x)(x - p)^2] dx,$$

where  $j = k/2$  and the factor  $\exp[(-1/2)(k/2)^2(x - p)^2 \cos^2 2\pi/x]$  has been set equal to one. Expanding the second exponential factor as a Taylor series and dropping the terms containing powers of  $j$  greater than one, we have

$$O(p) \approx \int_{-\infty}^{\infty} [(1 + j \cos 2\pi/x)/\sqrt{(2\pi)}] \\ \times \exp[(-1/2)(x - p)^2] \times [1 - j(x - p)^2 \cos 2\pi/x] dx \\ = 1 - j \int_{-\infty}^{\infty} [1/\sqrt{(2\pi)}](x - p)^2 \cos 2\pi/x \\ \times \exp[(-1/2)(x - p)^2] dx \\ + j \int_{-\infty}^{\infty} [1/\sqrt{(2\pi)}] \cos 2\pi/x \exp[(-1/2)(x - p)^2] dx \\ - j^2 \int_{-\infty}^{\infty} [1/\sqrt{(2\pi)}](x - p)^2 \cos 2\pi/x \\ \times \exp[(-1/2)(x - p)^2] dx.$$

Dropping the last term (which is less than  $j^2$ ) and making the change of variable  $v = x - p$ , we obtain

$$O(p) \approx 1 - j \int_{-\infty}^{\infty} [1/\sqrt{(2\pi)}] v^2 \cos 2\pi/(v + p) \\ \times \exp[(-1/2)v^2] dv + j \int_{-\infty}^{\infty} [1/\sqrt{(2\pi)}] \\ \times \cos 2\pi/(v + p) \exp[(-1/2)v^2] dv,$$

which can be solved exactly. Expanding the cosine factors into  $(\cos 2\pi/v)(\cos 2\pi/p) - (\sin 2\pi/v)(\sin 2\pi/p)$  and noting that the integrals involving sine factors all vanish, we have

$$O(p) \approx 1 - j \cos 2\pi/p \int_{-\infty}^{\infty} [1/\sqrt{(2\pi)}] v^2 \\ \times \cos 2\pi/v \exp[(-1/2)v^2] dv \\ + j \cos 2\pi/p \int_{-\infty}^{\infty} [1/\sqrt{(2\pi)}] \cos 2\pi/v \exp[(-1/2)v^2] dv.$$

The third term can be obtained from integral tables: It works out to  $j \cos 2\pi/p \exp(-2\pi^2/p^2)$ . To evaluate the second term we note that the integral is the Fourier transform of  $[1/\sqrt{(2\pi)}] v^2 \exp[(-1/2)v^2]$ , which is  $[1 - (2\pi f)^2] \exp(-2\pi^2 f^2)$ . The entire second term then is  $-j \cos 2\pi/p$  times that expression. Combining all three terms and replacing  $j$  with  $k/2$ , we have finally

$$O(p) \approx 1 + [2\pi^2 f^2 \exp(-2\pi^2 f^2)] k \cos 2\pi/p,$$

which is Eq. (7).

## ACKNOWLEDGMENTS

Research for this paper was supported in part by NASA grant NCA2-OR345-301 to John I. Yellott, Jr. We thank A. Ahu-

mada, S. Hersch, D. Kelly, and S. Reuman for discussions and assistance.

## REFERENCES

1. Psychophysical demonstrations of spatial summation begin with A. Ricco, "Relazione fra il minimo angolo visuale e l'intensita luminosa," *Ann. Ottalmol.* **6**, 373-479 (1877); the literature is reviewed by P. E. Hallett, "Spatial summation," *Vision Res.* **3**, 9-24 (1963) and by B. Sakitt, "Configuration dependence of scotopic spatial summation," *J. Physiol. (London)* **216**, 513-529 (1971); Physiological demonstrations of spatial summation in the vertebrate retina begin with H. K. Hartline, "The receptive fields of optic nerve fibers," *Am. J. Physiol.* **130**, 690-699 (1940); a recent review of that literature is P. O. Bishop, "Processing of visual information within the retinostriate system," in *Volume III of the Handbook of Physiology: The Nervous System*, I. Darian-Smith, ed. (American Physiological Society, Bethesda, Md., 1984); spatial summation at the photoreceptor level (receptor coupling) was first reported by D. A. Baylor, M. G. F. Fourtes, and P. M. O'Bryan, "Receptive fields of cones in the retina of the turtle," *J. Physiol. (London)* **214**, 265-294 (1971); many studies are described in H. B. Barlow and P. Fatt, eds., *Vertebrate Photoreception* (Academic, New York, 1977).
2. H. B. Barlow, "Temporal and spatial summation in human vision at different background intensities," *J. Physiol. (London)* **141**, 337-350 (1958).
3. V. D. Glezer, "The receptive fields of the retina," *Vision Res.* **5**, 497-525 (1965).
4. When the illuminance is  $I$ , the quantum catch is a Poisson random variable with mean and variance  $IA$ , and when the illuminance rises to  $I + cI$ , the catch is Poisson with mean and variance  $(1 + c)IA$ . Taking the probability of detecting the change to be the probability that the catch for  $I + cI$  exceeds the catch for  $I$  and using the normal approximation to the Poisson, it follows that the detection probability is the probability that a normal random variable with mean  $cIA$  and variance  $IA(2 + c)$  is greater than zero. To make this probability greater than 0.999,  $cIA/[IA(2 + c)]^{1/2}$  must be greater than 3. The order-of-magnitude value  $10/c^2$  underestimates the actual required value of  $IA$  [i.e.,  $(9/c^2)(2 + c)$ ] by a factor ranging from 0.55 (when  $c = 0.01$ ) to 0.37 (when  $c = 1$ ).
5. A. Rose, "The sensitivity performance of the human eye on an absolute scale," *J. Opt. Soc. Am.* **49**, 645-663 (1948); *Vision: Human and Electronic* (Plenum, New York, 1974).
6. D. Marr and E. Hildreth, "Theory of edge detection," *Proc. R. Soc. London Ser. B* **207**, 187-217 (1980).
7. S. Schlaer, "The relation between visual acuity and illumination," *J. Gen. Physiol.* **21**, 165-188 (1937). [Schlaer's data are shown in Fig. 3 of J. P. Thomas, "Spatial resolution and spatial interaction," in *Handbook of Perception*, E. C. Carterette and M. P. Friedman, eds. (Academic Press, New York, 1975), Vol. V, Chap. 7.]
8. H. B. Barlow, R. Fitzhugh, and S. W. Kuffler, "Change of organization in the receptive fields of the cat's retina during dark adaptation," *J. Physiol. (London)* **137**, 338-354 (1957).
9. C. Enroth-Cugell and J. G. Robson, "The contrast sensitivity of the ganglion cells of the cat," *J. Physiol. (London)* **187**, 517-552 (1966); A. M. Derrington and P. Lennie, "The influence of temporal frequency and adaptation level on receptive field organization of retinal ganglion cells in cat," *J. Physiol. (London)* **333**, 343-366 (1982). These experiments measured spatial CSF's for individual X cells over a wide range of mean luminance levels and fit them with modulation transfer functions implied by a linear difference-of-Gaussians receptive field model. In both cases the X-cell CSF changed from bandpass to low pass as mean luminance fell from photopic levels to near absolute threshold, indicating a loss of lateral inhibitory effects. The parameters of the best fitting MTF's implied that this change was due almost entirely to changes in the relative sensitivities of the center and surround mechanisms: The spatial areas of the center and surround apparently changed very little with mean luminance. Analyzing these data from a signal-detection standpoint, we find that that interpretation implies a very large decrease in the

quantum efficiency of the cat retina with light adaptation: for Derrington and Lennie's X-cell 25-J (their Fig. 9) quantum efficiency apparently fell by around 4 log units as mean luminance increased from  $3.8 \times 10^{-5}$  to  $200 \text{ cd/m}^2$ . Psychophysical evidence indicates that human quantum efficiency falls by only a factor of 10 over the same range (Ref. 5). Comparative visual-acuity measurements show that as mean luminance rises from  $10^{-5}$  to  $10 \text{ cd/m}^2$ , human visual acuity improves by a factor of 30, whereas cat acuity rises by only a factor of 3. [T. Pasternak and W. H. Merigan, "The luminance dependence of spatial vision in the cat," *Vision Res.* 21, 1333-1339 (1981)]. Taken altogether, these results suggest that cat and human retinas respond quite differently to changes in the light level. We are not aware of any study measuring spatial CSF's for primate retinal ganglion cells as a function of mean luminance, but we would expect substantial changes in the apparent size of receptive fields.

10. F. L. Van Ness and M. A. Bouman, "Spatial modulation transfer in the human eye," *J. Opt. Soc. Am.* 57, 401-406 (1967).
11. D. H. Kelly, "Adaptation effects on spatio-temporal sine-wave thresholds," *Vision Res.* 12, 89-101 (1972).
12. H. B. Barlow, "Increment thresholds at low intensities considered as signal/noise discriminations," *J. Physiol. (London)* 136, 469-488 (1957).
13. M. Aguilar and W. S. Stiles, "Saturation of the rod mechanism of the retina at high levels of stimulation," *Opt. Acta* 1, 59-65 (1954).
14. H. R. Wilson and J. R. Bergen, "A four mechanism model for spatial vision," *Vision Res.* 19, 19-32 (1979).
15. B. Sakitt, "Configurational dependence of scotopic spatial summation," *J. Physiol. (London)* 216, 513-529 (1971).
16. B. H. Crawford, "Visual adaptation in relation to brief conditioning stimuli," *Proc. R. Soc. London Sec. B* 134, 283-302 (1947). [Data shown as Fig. 3.10 in H. Ripps and R. A. Weale, "Visual adaptation," in *The Eye*, 2nd ed., H. Davson, ed. (Academic, New York, 1976), Vol. 2A.]
17. F. Ratliff, *Mach Bands: Quantitative Studies on Neural Networks in the Retina* (Holden-Day, San Francisco, Calif., 1965).
18. J. Krauskopf, "The effect of retinal image stabilization on the appearance of heterochromatic targets," *J. Opt. Soc. Am.* 53, 741-744 (1963).

**IDS CYLINDRICAL KERNEL RESPONSE TO A STEP EDGE**

## APPENDIX A

### IDS Cylindrical Kernel Response to a Step Edge

Since much of the analysis is predicated upon evaluation of the IDS response to an ideal step edge, we include here a short derivation of the basic properties of the cylindrical kernel IDS step edge response.

The IDS response  $O$  at a point  $(p,q)$  in an output image is the sum of each of the point spread functions (psf)  $h$  at  $(p,q)$ . By point spread function (kernel), we mean the response of the system to input of magnitude  $I$  at a sample point  $(x,y)$  in the input image. That is

$$O(p,q) = \int_{-\infty}^{\infty} \int_{-\infty}^{\infty} h(x,y;p,q,I) dx dy$$

The psf's are defined to be surfaces which encompass a constant volume  $V$  above the  $xy$  image plane. Without loss of generality we take this volume to be one. The psf is also assumed to have radial symmetry. For implementation of the psf it is useful to restrict it to a finite extent, so that the sum can be calculated "exactly" in a reasonable time. That is the sum includes only those psfs that lie with a radius  $r$ , here  $r^2 = (x-p)^2 + (y-q)^2$ . The simplest psf is then a cylinder (right circular) perpendicular to the  $xy$  plane of radius  $r$  and height  $l$ , ie.  $h(x,y;p,q,I) = h(r^2,I)$ . We further define the psf such that the height  $l$  is proportional to the intensity i.e.  $l = KI$ . Thus,  $V = 1 = \pi r^2 KI$  so that the psf is simply,

$$h(r^2,I) = KI \begin{cases} 1 & 0 < r < \frac{1}{\sqrt{\pi KI}} \\ 0 & \text{elsewhere} \end{cases}$$

Recall the circ function is defined as

$$\zeta(r) = \begin{cases} 1 & 0 < r < 1 \\ 0 & r \geq 1 \end{cases}$$

so that the integral can be written

$$O(p, q) = \int_{-\infty}^{\infty} \int_{-\infty}^{\infty} KI(x, y) \zeta(r\sqrt{\pi KI}) dx dy$$

We now invoke the essential one dimensionality of the original image i.e.  $I(x, y) = I(x)$ . Without loss of generality we will consider a step edge along the x direction, then

$$O(p, q) = \int_{-\infty}^{\infty} KI(x) \left\{ \int_{-\infty}^{\infty} \zeta(r\sqrt{\pi KI}) dy \right\} dx$$

The limits on the inner integral collapse to  $\pm y$ , where the kernel is nonzero. Then by expressing  $y = y(x, p, q, I)$  over the kernel we have

$$O(p) = 2 \int_{p - \frac{1}{\sqrt{\pi KI(x)}}}^{p + \frac{1}{\sqrt{\pi KI(x)}}} KI(x) \sqrt{\frac{1}{\pi KI(x)} - (x-p)^2} dx$$

where we have lost the dependency on  $q$  in the output image.

To proceed further we must now be explicit about the image. Specifically consider a step function at the x axis origin.

$$I(X) = \begin{cases} I_0 & x \leq 0 \\ I_0 + \Delta I & x > 0 \end{cases}$$

substituting

$$O(p) = \frac{2}{\pi r_0^2} \int_{p-r_0}^{p+r_0} \sqrt{r_0^2 - (x-p)^2} dx + \frac{2}{\pi r_\Delta^2} \int_{p-r_\Delta}^{p+r_\Delta} \sqrt{r_\Delta^2 - (x-p)^2} dx$$

where  $r_0 = (\pi K I_0)^{-1/2}$  is the radius of the kernel to the left of the origin and  $r_\Delta = (\pi K (I_0 + \Delta I))^{-1/2}$  is the smaller kernel to the right of the origin. It is useful to partition the x axis into the segments corresponding to the different limits of integration as shown in the Figure below

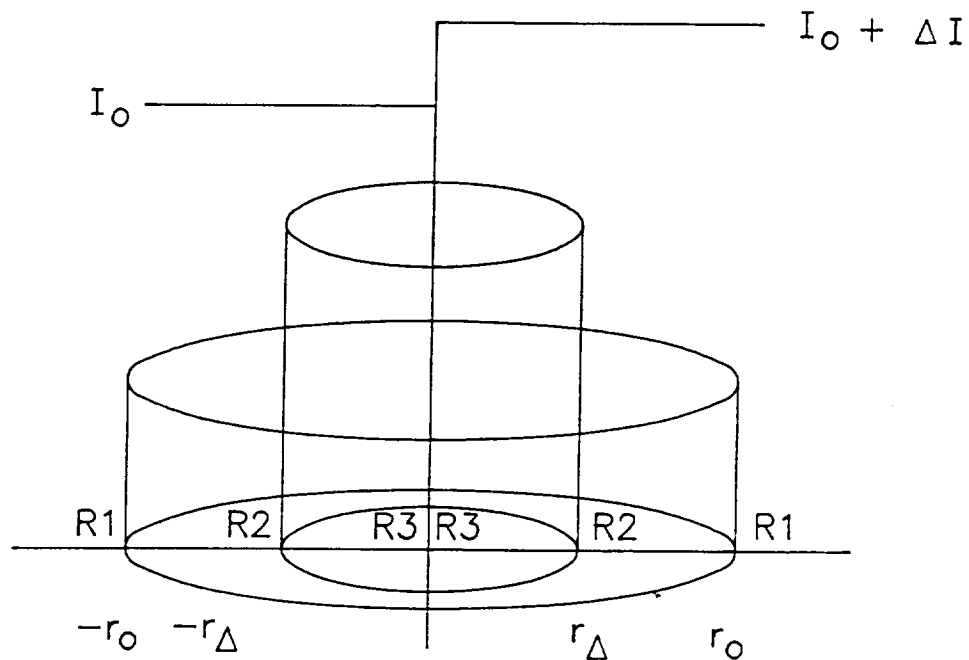


Figure A-1. Limits of Integration



Over the regions the integrals are:

$$\underline{R1} \quad |p| > r_0$$

$$O(p) = 1$$

$$\underline{R2} \quad r_\delta < |p| < r_0$$

$$O(p) = \frac{2}{\pi r_0^2} \int_{p-r_0}^0 \sqrt{r_0^2 - (x-p)^2} dx + H(p)$$

$$\underline{R3} \quad |p| < r_\delta$$

$$O(p) = \frac{2}{\pi r_0^2} \int_{p-r_0}^0 \sqrt{r_0^2 - (x-p)^2} dx + \frac{2}{\pi r_\delta^2} \int_0^{p+r_\delta} \sqrt{r_\delta^2 - (x-p)^2} dx$$

Where H is the Heaviside function

$$H(x) = \begin{cases} 1 & x > 0 \\ 0 & x < 0 \end{cases}$$

These integrals evaluate to

$$\underline{R1} \quad |p| > r_0$$

$$O(p) = 1$$

$$\underline{R2} \quad r_\delta < |p| < r_0$$

$$O(p) = \frac{1}{2} - \frac{1}{\pi} \left( \frac{p}{r_0} \right) \sqrt{1 - \left( \frac{p}{r_0} \right)^2} - \frac{1}{\pi} \sin^{-1} \left( \frac{p}{r_0} \right) + H(p)$$

$$\underline{R3} \quad |p| < r_\delta$$

$$O(p) = 1 - \frac{1}{\pi} \left( \frac{p}{r_0} \right) \sqrt{1 - \left( \frac{p}{r_0} \right)^2} - \frac{1}{\pi} \sin^{-1} \left( \frac{p}{r_0} \right) \\ + \frac{1}{\pi} \left( \frac{p}{r_\delta} \right) \sqrt{1 - \left( \frac{p}{r_\delta} \right)^2} - \frac{1}{\pi} \sin^{-1} \left( \frac{p}{r_\delta} \right)$$

By substituting  $r_0$  and  $r_\delta$  one can immediately obtain the expressions for the output as a function of the original step edge intensities. A more succinct form can be obtained by defining an angle  $\psi = \sin^{-1}(p/r)$  to give

$$R1 \quad |p| > r_0$$

$$O(p) = 1$$

$$R2 \quad r_\Delta < |p| < r_0$$

$$O(p) = \frac{1}{2} - \frac{1}{2\pi} [\psi_0 + \sin\psi_0] + H(p)$$

$$R3 \quad |p| < r_\Delta$$

$$O(p) = 1 - \frac{1}{2\pi} [(\psi_0 + \sin\psi_0) - (\psi_\Delta + \sin\psi_\Delta)]$$

The above functions and their first derivative are continuous across the region boundaries.

The extrema can be formed by finding  $\partial O(p)/\partial p = 0$  from either the integral or the explicit forms above. Differentiating the output expression over region 3 gives their location  $p'$  on the  $p$  axis as

$$p' = \pm \frac{r_0 r_\Delta}{\sqrt{r_0^2 + r_\Delta^2}}$$

substituting for  $r_0$  and  $r_\Delta$  gives the form

$$p' = \pm [\pi K I_0 (\omega + 2)]^{-1/2}$$

which should be compared with expression (7a) in Alter-Gartenberg<sup>1</sup>.

At this value of  $p$  we can find the peak value directly from the output expression in region 3. The three equivalent expressions are

$$\begin{aligned} O(p') &= 1 + \frac{1}{\pi} \sin^{-1} \left( \frac{1+\omega}{2+\omega} \right)^{1/2} - \frac{1}{\pi} \sin^{-1} \left( \frac{1}{2+\omega} \right)^{1/2} \\ &= 1 + \frac{1}{\pi} \sin^{-1} \left( \frac{r_0}{\sqrt{r_0^2 + r_\Delta^2}} \right) - \frac{1}{\pi} \sin^{-1} \left( \frac{r_\Delta}{\sqrt{r_0^2 + r_\Delta^2}} \right) \\ &= \frac{1}{2} + \frac{1}{\pi} \psi_\Delta' = \frac{3}{2} - \frac{1}{\pi} \psi_0' \end{aligned}$$

where  $\omega = \Delta I/I_0$  is the Weber fraction or contrast at the step edge. The first form is (7j) in Alter-Gartenberg<sup>1</sup>. The minimum is then  $O(-p') = 2 - O(p')$ . At infinite contrast the extrema are 1/2 and 3/2.

# APPROACHES TO IDS RECONSTRUCTION

## 1.1 Introduction

Given the IDS output, we would like to be able to reconstruct the input. Actually, we don't want to recreate the input itself, but a version of the input that has ratios of reflectances instead of intensities. Currently, Odetics is using an algorithm that goes through the output line-by-line, finds peaks and troughs, decodes the ratio of the step in intensities that is presumed to cause the peak and trough, and reconstructs the step as a ratio of reflectances. This method is a heuristic one. We can more or less tell from experience that this should work for certain images and under certain conditions. However, there is no mathematical proof or formal analysis of the algorithm, its benefits and drawbacks.

In this report, I will present four different approaches to IDS reconstruction. I haven't succeeded in solving the actual problem itself. However, I feel these techniques provide insight into the problem and may serve as trailheads to those who wish to continue on the path of reconstruction.

Figure 1.1 shows a one-dimensional slice of a two-dimensional step input. It also shows a slice of the IDS output. The output has odd symmetry about the point  $(0,1)$ .

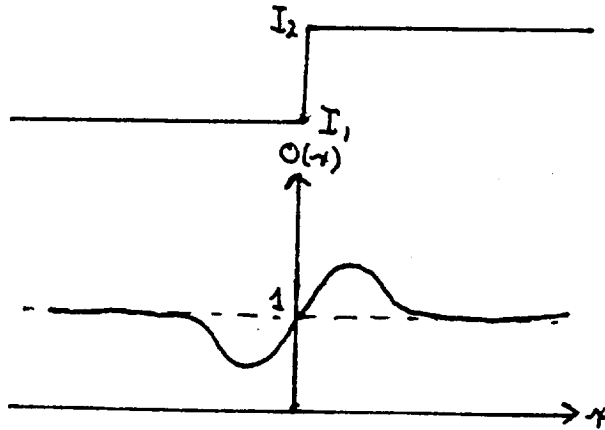
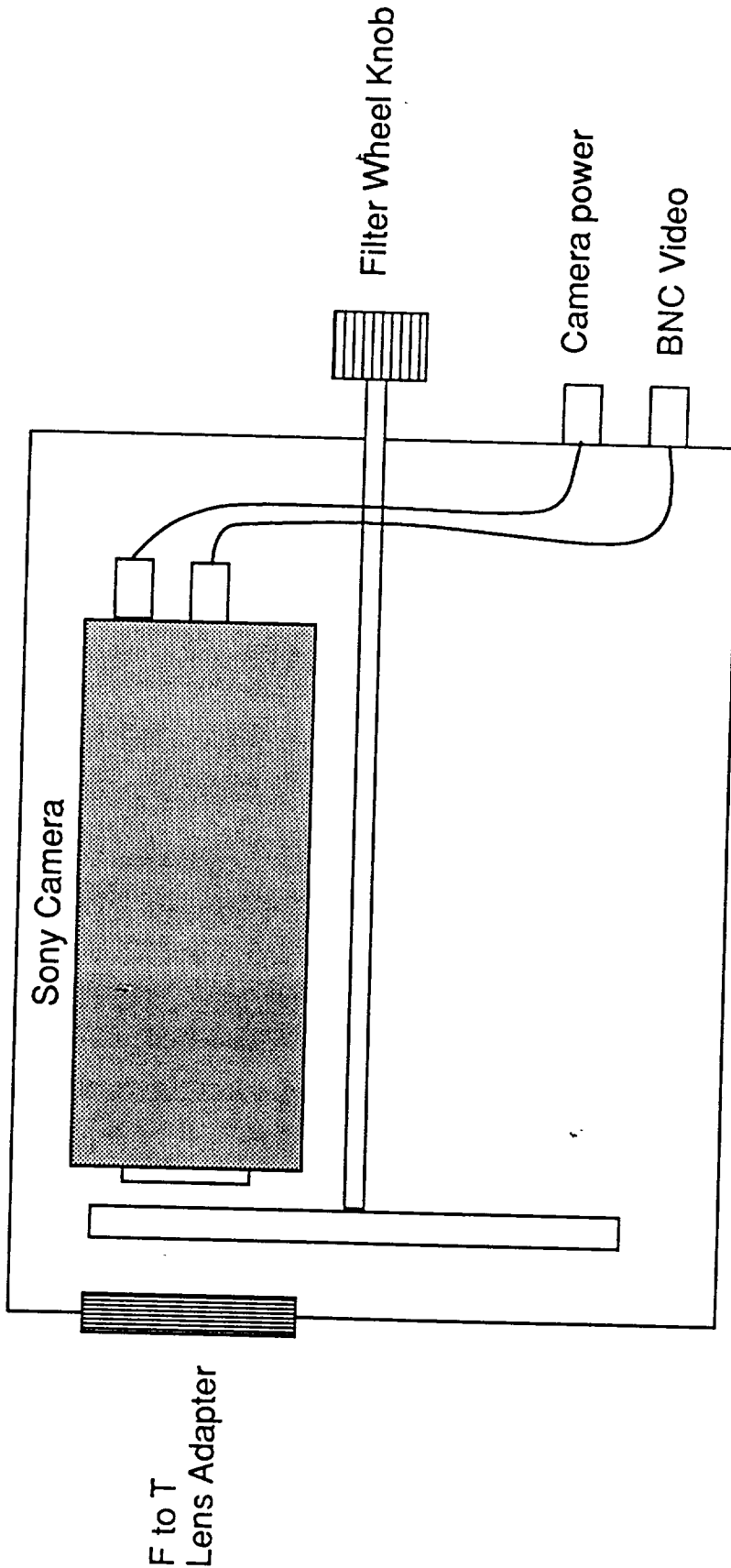


Figure 1.1: Step input and IDS response

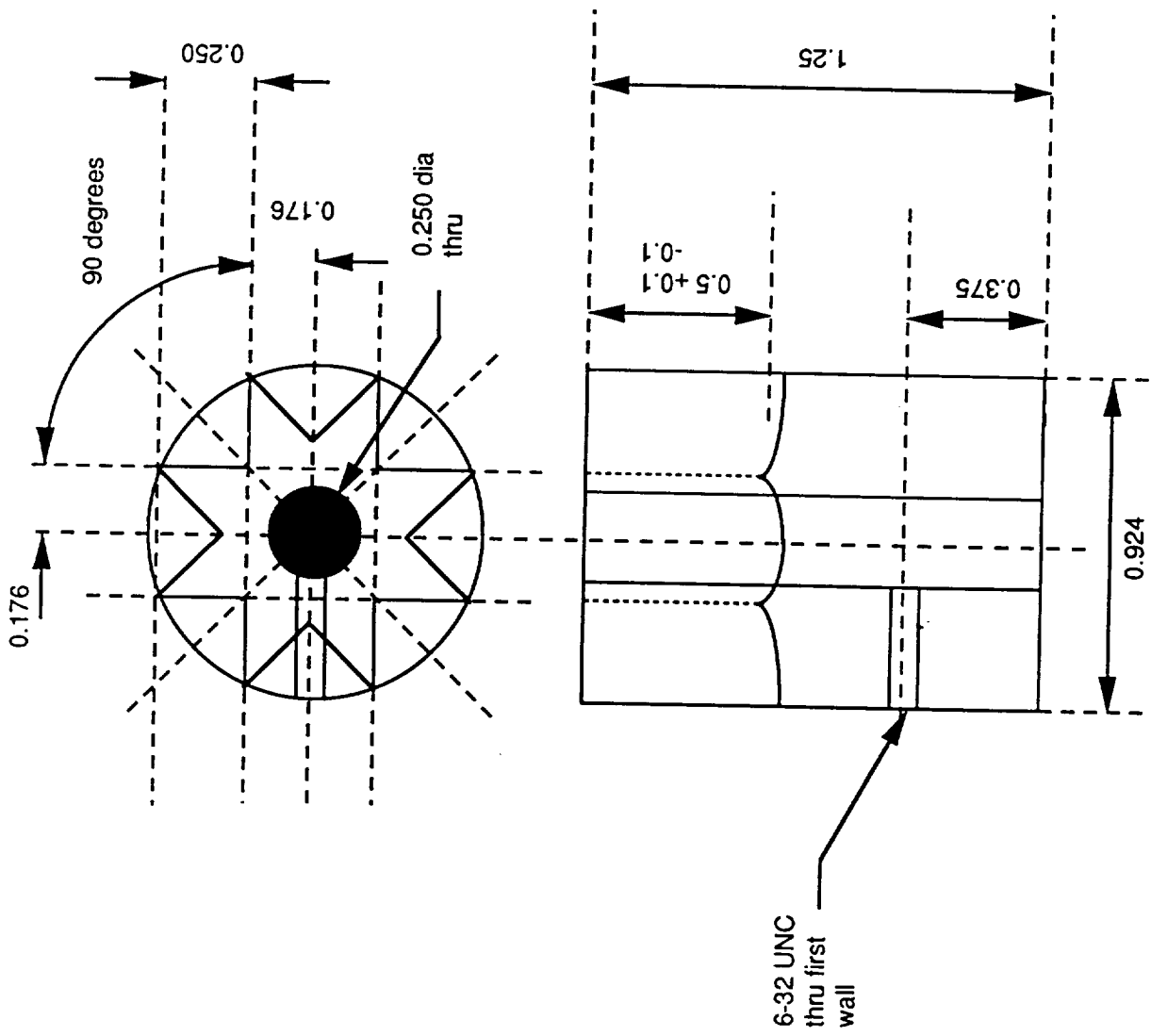
# Bibliography

- [1] Tom N. Cornsweet and John I. Yellott, Jr. Intensity-dependent spatial summation. *Journal of the Optical Society of America A*, 2:1769-1786, 1985.
- [2] Gregory Joel Reese. *Analysis and Application of Intensity-Dependent Spread Functions*. PhD thesis, University of California, Irvine, 1989.

**MULTISPECTRAL CAMERA DESIGN USING A SONY XC-77 CAMERA**



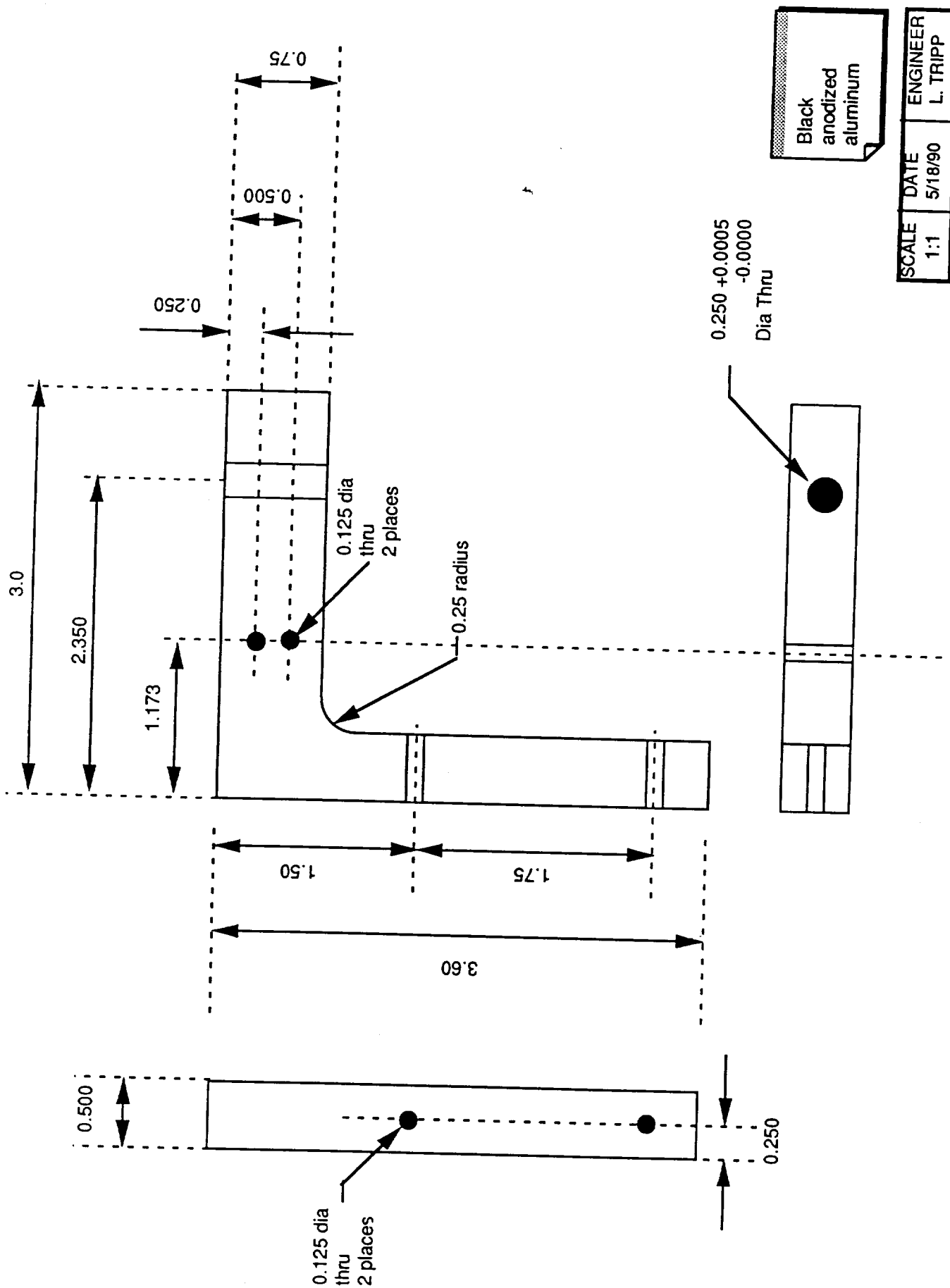
SCALE none	DATE 5/24/90	ENGINEER L. TRIPP
TITLE PLAN VIEW		



Mild steel

SCALE	DATE	ENGINEER
2:1	5/21/90	L. TRIPP
TITLE		
FILTER INDEX RING		





SCALE	DATE	ENGINEER	TITLE
1:1	5/18/90	L. TRIPP	
			FILTER WHEEL BRACKET

The peak height depends only on the ratio of the intensities on the two sides. If the input is due to a step in reflectances that is lit by a uniform illumination, the ratio of intensities will be independent of the actual illumination.

The output crosses one right where the intensity jump in the input is. The distance of the peak from the one crossing depends on the actual intensities themselves. If the intensities in the input are both multiplied by a constant greater than one, the peak height will remain the same but the peak will move closer to the origin.

The IDS response to a step illustrates a fundamental idea behind reconstruction processes. This idea is that we *want* to lose some of the information that is in the IDS output. To reconstruct the step as a ratio of intensities we only need to know three things — where to put the jump, what the ratio of the two sides is and which side is higher. We put the jump right where the one-crossing in the output is. We decode the ratio of the reflectances of the two sides from the peak height. We make the high side of the reconstruction the same as the side of the IDS output that has the peak.

Notice that we didn't use the information contained in the distance of the peak from the one-crossing. This makes sense because this information tells us the absolute values of the intensities in the input and that is precisely what we want to ignore.

The approaches that I illustrate below all attempt to reconstruct intensities instead of ratios. This comes about because the mathematical results that are available are stated in terms of the output for a given input and not as the output for ratios within the given input. In fact, it is impossible to always be able to reconstruct the input from the output. A simple example of this is an input that is a uniform field. Regardless of the intensity of the input, the output is always a uniform field whose value is one. Therefore, given an output that is one everywhere, we can't tell what the particular intensity of the input

was. However, if we relax the restriction of exact reconstruction to that of finding the ratio of all points to any one point, we can easily say that this ratio is one.

Because these approaches attempt an exact reconstruction, we already know that they will fail. My motivation for demonstrating these techniques is not to actually make the exact reconstruction, but to provide models and ideas for methods that can be modified to reconstruct an image of ratios of reflectances. I hope that someone will be able to do this.

## 1.2 An important approximation

Before I demonstrate the approaches to reconstruction, I'd like to derive and explain an important approximation that I'll use as a bridge between the continuous IDS that is used to derived mathematical results and the discrete IDS that is used on the computer for image processing. It is this:

**Approximation:** *The value of the discrete-IDS spread function at  $(x, y)$  from the input intensity  $I$  at the pixel at  $(p, q)$  is approximately equal to the continuous-IDS output at  $(x, y)$  from a square at  $(p, q)$  that is the size of the pixel at  $(p, q)$  and is uniformly covered by an intensity  $I$ .*

Let the square centered at  $(p, q)$  have sides of length  $2\Delta$ , with  $2\Delta$  being one pixel width. The continuous-IDS output at  $(x, y)$  from the square at  $(p, q)$  is given by

$$\int_{-\Delta}^{\Delta} \int_{-\Delta}^{\Delta} I(p, q) S \left\{ I(p, q) \left[ (x - p)^2 + (y - q)^2 \right] \right\} dp dq.$$

Since  $I(p, q)$  is constant over the square, we can write the output as

$$\int_{-\Delta}^{\Delta} \int_{-\Delta}^{\Delta} I S \left\{ I \left[ (x - p)^2 + (y - q)^2 \right] \right\} dp dq.$$

Now assume that the square is small enough so that the spread function is approximately constant over the square. (In practice, the spread functions in the discrete version of IDS are constructed so that this assumption is true.) Since the spread function is constant, it can be factored out of the integral to yield

$$IS \left\{ I \left[ (x - p)^2 + (y - q)^2 \right] \right\} \int_{-\Delta}^{\Delta} \int_{-\Delta}^{\Delta} dp dq.$$

The integral is just the area of the square. If we choose the unit of length to be one pixel width, this area will be equal to one. The output becomes

$$IS \left\{ I \left[ (x - p)^2 + (y - q)^2 \right] \right\},$$

which is the discrete IDS output at  $(x, y)$  from the pixel at  $(p, q)$ .

We'll use this equivalence throughout the report. In particular, note that the discrete IDS input can be considered to be a continuous input made up of little squares of uniform intensity. Since many of the results in the rest of this report depend on the input consisting of only regions of uniform intensity, this approximation will prove to be quite valuable.

### 1.3 Orthogonality

The first approach to reconstruction uses orthogonal functions. As an example of the concept of orthogonality, suppose the function  $f(x)$  is periodic. It can be expanded in a Fourier series, namely

$$f(x) = \sum_{i=-\infty}^{\infty} a_i e^{j i \alpha x}, \quad (1.1)$$

where

$i$  is an integer

$a_i$  is the Fourier coefficient

$j$  is  $\sqrt{-1}$

$\alpha$  is the fundamental spatial frequency.

To find  $a_i$ , we multiply both sides of Equation 1.1 by  $e^{-jk\alpha x}$  ( $k$  is some integer) and integrate over one period  $T$  ( $= \frac{2\pi}{\alpha}$ ).

$$\begin{aligned}\int_0^T f(x)e^{-jk\alpha x} dx &= \int_0^T \left[ \sum_{i=-\infty}^{\infty} a_i e^{ji\alpha x} \right] e^{-jk\alpha x} dx \\ &= \sum_{i=-\infty}^{\infty} a_i \int_0^T e^{j(i-k)\alpha x} dx\end{aligned}\tag{1.2}$$

The key to the procedure of orthogonality is that the integral on the right side is given by

$$\int_0^T e^{j(i-k)\alpha x} dx = \begin{cases} T & \text{for } i = k \\ 0 & \text{otherwise.} \end{cases}\tag{1.3}$$

Suppose two functions (such as  $e^{ji\alpha x}$  and  $e^{-jk\alpha x}$ ) are multiplied together and integrated over some range. If the result is a constant when the parameters in each function are equal ( $i = k$ ) but zero otherwise, the functions are *orthogonal*.

To continue the derivation of  $a_i$ , insert Equation 1.3 into Equation 1.2 to get

$$\begin{aligned}\int_0^T f(x)e^{-jk\alpha x} dx &= \sum_{i=-\infty}^{\infty} a_i \begin{cases} T & \text{for } i = k \\ 0 & \text{otherwise} \end{cases} \\ &= Ta_k\end{aligned}$$

or

$$a_k = \frac{1}{T} \int_0^T f(x)e^{-jk\alpha x} dx.$$

The technique which I will now outline is only applicable to inputs that just contain regions of uniform intensity. Each region must have positive<sup>1</sup> area, but the area can be infinite. By the approximation in Section 1.2, all discrete inputs on the computer can be treated as continuous inputs with only regions of uniform intensity. In [2, page 71, Theorem 2.6], I showed that for this type of input the output  $O(x, y)$  is given by

$$O(x, y) = \sum_{i=1}^N I_i S \{ I_i(x^2 + y^2) \} * u_{\mathfrak{R}_i}(x, y) \quad (1.4)$$

where

$N \geq 1$  is the number of regions of distinct intensities

$\mathfrak{R}_i$  is the region containing intensity  $I_i$

$*$  is the convolution operator

and  $u_{\mathfrak{R}_i}(x, y)$ , called an *indicator function*, is given by

$$u_{\mathfrak{R}_i}(x, y) = \begin{cases} 1 & \text{for } (x, y) \in \mathfrak{R}_i \\ 0 & \text{otherwise.} \end{cases}$$

Under this notation, the input  $I(x, y)$  can be written as

$$I(x, y) = \sum_{i=1}^N I_i u_{\mathfrak{R}_i}(x, y).$$

We want to find  $u_{\mathfrak{R}_i}(x, y)$  for all values of  $i$ . Since  $I_i$  goes with  $u_{\mathfrak{R}_i}(x, y)$ , we can then reconstruct the input. To find  $u_{\mathfrak{R}_i}(x, y)$ , we will use a more general version of orthogonality in which  $\langle \rangle$  is an unknown operation that replaces integration and  $Q(I_k, x, y)$  is a set of orthogonal functions. We will require  $Q(I_k, x, y)$  to be “orthogonal”<sup>2</sup> to the

---

<sup>1</sup>Throughout this report, “positive” means “greater than zero”.

<sup>2</sup>I put in quotation marks because the nonzero response in Equation 1.5 is a function, not a constant as the definition of orthogonality states.

function  $I_k S \{I_k(x^2 + y^2)\} * u_{\mathfrak{R}_k}(x, y)$  under the operation  $\langle \rangle$  so that

$$\langle Q(I_k, x, y), I_i S \{I_i(x^2 + y^2)\} * u_{\mathfrak{R}_i}(x, y) \rangle = \begin{cases} u_{\mathfrak{R}_i}(x, y) & \text{for } i = k \\ 0 & \text{otherwise.} \end{cases} \quad (1.5)$$

We reconstruct the input by finding one region  $u_{\mathfrak{R}_i}(x, y)$  at a time. To do this, apply the operator to both sides of Equation 1.4 to get

$$\langle Q(I_k, x, y), O(x, y) \rangle = \langle Q(I_k, x, y), \sum_{i=1}^N I_i S \{I_i(x^2 + y^2)\} * u_{\mathfrak{R}_i}(x, y) \rangle$$

Assume that  $\langle \rangle$  can be moved inside the summation sign. This gives

$$\langle Q(I_k, x, y), O(x, y) \rangle = \sum_{i=1}^N \langle Q(I_k, x, y), I_i S \{I_i(x^2 + y^2)\} * u_{\mathfrak{R}_i}(x, y) \rangle,$$

which through the use of Equation 1.5 reduces to

$$\langle Q(I_k, x, y), O(x, y) \rangle = \begin{cases} u_{\mathfrak{R}_k}(x, y) & \text{for } i = k \\ 0 & \text{otherwise} \end{cases}$$

or

$$u_{\mathfrak{R}_k}(x, y) = \langle Q(I_k, x, y), O(x, y) \rangle. \quad (1.6)$$

In image processing there are only a finite number of intensities  $I_k$ . We can use Equation 1.6 to go through the output and find the region in the input that corresponds to each intensity.

As an example, suppose that the operator  $\langle \rangle$  is the convolution operator  $*$  and the function  $Q(I_k, x, y)$  is such that

$$Q(I_k, x, y) * I_i S \{I_i(x^2 + y^2)\} = \begin{cases} \delta(x, y) & \text{for } i = k \\ 0 & \text{otherwise} \end{cases}$$

Then starting with Equation 1.4, we get

$$\begin{aligned}
O(x, y) &= \sum_{i=1}^N I_i S \{I_i(x^2 + y^2)\} * u_{\mathfrak{R}_i}(x, y) \\
Q(I_k, x, y) * O(x, y) &= Q(I_k, x, y) * \sum_{i=1}^N I_i S \{I_i(x^2 + y^2)\} * u_{\mathfrak{R}_i}(x, y) \\
&= \sum_{i=1}^N Q(I_k, x, y) * I_i S \{I_i(x^2 + y^2)\} * u_{\mathfrak{R}_i}(x, y) \\
&= \sum_{i=1}^N [Q(I_k, x, y) * I_i S \{I_i(x^2 + y^2)\}] * u_{\mathfrak{R}_i}(x, y) \\
&= \delta(x, y) * u_{\mathfrak{R}_k}(x, y).
\end{aligned}$$

Since the convolution of a delta function with a second function is the second function itself, the above equation becomes

$$u_{\mathfrak{R}_k}(x, y) = Q(I_k, x, y) * O(x, y),$$

which is what we were looking for.

Of course, the trick is to find an operator  $\langle \rangle$  and a set of functions  $Q(I_k, x, y)$  that will make this technique work. Moreover, even if we found these items, this method would still have to be modified to produce ratios of reflectances and not an exact reconstruction.

## 1.4 Algebraic reconstruction

Each point in the IDS output is the sum of spread functions from numerous input points. Given a group of such sums, can we deduce the constituent input values? I will now study this idea, which I call *algebraic reconstruction*.

Figure 1.2 is a very simple example. The input contains only two pixels. Let  $X(Y)$  be the value at pixel  $Y$  of the spread function centered at pixel  $X$ . In Figure 1.2,  $A_1(A_2)$  is the value at the right pixel of the spread function from the left pixel.



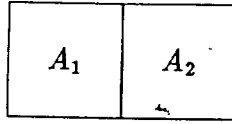


Figure 1.2: Input of two pixels

There are four unknowns in this problem —  $A_1(A_1), A_1(A_2), A_2(A_1), A_2(A_2)$ . We are given  $O(A_1)$  and  $O(A_2)$ , the outputs at the two pixels. Each output is the sum of the spread function centered above it and the spread function from the other pixel. Thus we get two equations,

$$\begin{aligned} O(A_1) &= A_1(A_1) + A_2(A_1) \\ O(A_2) &= A_1(A_2) + A_2(A_2) \end{aligned} \tag{1.7}$$

But we also know that the volume under the spread function is one. This means that the sum of all the values of any spread function must be one. This gives us another two equations,

$$\begin{aligned} 1 &= A_1(A_1) + A_1(A_2) \\ 1 &= A_2(A_1) + A_2(A_2) \end{aligned} \tag{1.8}$$

We now have four equations in four unknowns. Unfortunately, the equations aren't independent. We can see this by noting that the right side of the sum of the first two equations is the same as the right side of the sum of the second two equations. Thus there are more unknowns than (independent) equations.

We're also operating under other restrictions. The spread functions are non-negative

and the center heights are positive.<sup>3</sup> This leads to the four restrictions

$$A_1(A_1) > 0$$

$$A_1(A_2) \geq 0$$

$$A_2(A_1) \geq 0$$

$$A_2(A_2) > 0.$$

To fully understand the problem in this example, we would have to study the solutions to equations 1.7 and 1.8 under the above four restrictions.

When there are more than two input pixels (there usually are!), the situation is the same. Suppose the input is an  $n \times n$  array of pixels. There are  $n^2$  input points and  $n^2$  output points. Since each output is a sum of the spread functions from the inputs, there are  $n^2$  equations similar to those in Equation 1.7. Since each of the spread functions from the  $n^2$  inputs must sum to one, there will be  $n^2$  more equations like Equation 1.8. This gives a total of  $2n^2$  equations. However, as before, the sum of the two sets of equations is the same, so there are really  $2n^2 - 1$  independent equations. Each of the center heights must be positive and the other values of the spread function must be non-negative.

On the computer, all spread functions are set to zero past a certain distance. Call this maximum distance from the center  $r$ . There are approximately  $\pi r^2$  values for each spread function. This can be reduced to about  $\frac{1}{8}\pi r^2$  different values by symmetry arguments. Thus each image contains about  $\frac{1}{8}\pi r^2 n^2$  unknowns, but only  $2n^2 - 1$  independent equations. In general, there are always more unknowns than independent equations, and so there is no unique solution to the problem. Nevertheless, I think that algebraic

---

<sup>3</sup>This latter restriction comes about because the center height is proportional (with a positive constant of proportionality) to the intensity, and intensities in IDS are defined to be positive.

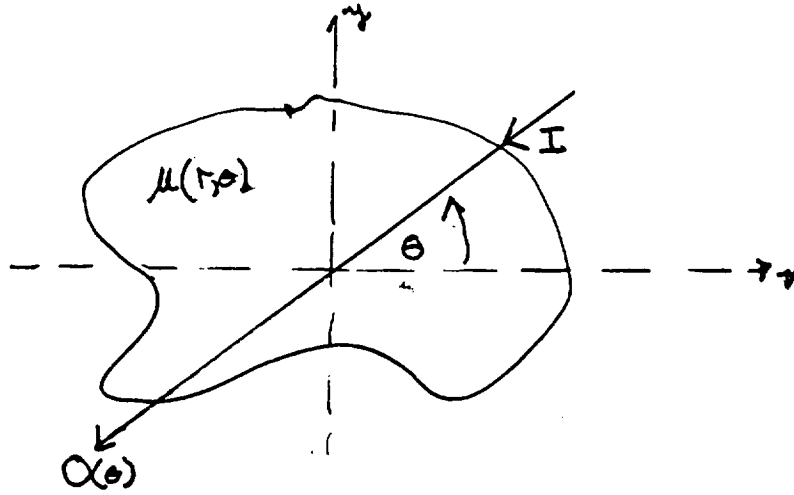


Figure 1.3: CAT scan

reconstruction needs to be investigated further for two reasons.

The first is that the technique attempts to reconstruct the values of the inputs exactly. As I explained in Section 1.1, we really want to find the ratios of reflectances. This involves a loss of information. It would be good to examine the solutions to the underdetermined equations that occur in algebraic reconstruction. What kind of information is lost in these equations? Is the loss such that the solution involves ratios of reflectances?

The second reason to further pursue algebraic reconstruction is that it may be similar to the techniques used in computer-aided tomography (CAT). Figure 1.3 shows the idea of CAT scans. There is a two-dimensional object which partially absorbs x-rays. The absorption varies throughout the object and is given (in polar coordinates) by  $\mu(r, \theta)$ . During a scan, a beam of x-rays passes through the object at a particular angle. The input intensity of the beam is known and the output intensity is measured. If this procedure is repeated at many different angles, the absorption can be accurately approximated at all points  $(r, \theta)$ .

For a given angle  $\theta$ , the relationship between the input intensity  $I$  of the beam and

the output intensity  $O(\theta)$  is

$$O(\theta) = Ie^{-\int_{-\infty}^{\infty} \mu(r, \theta) dr},$$

where the integral is along the path of the beam. Loosely speaking, even though the output always depends on a sum (integral) of the values we're trying to reconstruct ( $\mu(r, \theta)$  for various  $r$  and  $\theta$ ), we can still determine the absorption at each individual point  $(r, \theta)$ .

The situation in IDS is similar, though not exactly the same. Each output depends on a sum of functions of the object we're trying to reconstruct. The differences between IDS and CAT scans are that in IDS the sum is over two dimensions (a neighboring area) instead of one dimension and the input is unknown. However, the concepts are similar and it would be worthwhile to pursue the analogy further.

## 1.5 Geometry at corners

The previous approaches to reconstruction involve algebraic techniques. Another tack towards solving the problem is to look at the geometry of the output. By graphing the output as a height above the  $xy$ -plane, we get a three-dimensional landscape. As I explained in Section 1.1, there are geometrical features in the output that relate to geometrical features in the input. For example, in the step response, the output crosses one right where the jump in the input occurs. A geometrical approach to reconstruction would be to go through the output and look for one-crossings, peaks, valleys and other such figures and reconstruct the input from information in these figures. This idea has been used by people at NASA and is similar to the one currently being tested at Odetics.

A big problem with the geometrical approach is that it is hard to reconstruct the

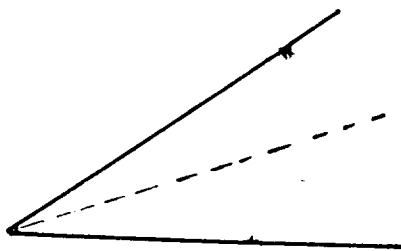


Figure 1.4: Bisector at a corner

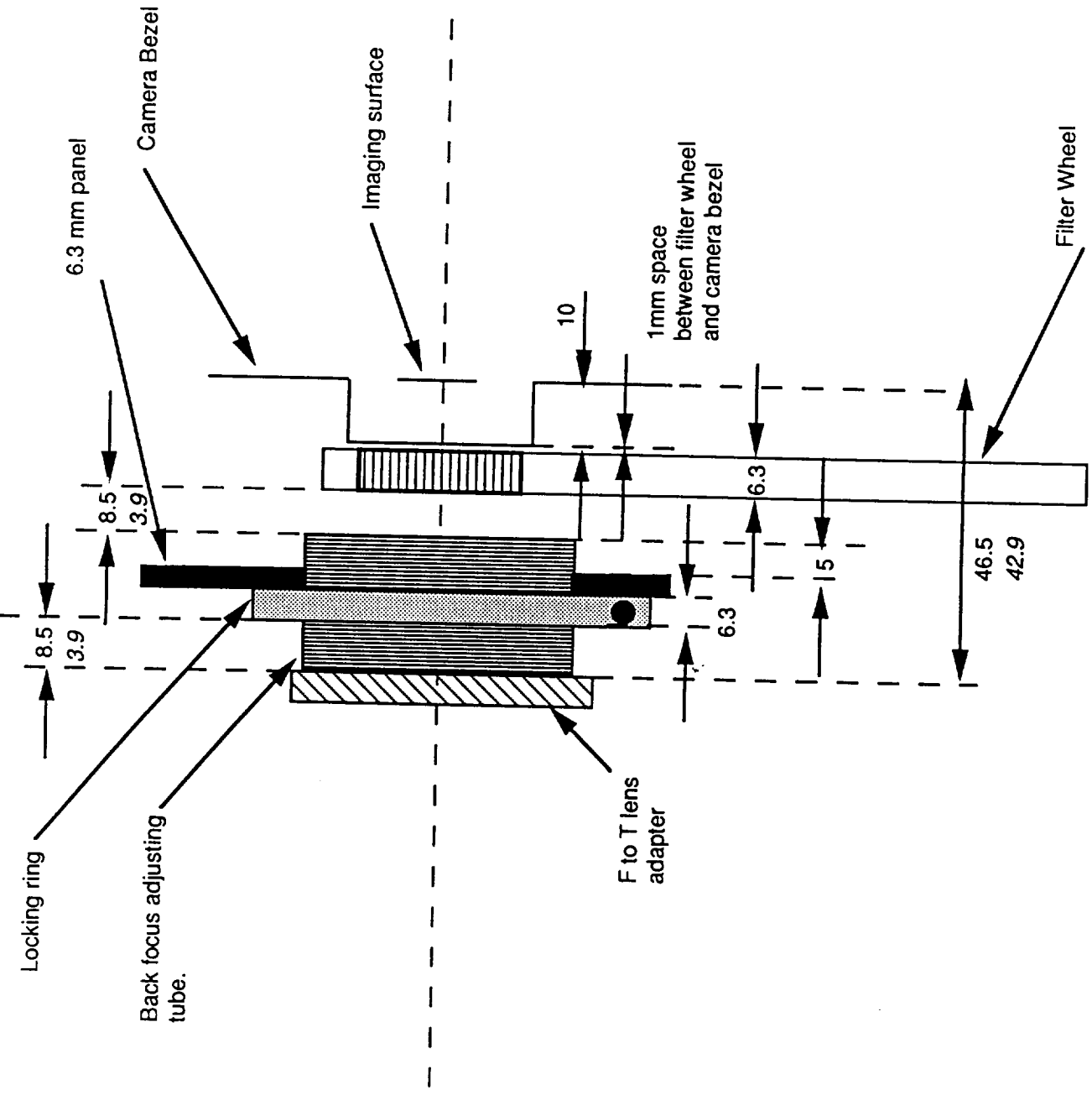
input at spots where there is a lot of detail, such as the vertex where polygons meet. (I'll discuss the specific nature of the problem in the next section.) In this section, I'd like to propose some mathematical results which may help determine corners more accurately.

In [2, page 110, Theorem 2.8], I showed that, under fairly general conditions, the output at the vertices of polygons is exactly one. I propose here that the local extrema (maxima or minima) occur along the bisector of the vertex angle. (In Figure 1.4, the dashed line is the bisector.) This proposition should be investigated and proven or disproven. For the rest of this section, I will assume that it is true.

These two properties of vertices could be used to pinpoint the intersection of two edges. Suppose that we have detected two edge segments, have calculated the formulas of the lines going through them and that we know that these lines intersect. Should these segments be extended to their intersection point to form a corner?

One supporting piece of evidence would be a pixel at the intersection whose value is one. In the continuous version of IDS, the point right at the intersection would be exactly one. Because IDS is discrete on the computer, we would check the pixels close to the calculated intersection (probably the nearest four pixels) to see if one of them is approximately one. If it were one, we would have more confidence in extending the segments.

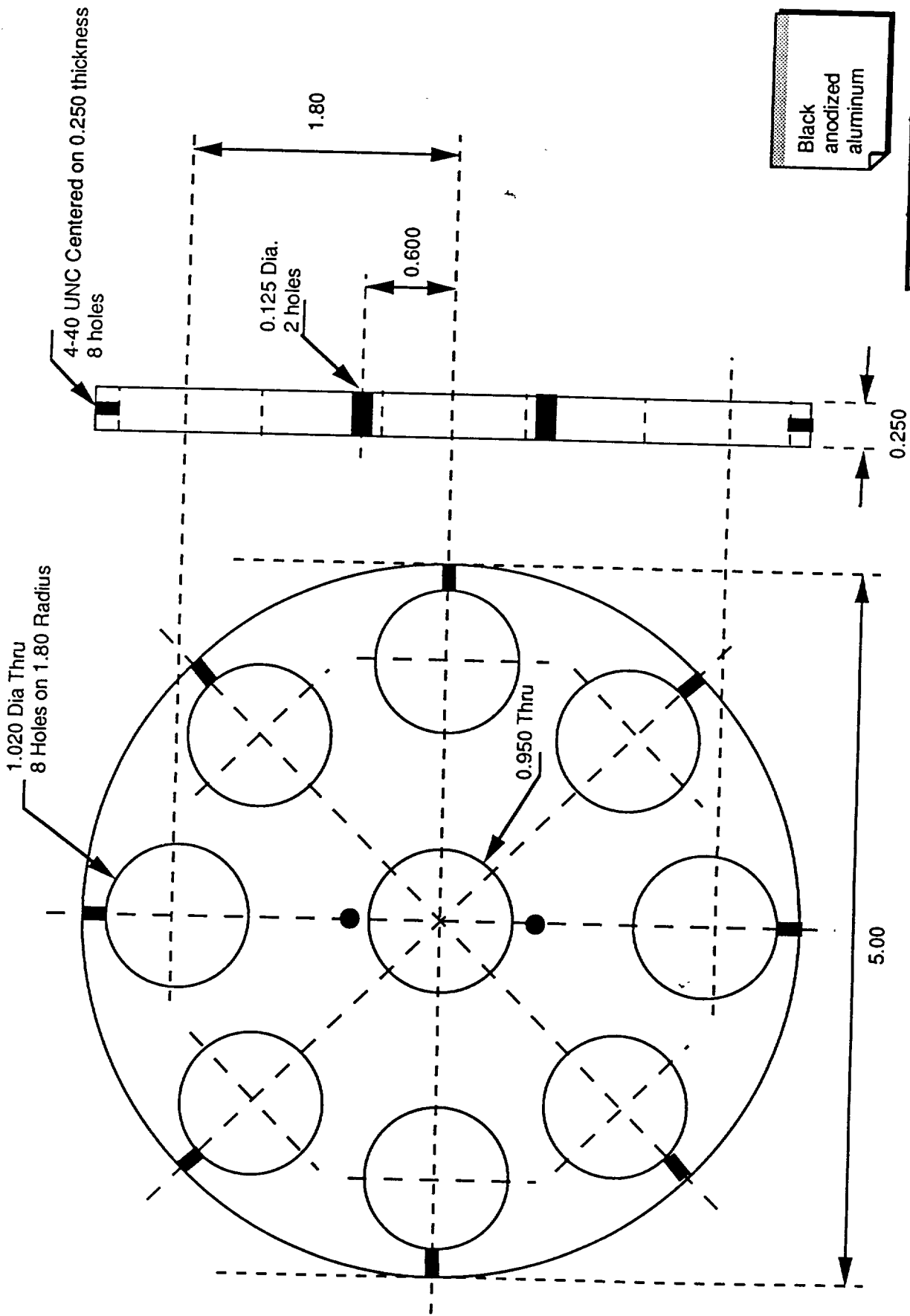
We could also calculate the bisector of the angle formed by the two intersecting lines



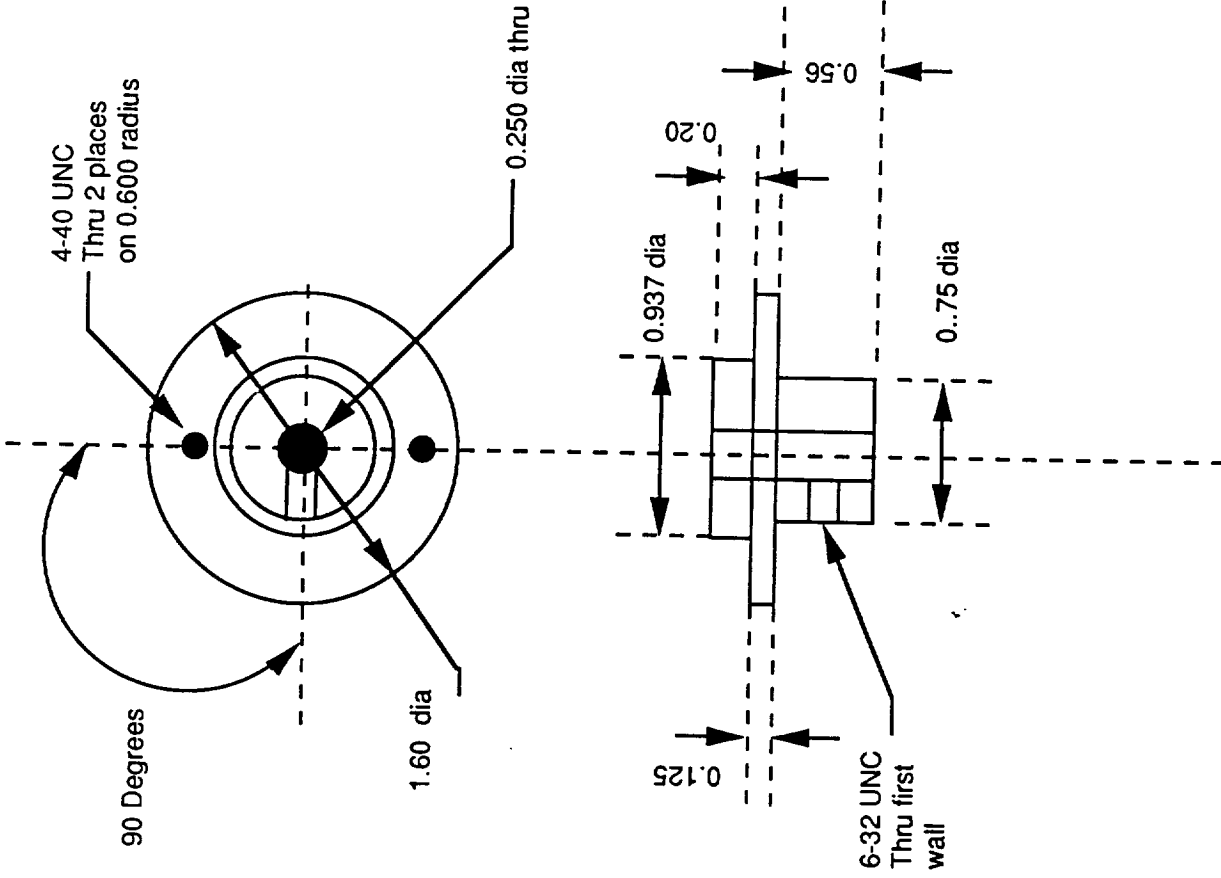
Optical path distances for air are shown in plain font. Path distances with 7mm of optical elements with refractive index=1.52 is shown in italics.

With 0.25 (6.3 mm) thick back focus tube locking ring.

SCALE	DATE	ENGINEER
		L. TRIPP
TITLE		
Optical Path		



SCALE	DATE	ENGINEER	TITLE
	5/14/90	L. TRIPP	
			FILTER WHEEL



Black anodized aluminum		SCALE	DATE 6/8/90	ENGINEER L. TRIPP	TITLE FILTER WHEEL HUB



and check on the bisector and near the intersection for a local extremum. If we found an extremum, we would feel even more confident in constructing the corner. Moreover, it might turn out that the distance of the extremum to the intersection may provide information about the intensities around the corner. If Odetics is going to pursue a geometric form of reconstruction, it would be worthwhile to have someone investigate this proposition on the extrema and the bisector.

## 1.6 One-dimensional response

Figure 1.1 is the IDS response to a step input. To reconstruct a step of ratios, we could find the one-crossing, determine the ratio of the two sides from the peak height, and create a step whose two sides are in the desired ratio and whose jump occurs right at the one crossing.

Now imagine that to the right of the step in the input there is another step. If the two steps are far enough apart, the output will just be two step responses that are separated by a large distance. However, if the steps are close to each other, the output changes. The trough from the output to the step on the right merges with the peak from the output to the step on the left and decreases its height. If we were to calculate the ratio of the two sides of the step on the left, the answer would not be correct because the peak height would be smaller than it should be. If the step on the right were a step down in intensity, the left side of its output would be a peak. If the two steps were close enough, the two peaks would merge and the peak in the output of the left step would be higher than it should be. The ratio of reflectances calculated from this peak would not be correct. We call this change in output heights due to steps that are too close together

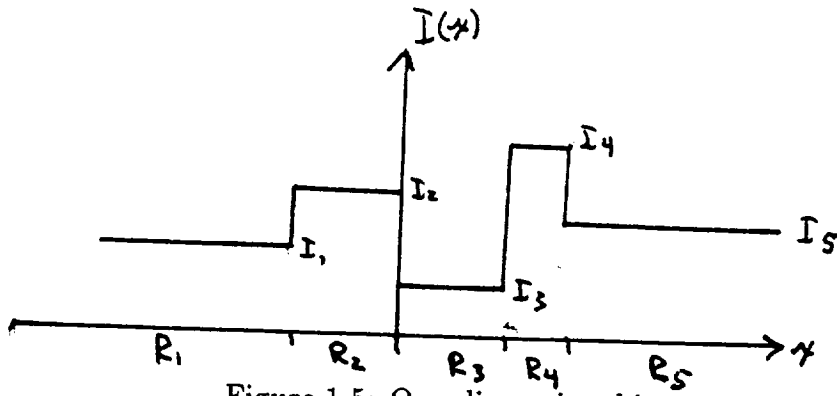


Figure 1.5: One-dimensional input

the *interference effect*.

In this section, I will state, prove and discuss a theorem about the IDS response to certain one-dimensional patterns. I haven't found the result to be helpful in actually leading to a reconstruction of the IDS input. Rather, it illuminates and quantifies the problem of interference in IDS reconstruction.

The theorem holds only for one-dimensional patterns and for inputs that consist solely of regions of uniform intensity. On the computer, this latter restriction is not important because of the approximation in Section 1.2. However, the former restriction is quite severe. Although patterns will in general not be one-dimensional, this theorem illustrates the problems with reconstruction in the simplest case. Interference only gets worse in two dimensions.

Actually, the theorem may have some immediate practical use. The current technique for reconstruction at Odetics involves only one-dimensional scans of the output. Thus as far as that method is valid, the theorem may also be valid and applicable.

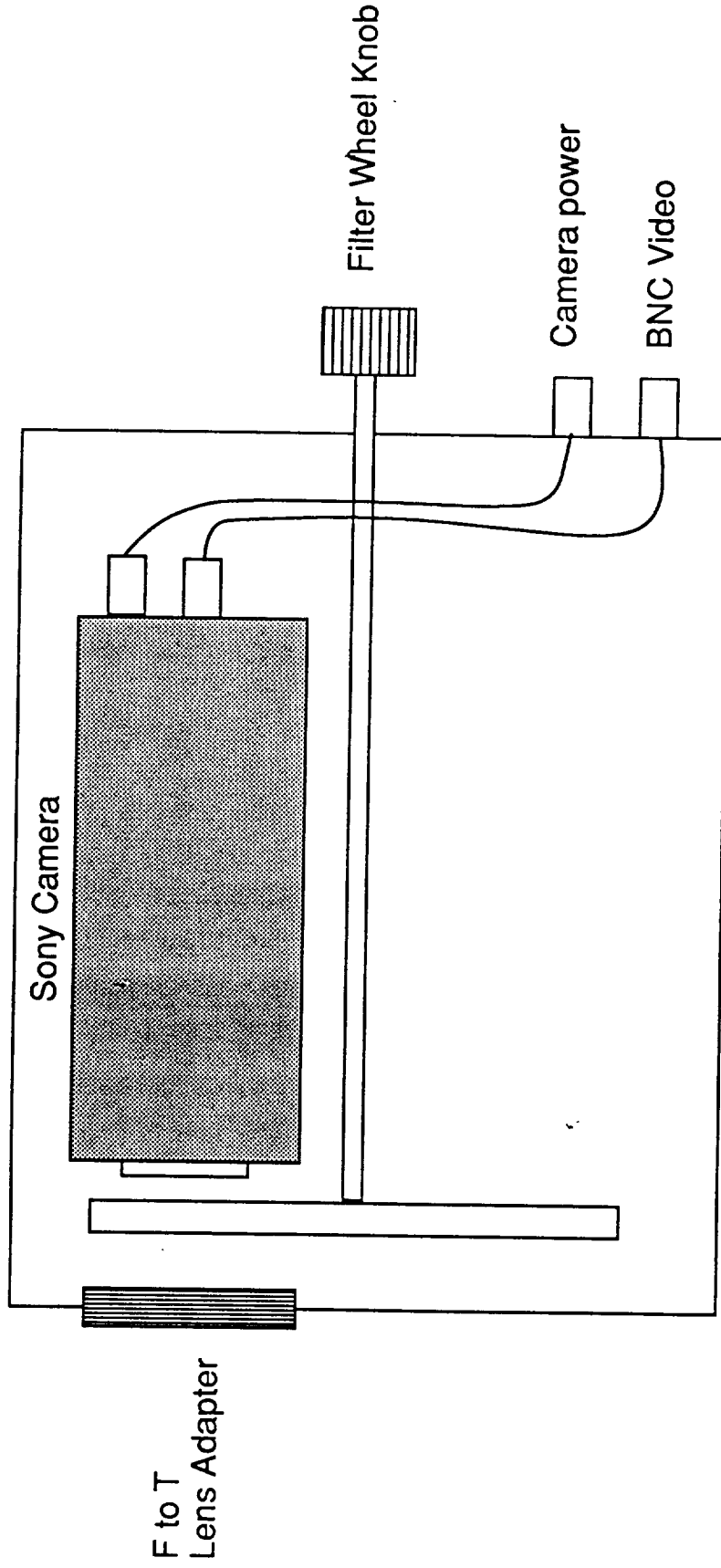
**Theorem 1** *Suppose the input varies only in one dimension and is composed solely of regions of uniform intensity. Let there be  $N$  regions and thus  $N - 1$  jumps or changes in intensity. Then the IDS output  $O(x)$  to the input is given by*

$$O(x) = \sum_{i=1}^{N-1} [O_i(x) - 1] + 1 \quad (1.9)$$

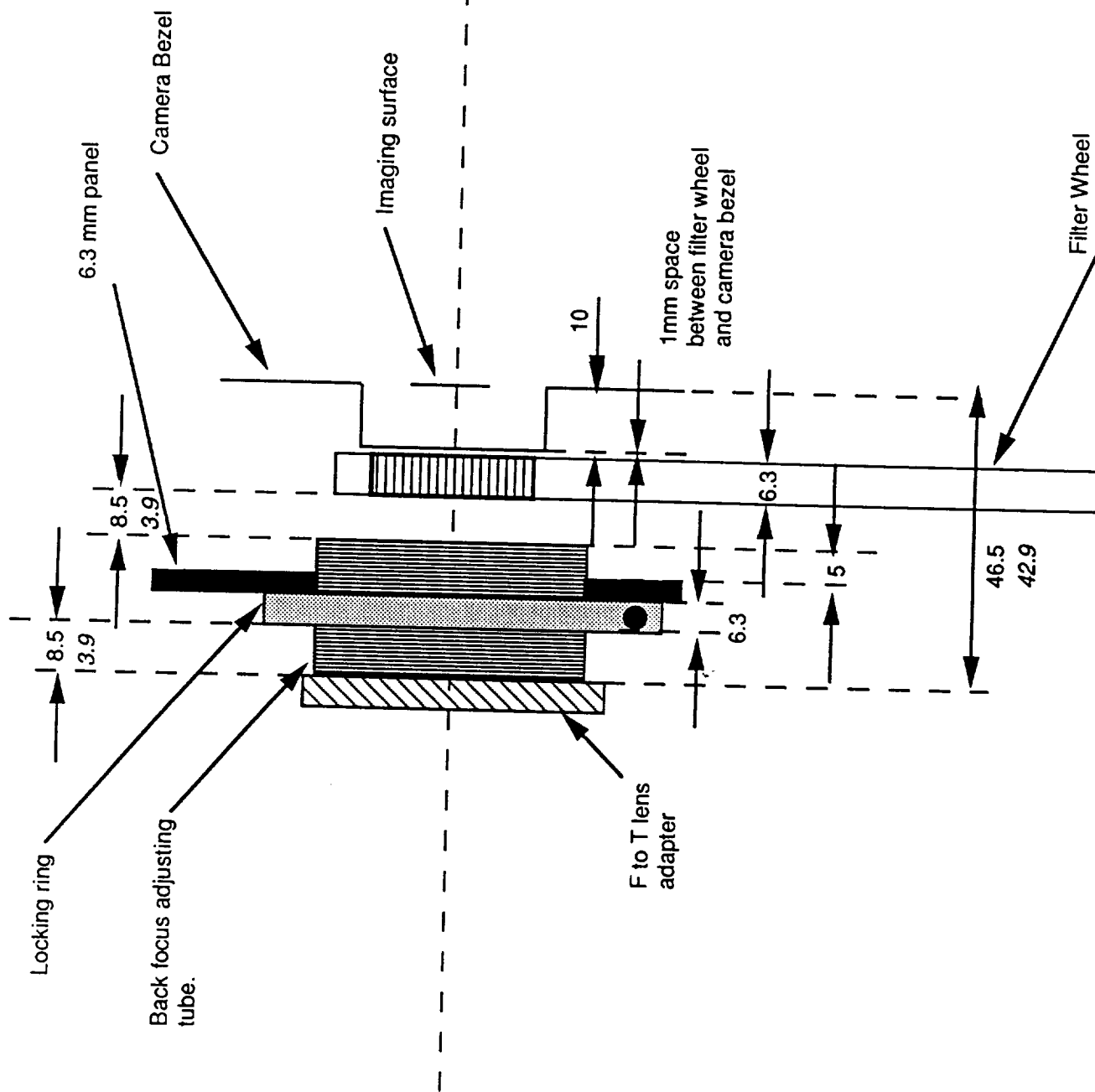
# Bibliography

- [1] Tom N. Cornsweet and John I. Yellott, Jr. Intensity-dependent spatial summation. *Journal of the Optical Society of America A*, 2:1769-1786, 1985.
- [2] Gregory Joel Reese. *Analysis and Application of Intensity-Dependent Spread Functions*. PhD thesis, University of California, Irvine, 1989.

**MULTISPECTRAL CAMERA DESIGN USING A SONY XC-77 CAMERA**



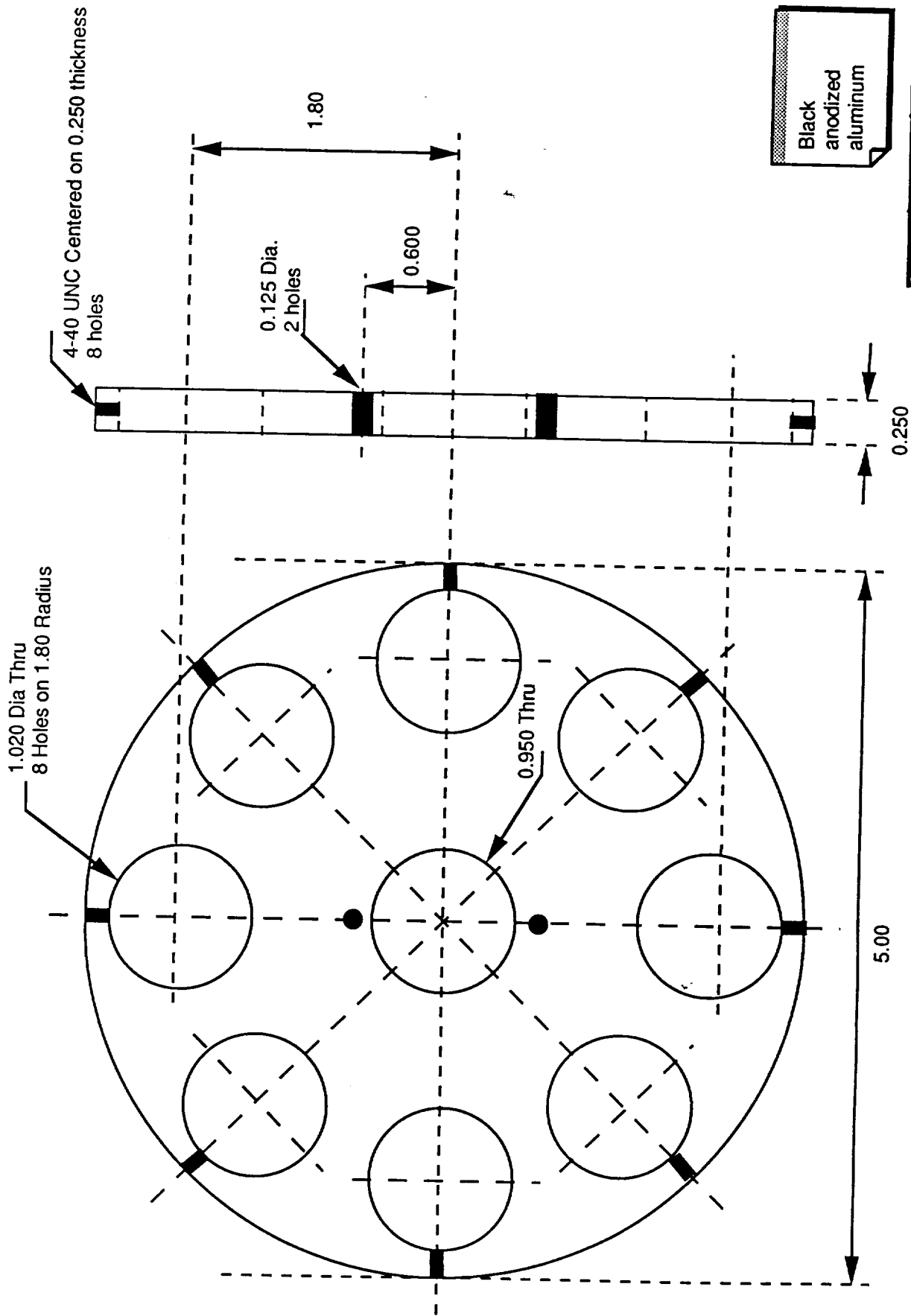
SCALE none	DATE 5/24/90	ENGINEER L. TRIPP
TITLE PLAN VIEW		



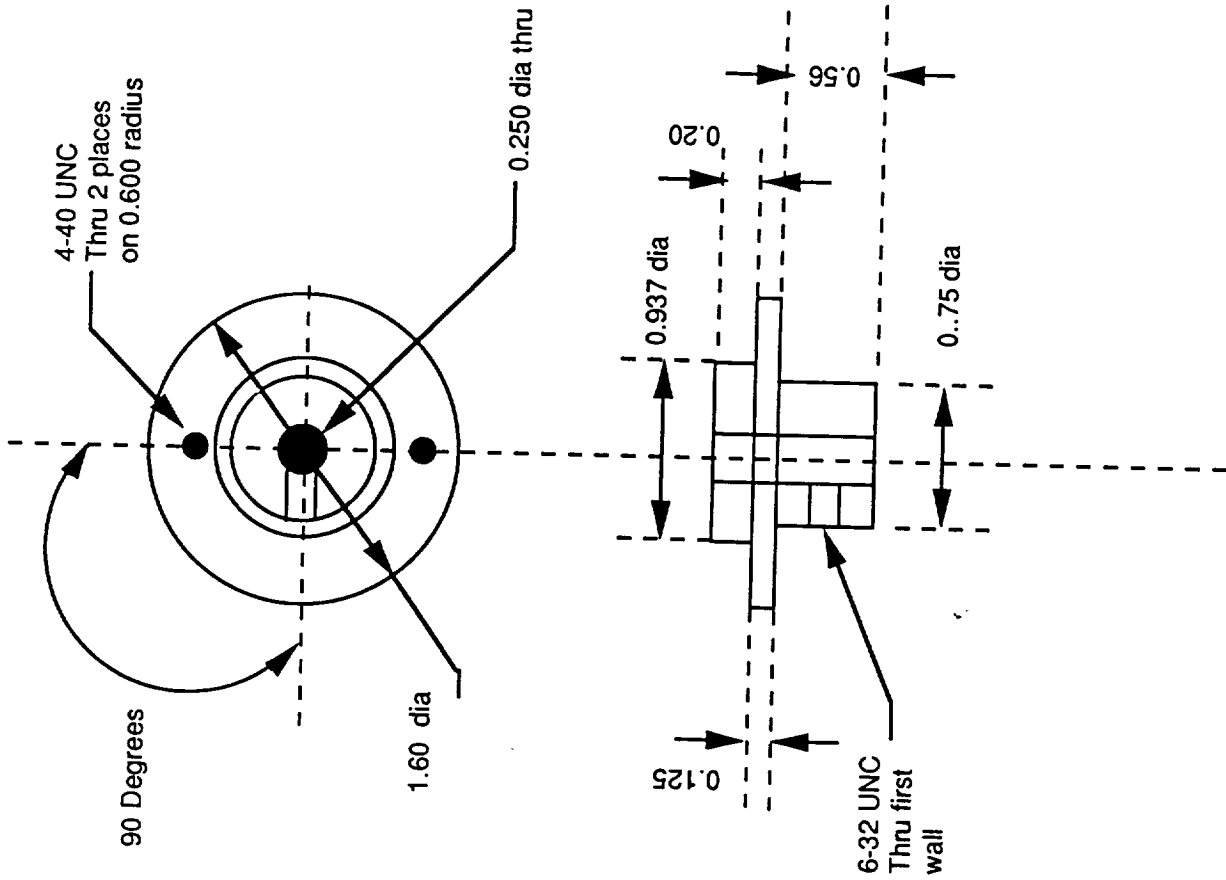
Optical path distances for air are shown in plain font. Path distances with 7mm of optical elements with refractive index=1.52 is shown in italics.

With 0.25 (6.3 mm) thick back focus tube locking ring.

SCALE	DATE	ENGINEER L. TRIPP
TITLE Optical Path		



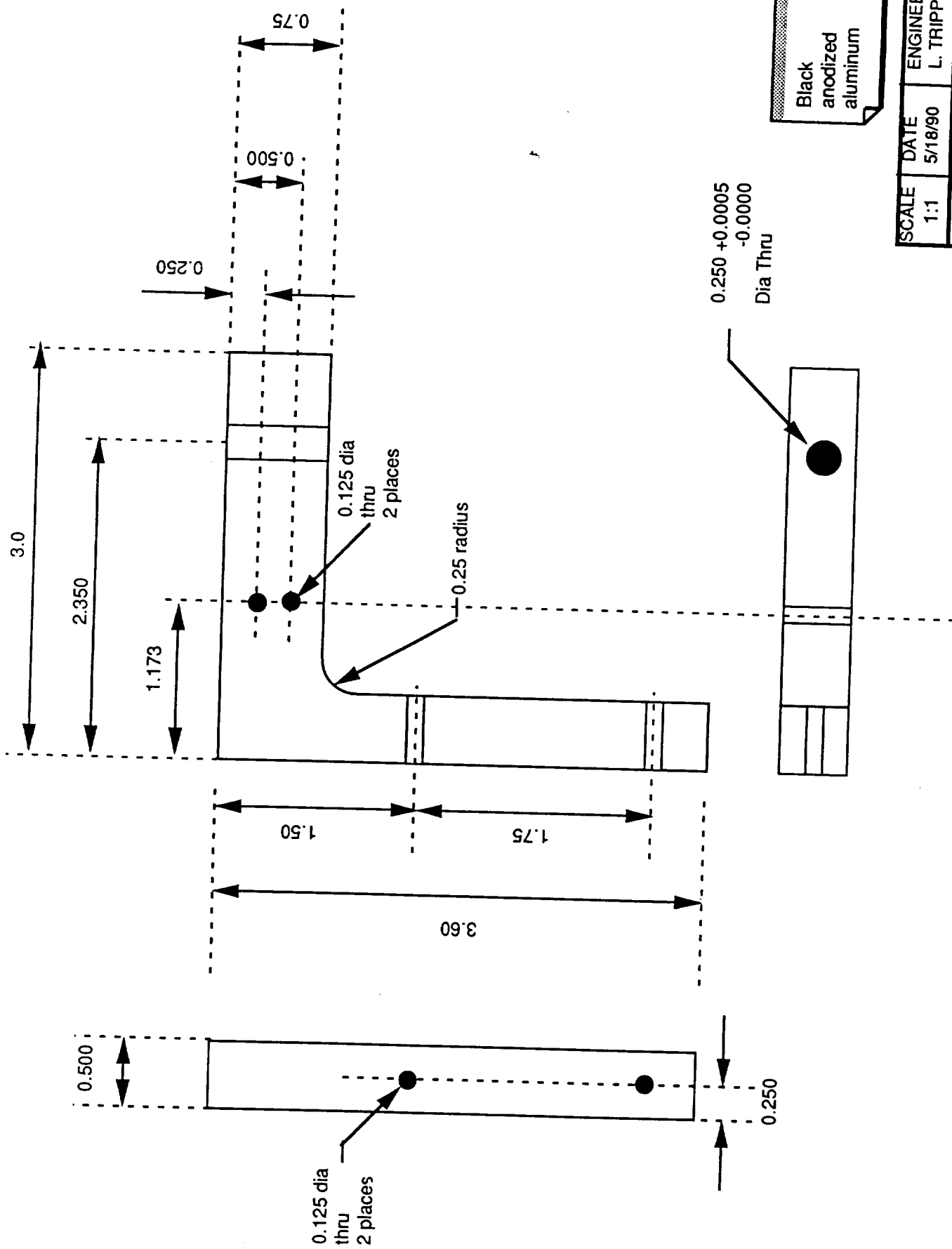
SCALE	DATE	ENGINEER	TITLE
	5/14/90	L. TRIPP	
FILTER WHEEL			



Black  
anodized  
aluminum

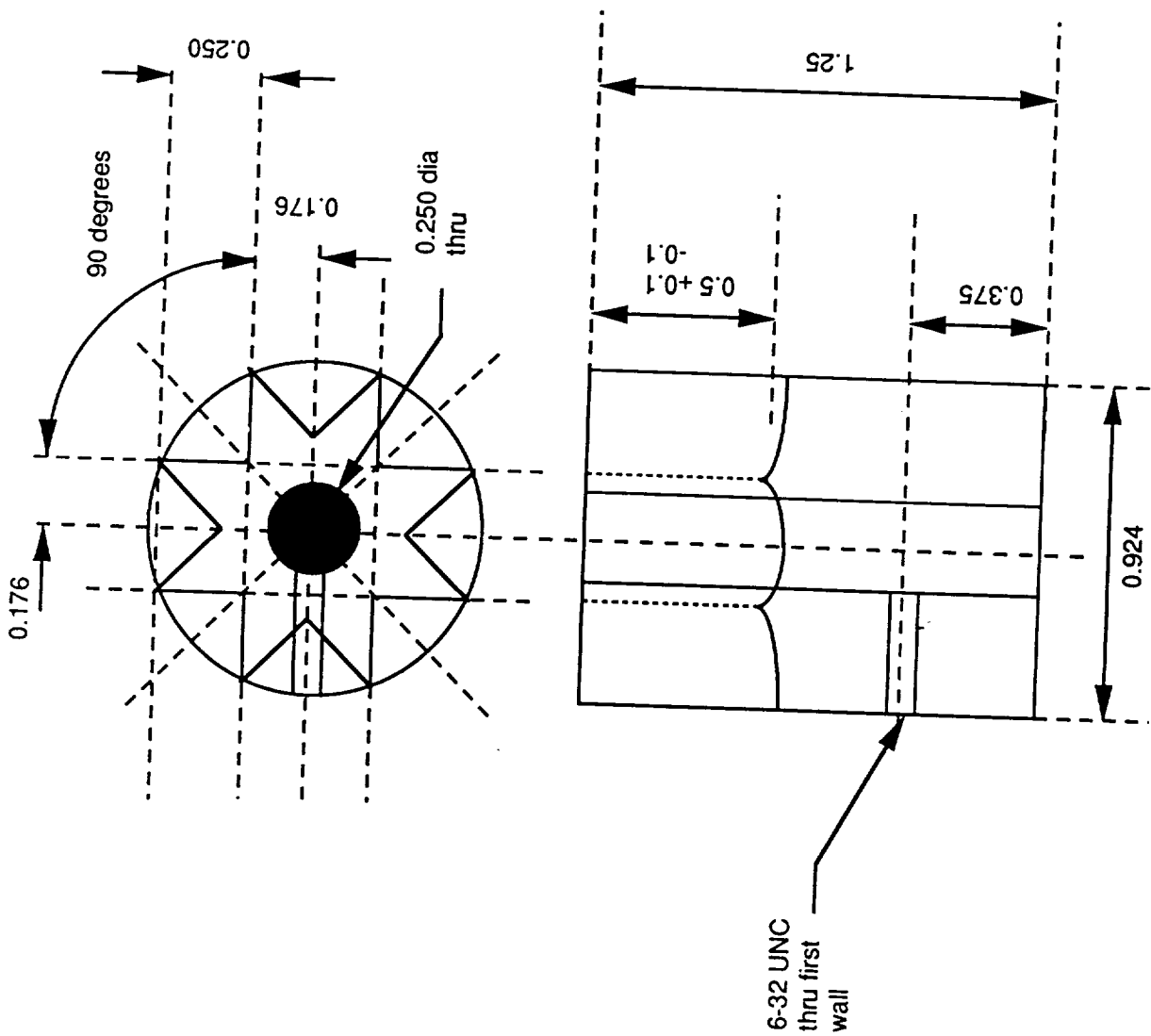
SCALE	DATE	ENGINEER	TITLE
	6/8/90	L. TRIPP	
			FILTER WHEEL HUB





Black  
anodized  
aluminum

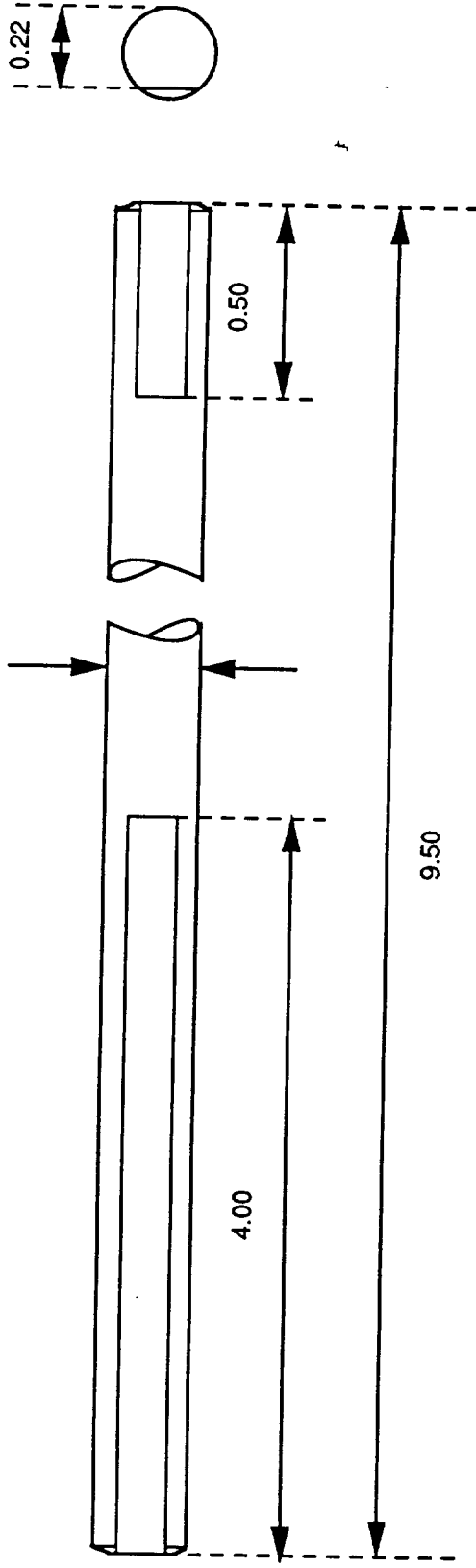
SCALE	DATE	ENGINEER	TITLE
1:1	5/18/90	L. TRIPP	FILTER WHEEL BRACKET



Mild steel

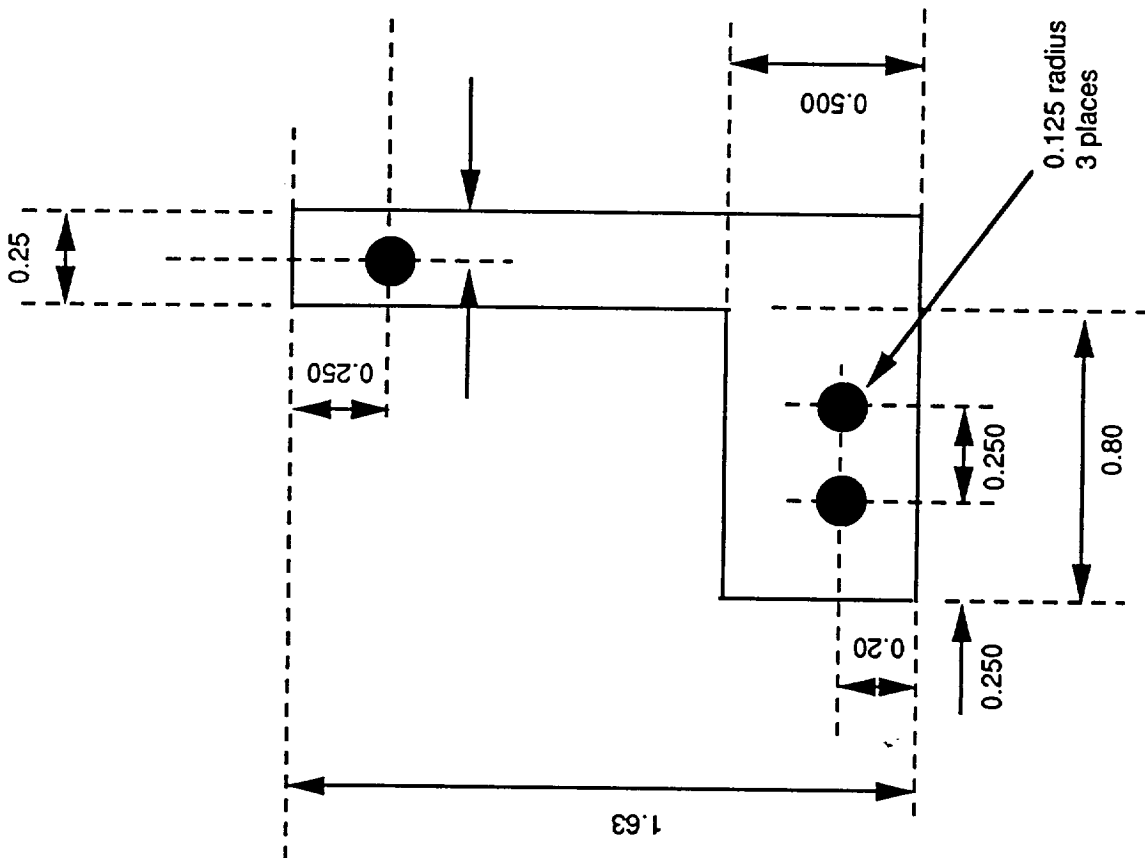
SCALE	DATE	ENGINEER
2:1	5/21/90	L. TRIPP
TITLE		
FILTER INDEX RING		

0.249 dia +0.0000  
-0.0005



Mild steel

SCALE	DATE	ENGINEER
2:1	6/8/90	L. TRIPP
TITLE		
FILTER WHEEL SHAFT		



MAKE TWO PIECES

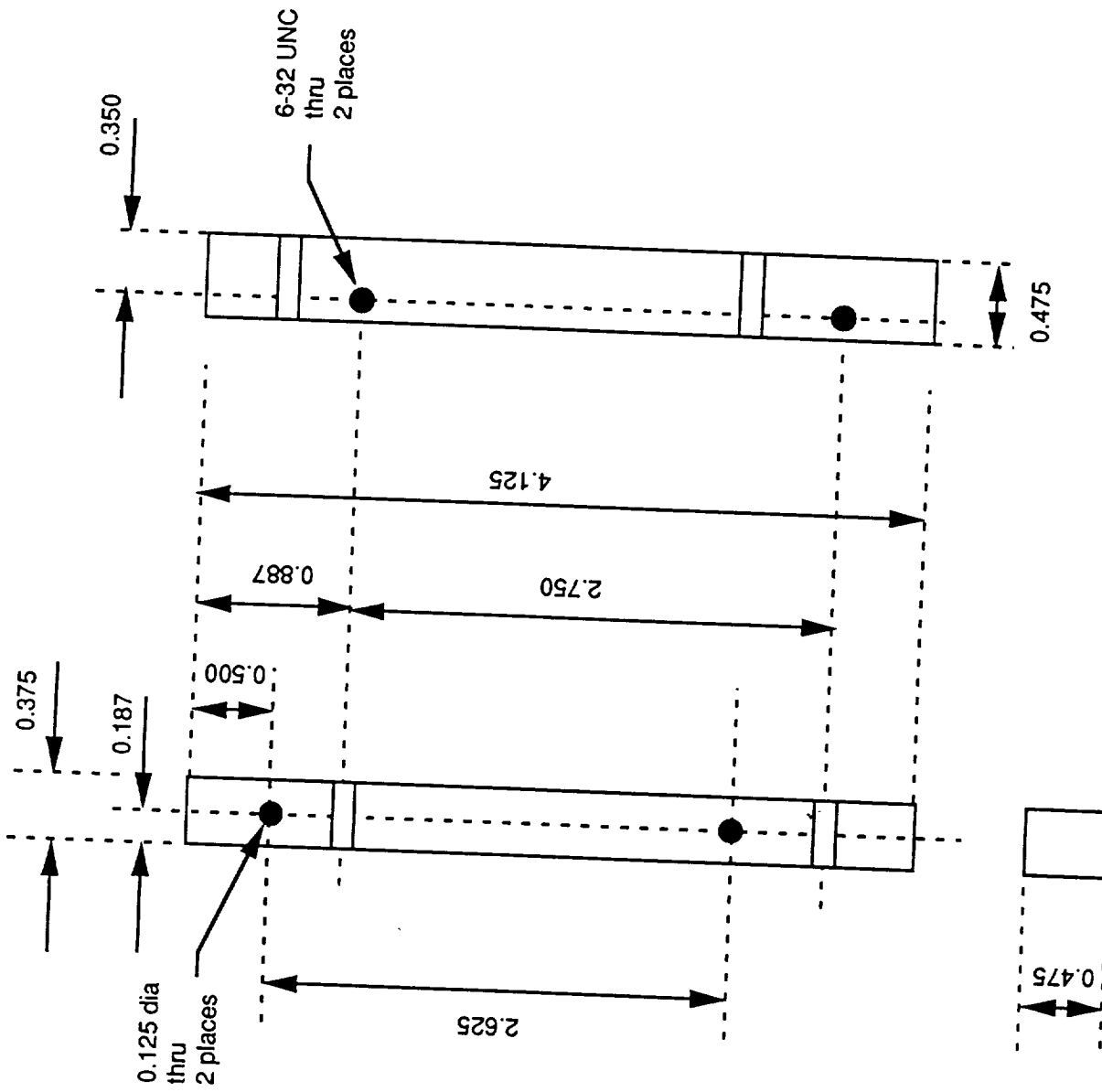
1. 0.02/0.03 Hard spring steel

2. 0.02/0.03 Stainless steel

SCALE	DATE	ENGINEER
2:1	6/890	L. TRIPP

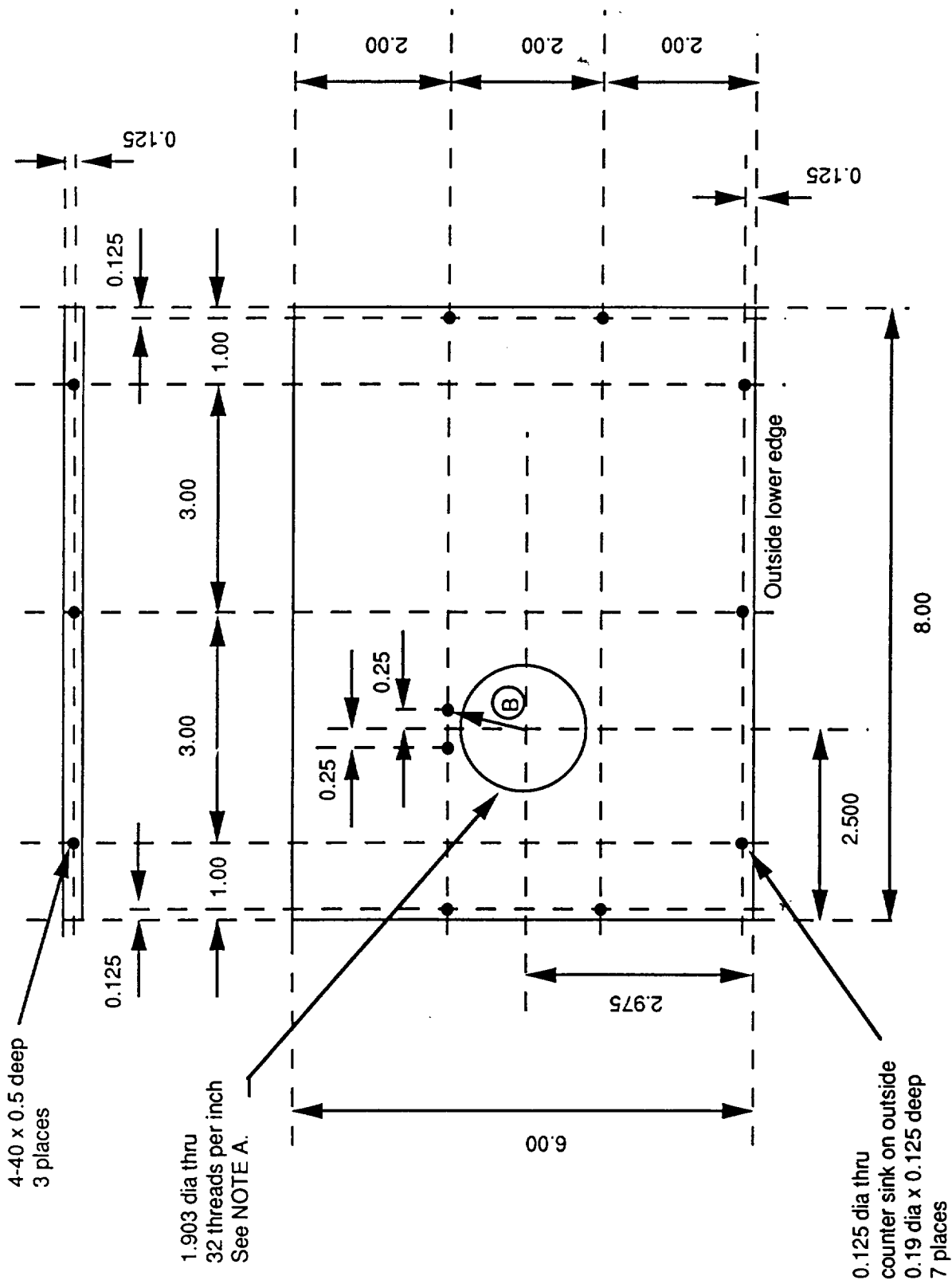
TITLE
ALT FILTER INDEX SPRING





Black  
anodized  
aluminum

SCALE 1:1	DATE 5/18/90	ENGINEER L. TRIPP
TITLE CAMERA MOUNTING BKT		



SCALE	DATE	ENGINEER
1:2	5/22/90	L. TRIPP
TITLE		
ALT		
FRONT PANEL		

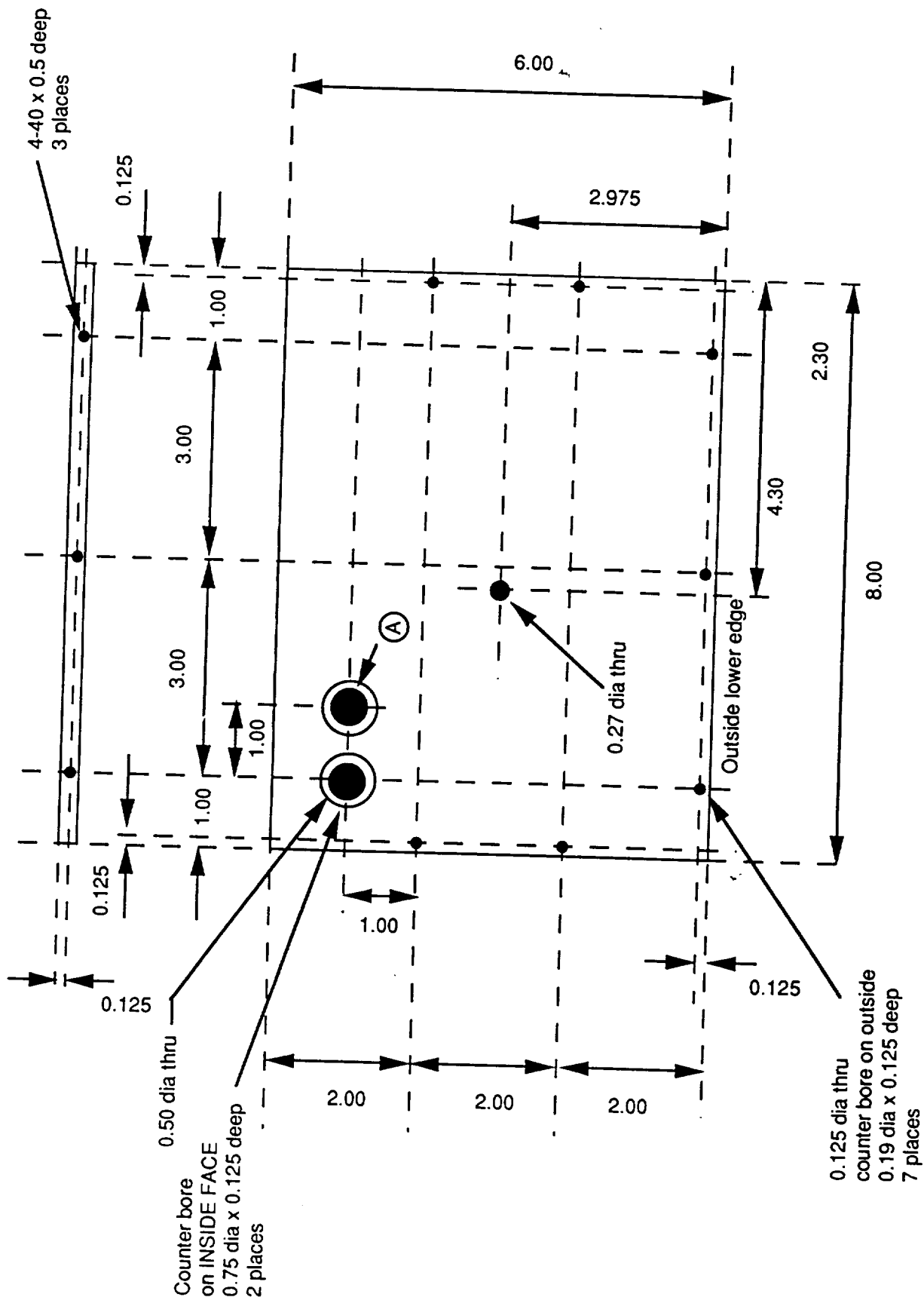
Black anodized aluminum  
0.25 thick

Diameter and thread pitch must match back focus tube OD and threads.

(A)

4-40 thru 1.062 radius 2 places

(B)

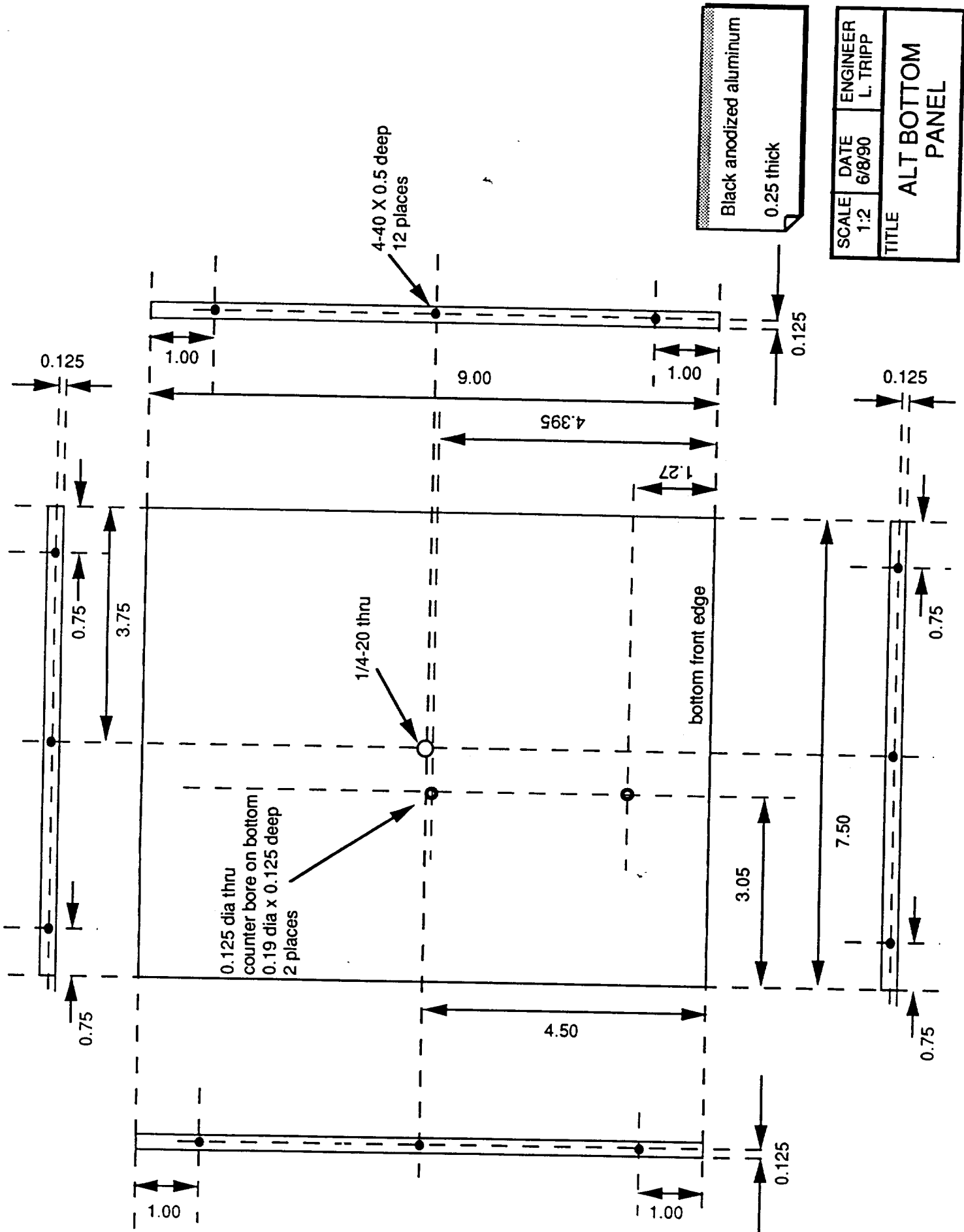


SCALE 1:2	DATE 6/8/90	ENGINEER L. TRIPP
TITLE ALT BACK PANEL		

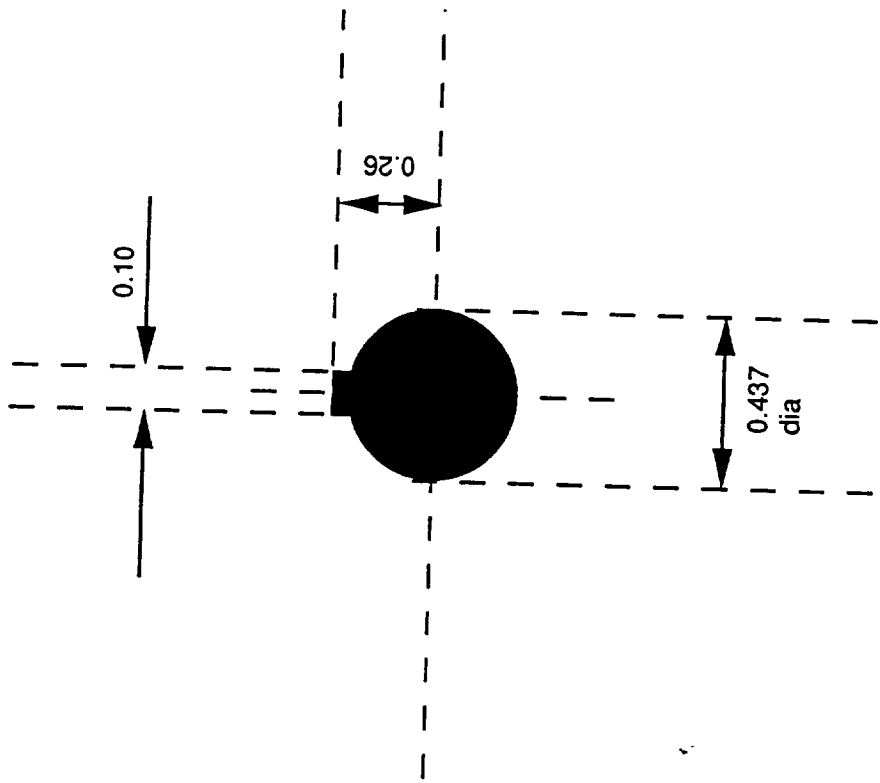
Black anodized aluminum  
0.25 thick

A See Hirose connector detail

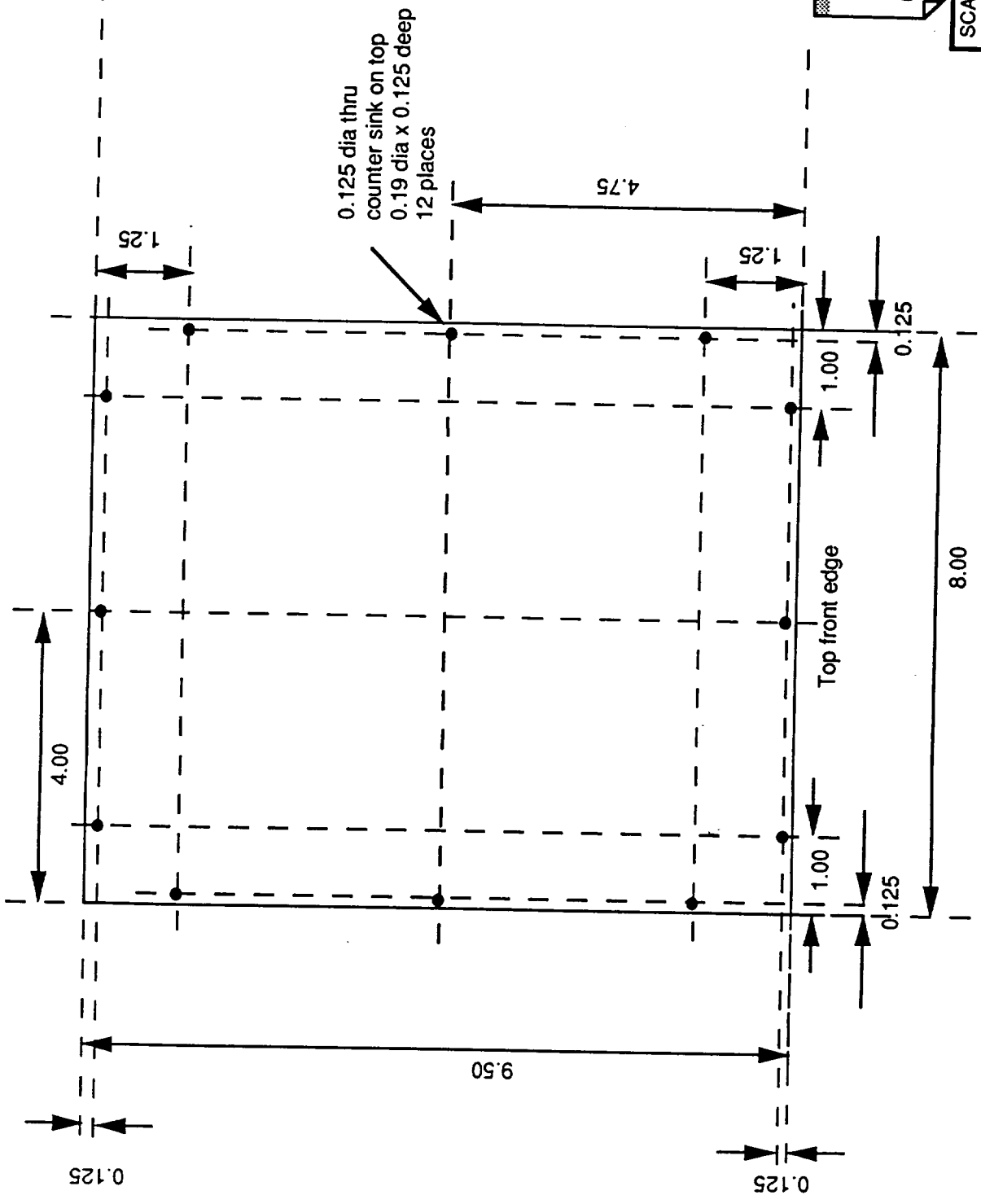




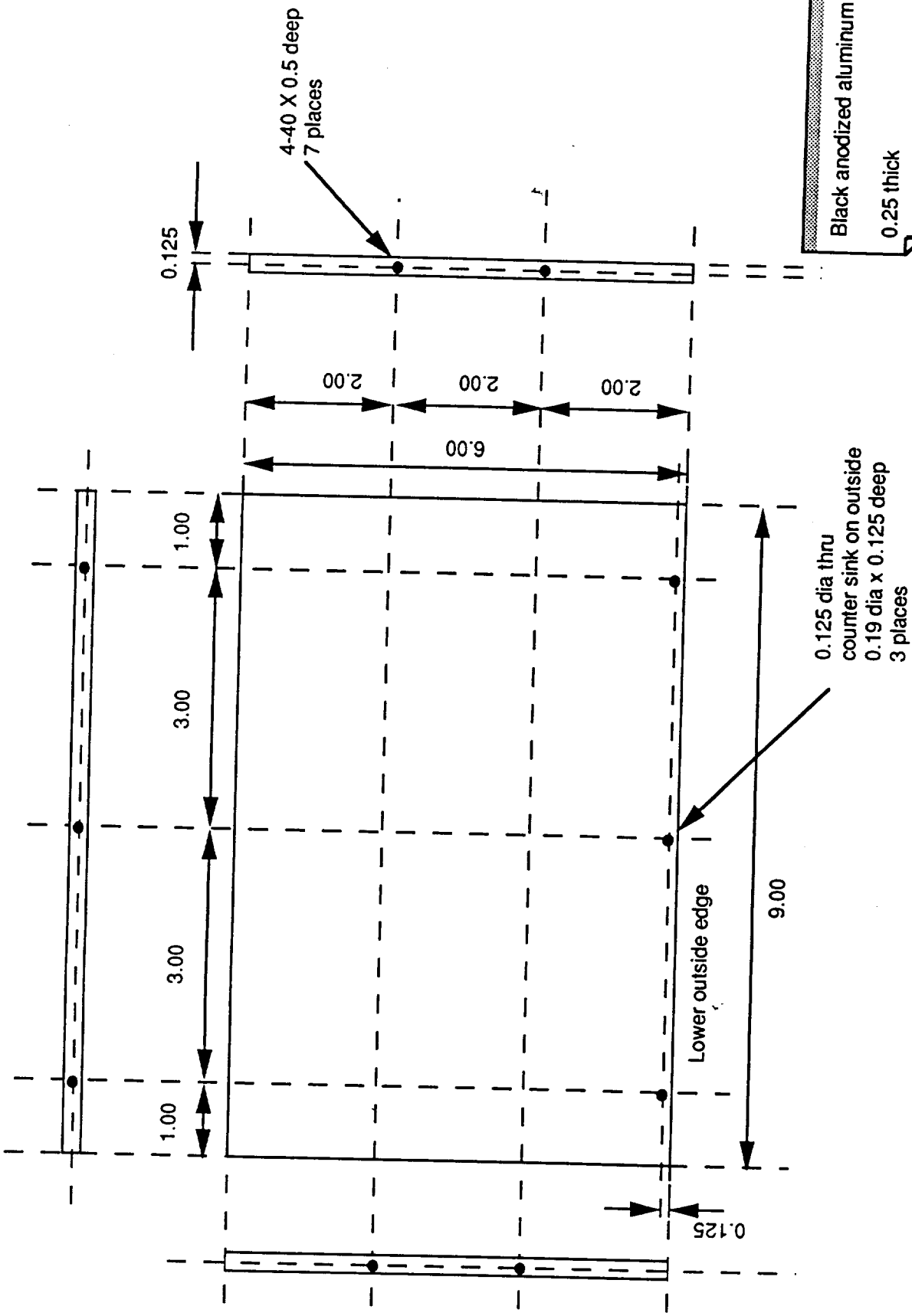
SCALE	DATE	ENGINEER	TITLE
1:2	6/8/90	L. TRIPP	
			ALT BOTTOM PANEL



SCALE 2:1	DATE 5/22/90	ENGINEER L. TRIPP
TITLE HIROSE CONNECTOR DETAIL		

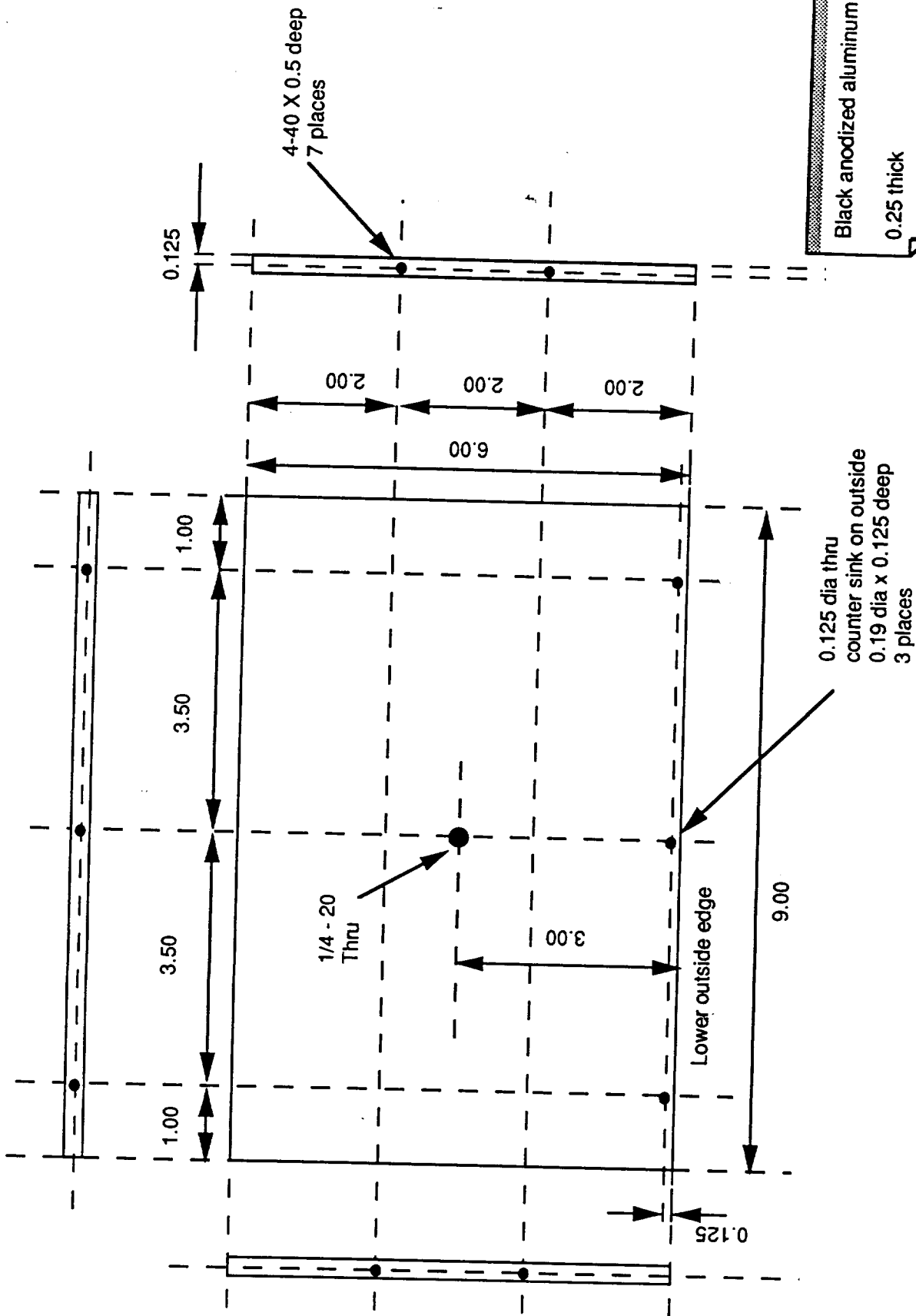


Black anodized aluminum		ENGINEER L. TRIPP		TOP PANEL
0.25 thick		DATE 5/22/90		
SCALE 1:2				
TITLE				

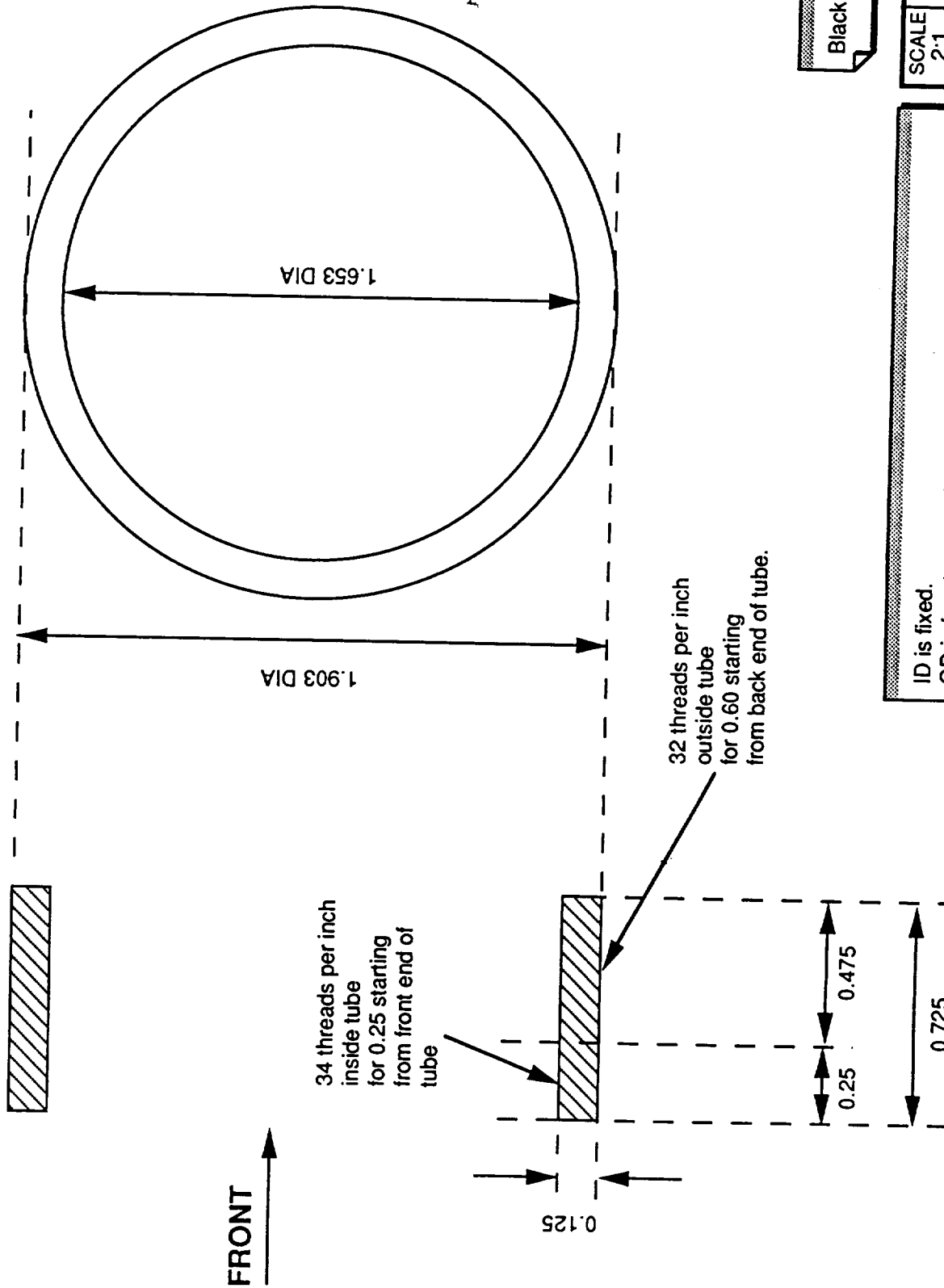


SCALE 1:2	DATE 5/22/90	ENGINEER L. TRIPP
TITLE  SIDE PANEL		

Make two side panels.



SCALE	DATE	ENGINEER	TITLE
1:2	6/8/90	L. TRIPP	
RIGHT SIDE PANEL			



Black anodized aluminum

SCALE	DATE	ENGINEER
2:1	6/12/90	L. TRIPP
TITLE		
BACK FOCUS TUBE		

ID is fixed.  
 OD is free to set as long as it mates with the hole in the ALT FRONT PANEL, and fits in the locking ring.  
 OD=1.903 was chosen to give a wall thickness of 0.125



**THE DETAILED SPECIFICATIONS OF THE SONY XC-77 CAMERA**



**SONY.**

CCD B/W VIDEO CAMERA MODULE

**XC-77/77CE**

JUNCTION BOX

**JB-77**

STANDARD LENS

**VCL-16Y-M**

TRIPOD ATTACHMENT

**VCT-37**

4-PIN M CONNECTOR

**PC-XC04**

12-PIN F CONNECTOR

**PC-XC12**

CAMERA CABLE

**CCXC-12P02/12P05**

**CCXC-12P10/12P25**



**SERVICE MANUAL**

**XCM-77/77CE**

# TABLE OF CONTENTS

1. OPERATION.....	1-1 (E)
1-1. Features .....	1-1 (E)
1-2. Composition .....	1-2 (E)
1-3. Parts location, function and operation.....	1-3 (E)
1-3-1. XC-77/77CE CCD video camera module...	1-3 (E)
1-3-2. VCT-37 tripod attachment.....	1-5 (E)
1-3-3. JB-77 junction box .....	1-6 (E)
1-4. Connections.....	1-8 (E)
1-4-1. When junction box is used.....	1-8 (E)
1-4-2. When junction box is not used .....	1-9 (E)
1-5. Initialization of the mode.....	1-10 (E)
1-6. Precautions.....	1-10 (E)
1-7. Special characteristics of a CCD .....	1-11 (E)

# SECTION 1 OPERATION

## 1-1. FEATURES

The XC-7777CE is a monochrome video camera module which uses a solid state image sensor — the CCD (Charge Coupled Device).

### High quality image

High quality, fine image is made possible by a large number of picture elements, as much as 768x493 for XC-77 and 753x581 for XC-77CE.

The XC-77CE's picture elements are equally arrayed in vertical and horizontal directions, and allow easy addressing. This makes XC-77CE most suitable for image processing systems which require highly accurate addressing.

### Adaptability to diversified signal processing

Gain can be internally selected either the AGC (Automatic Gain Control) or Fixed, and the  $\gamma$  (gamma) can be set either to the compensation mode or to the fixed (1) mode.

The accumulation mode of the electrical charge can be internally changed from the frame accumulation to the field accumulation. This enables the non-interlace mode sensitivity to be elevated up to the equivalent level to the sensitivity of the interlace mode by entering signals into the external sync input for the setting of the non-interlace mode.

### Three types of external sync signals

Synchronization with other cameras is possible by entering the three types of signals from the external sync signal generator. The capture range is set as wide as  $\pm 1\%$  of the horizontal frequency.

HD, VD signals: external synchronization is applied in accordance with the system, either the interlace or non-interlace system, which is automatically identified by the HD, VD signals.

VBS (Video, Burst, Sync) signal: the camera module is synchronized with the VBS signal (BB signal or composite sync signal.) (The sync system, whether by HD/VD signal or VBS signal, is automatically selected depending on the input signal.)

Reset pulse: this is used to set the timing for the read-out of register contents at an arbitrary moment.

### Internal sync signal output

Clock signals are constantly output. HD signal and field index signal can be output to the 12P connector by altering the internal wiring.

### Solid body

The body consists of aluminum diecast and steel sheet. On the bottom are 2 screw holes (reference holes) which can be used to keep deviation of the optical axis at a minimum.

### Compatibility with XC-37 series

XC-7777CE has common types of VIDEO OUT connector and 12-pin multi-connector pin assignment with the XC-37 series, as well as having identical cross section external dimensions, and can replace the XC-37 series camera module.

### Long life and high stability

### Precise image geometry

### Low lag and little image sticking

### High resistance to vibration and mechanical shock

### Quick start-up

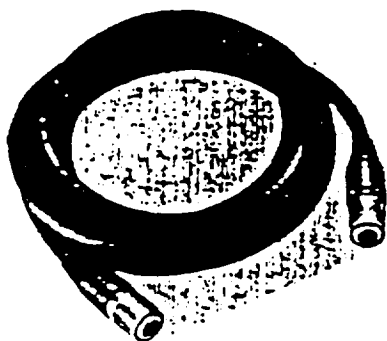
### Shooting in a strong magnetic field

### Low power consumption (2.2W)

## 1-2. COMPOSITION

The CCD video camera module system consists of the following optional products which can be purchased separately.

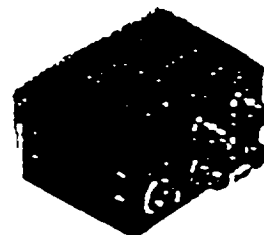
Camera cables  
CCXC-12P02 (2m)  
CCXC-12P05 (5m)  
CCXC-12P10 (10m)  
CCXC-12P25 (25m)



XC-7777CE CCD video camera module



JB-77 junction box



VCL-16Y-M standard lens



PC-XC12 12-pin connector



VCT-37 tripod attachment



PC-XC04 4-pin connector

**XC-7777CE CCD video camera module**

**VCL-16Y-M standard lens**

This is a standard lens of  $f = 16 \text{ mm}$ ,  $F1.4$ . The iris and focus are adjusted manually.

**JB-77 Junction box**

This is attached to the camera module using the CCXC-12P02/12P05/12P10/12P25 camera cable and will supply power, transmit video signals, and exchange external sync signals.

**PC-XC04 4-pin connector**

This is used to attach the lens cord of the auto iris lens to the LENS connector on the XC-7777CE video camera module.

**PC-XC12 12-pin connector**

This connector is prepared for system-up, and used to connect to the DC IN/SYNC connector of the camera module.

**VCT-37 tripod attachment**

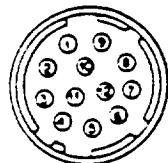
To attach the video camera module to a tripod, use this tripod attachment.

**CCXC-12P02 (2m), 12P05 (5m), 12P10 (10m) and 12P25 (25m) camera cables**

These cables can be attached to the 12-pin DC IN/SYNC connector on the rear of the camera module to supply power, transmit video signals and exchange sync signals.

**② DC IN/SYNC (DC power input/sync) connector (12-pin)**  
Connect a CCXC-12P02, CCXC-12P05, CCXC-12P10 or CCXC-12P25 camera cable to this connector to supply power (12 V DC) from an external power source and output the video signal from the video camera module. When a sync signal generator is connected to supply the sync signal (VBS, VS, BS or HD/VD), the camera module can be operated on external sync signals.

The pin configuration of this connector is shown in the diagram below.



Signal Pin No.	External Sync mode			Camera Sync output
	HD, VD	VBS/VS	RESTART RESET	
1	Ground	Ground	Ground	Ground
2	+ 12 V	+ 12 V	+ 12 V	+ 12 V
3	Video output (ground)	Video output (ground)	Video output (ground)	Video output (ground)
4	Video output (signal)	Video output (signal)	Video output (signal)	Video output (signal)
5	HD Input (ground)	—	HD Input (ground)	HD output (ground)
6	HD Input (signal)	—	HD Input (signal)	HD output* (signal)
7	VD Input (signal)	VBS Input (signal)	RESET PULSE (signal)	FIELD INDEX* output (signal)
8	—	—	—	CLOCK output (ground)
9	—	—	—	CLOCK output (signal)
10	Ground	Ground	—	Ground
11	+ 12 V	+ 12 V	—	+ 12 V
12	VD input (ground)	VBS input (ground)	RESET PULSE (ground)	FIELD INDEX output (ground)

\*It is necessary to modify connections of the circuits inside the camera in order to output the HD and FIELD INDEX signals.

**③ VIDEO OUT (output) connector (BNC connector)**

The video signal from the video camera module is output from this connector. This connector can be used only when a CCXC-12P02 camera cable is connected to the DC IN/SYNC connector and the video output of the 12-pin connector of the CCXC-12P02 cable is not terminated with 75 ohms.

### 1-3-3. JB-77 JUNCTION BOX

Front



#### ① Pilot Lamp

Lights up when 12 V DC is input.

#### ② CAMERA connector (12-pin)

Connect a CCXC-12P02/12P05/12P10 or CCXC-12P25 camera cable to this connector to supply power (12 V DC) from an external power source and external sync signals from an external sync system and input the video signal from the video camera module.

#### VIDEO OUT (output) connector (BNC connector)

The video signal from the video camera module is output from this connector when connected to a video monitor or VTR etc.

#### ③ CLOCK OUT (Internal sync signal output) connector

Clock signal is output through this connector for the independent use of the camera module.

#### ④ VD IN connector (BNC connector)

Connect the sync signal generator to input the VD signal or the VBS signal. This enables the camera module to be operated on external sync signals.

- When receiving VD signals, input HD signals to the HD connector.
- When receiving VBS signals, do not input HD signals to the HD connector.

For the independent use of the camera module, the field index signal (FLD, VD or composite sync signal) can be output by changing the camera's internal wiring.

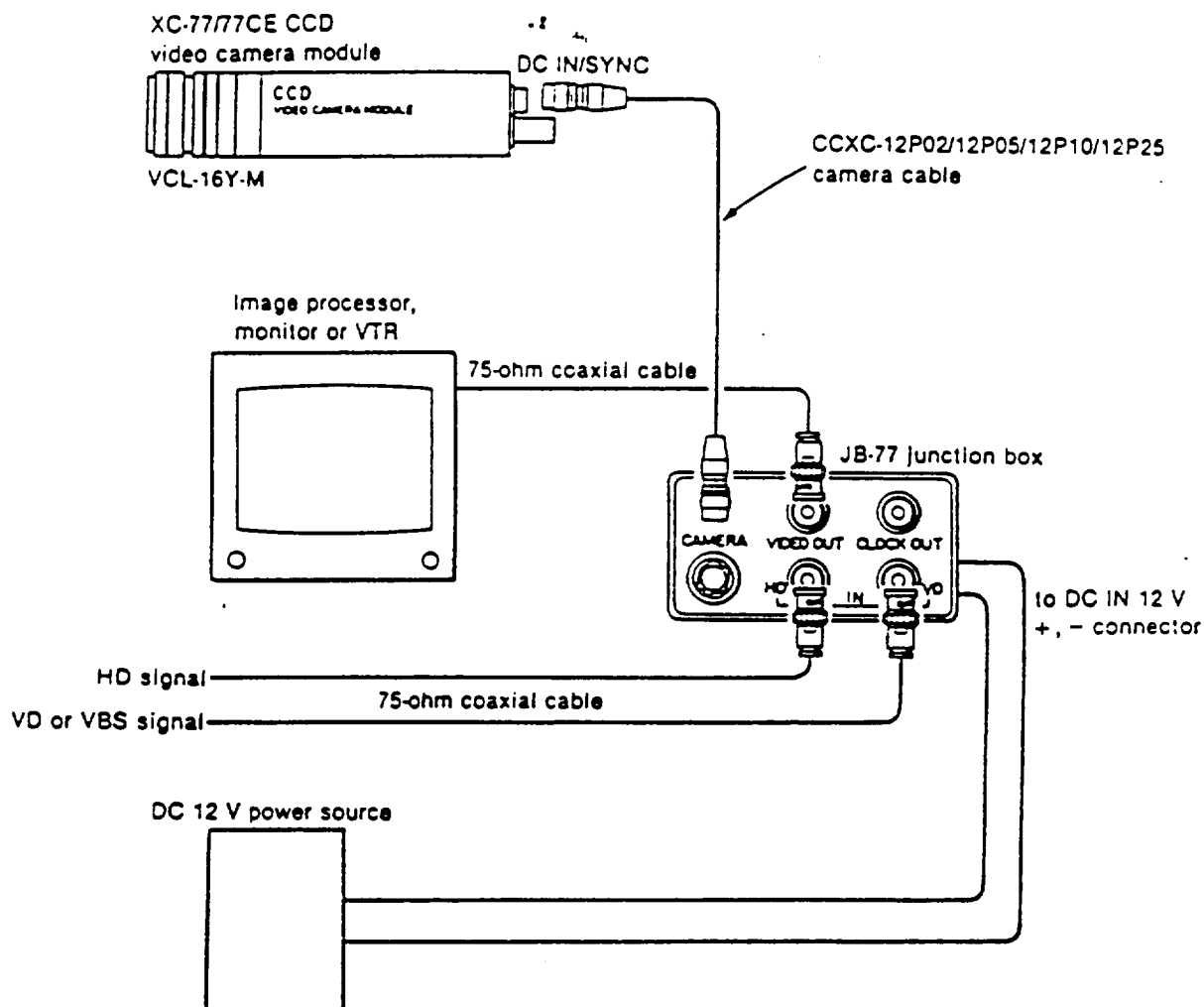
#### ⑤ HD IN connector

Connect the sync signal generator to input the HD signal. Combining it with the VD signal input from VD IN connector enables the camera module to be operated on external sync signals.

For the independent use of the camera module, the HD signal can be output by changing the camera's internal wiring.

## 1-4. CONNECTIONS

### 1-4-1. WHEN JUNCTION BOX IS USED



**Note**

When applying external sync by VBS or VB signal, the image may be affected by VBS signal during gen lock if a long type CCXC cable is used (especially CCXC-12P25). When this occurs use only BS or an S signals.

## 1-5. INITIALIZATION OF THE MODE

Modes for the following 8 items can be switched. At the time of delivery, each item is set to the upper mode in the list shown below.

Item	Mode	Remarks **
AGC	FIX GAIN	Gain fix
	AGC	Automatic gain control
$\gamma$	1	No $\gamma$ compensation
	compensate	$\gamma$ compensation
SUB	SUB1	Frame accumulation in use
	SUB2	Field accumulation in use
EIA/CCIR	EIA	ROM (EIA mode)
	CCIR	ROM (CCIR mode)
FRAME/ FIELD	FRAME	Frame accumulation
	FIELD	Field accumulation
FRAME	NORMAL	Normal scanning
	INVERSION	Inversion of even number field and odd number field
RESTART RESET	OFF	Frame not synchronizing
	ON	Frame synchronizing
EIA/CCIR	EIA	SG (EIA mode)
	CCIR	SG (CCIR mode)

### Note

EIA/CCIR mode settings vary depending on the CCD (EIA/CCIR).

## 1-6. PRECAUTIONS

### Power source

Operates on 12 V DC. Use a stable power source, free from ripples or noise.

### Foreign objects

Do not spill any liquid, drop any inflammable or metal objects inside. This could result in fire, electrification, malfunction or accident.

Do not wrap in cloth while in operation

### Locations for operation and storage

Avoid operating or storing in the following places.

- An extremely hot or cold location.  
Operating temperature: 0°C to 40°C (32°F to 104°F)
- A location exposed to high humidity or dust.
- A location exposed to rain.
- A location subjected to strong vibrations.
- A location near a TV or radio station which radiates high powered radio frequencies.

### Care

Clean the dust on the surface of the lens and optical filter with a blower. Clean the exterior with a soft, dry cloth. If it becomes very dirty, clean with a cloth slightly moistened with a mild detergent solution. Do not use any type of solvent, such as alcohol or benzene, which may damage the finish.




# SECTION 2

## COMPREHENSIVE SPECIFICATIONS

### 2-1. SPECIFICATIONS

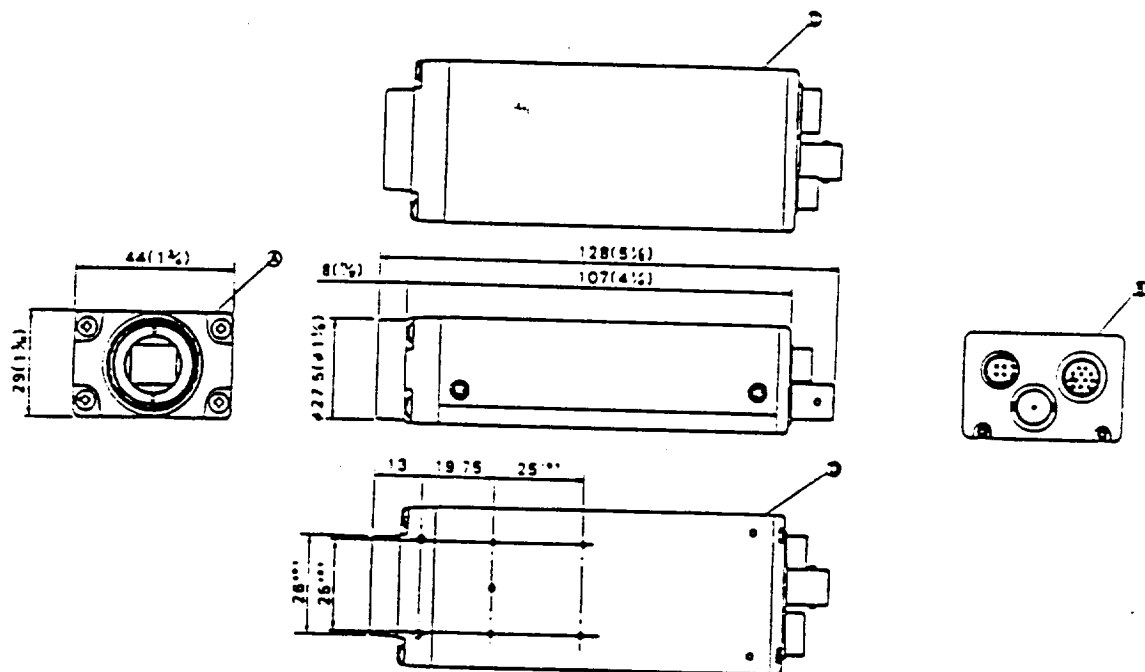
#### <CAMERA MODULE XC-77>

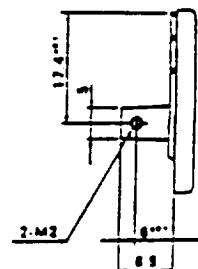
Pickup Device	Interline transfer CCD
Picture elements	768 (H) x 493 (V)
Sensing area	8.8 mm x 6.6 mm (the same as the 2/3-inch camera tube)
Optical black	22 pixels each horizontal line
Vertical drive frequency	15.734 kHz
Horizontal drive frequency	9.545 MHz
Signal system	EIA standard
Structure	Interline transfer
Cell size	17 $\mu$ m (H) x 13 $\mu$ m (V)
Chip size	10.0 mm (H) x 9.3 mm (V)
Optical System	
Lens mount	C mount
Flange back length	17.526 mm
Sync System	Internal/External automatic change
External sync input	VBS, VS, BS (SYNC LEVEL 0.3 Vp-p = 6 dB) = 1%
External sync frequency tolerance	Within $\pm$ 100 n sec
Jitter	Within 10 sec
Locking time when power is on.	2 : 1 Interlace : 525 lines
Scanning System	1.0 Vp-p sync negative, 75 ohms unbalanced.
Video Output	570  TV lines
Horizontal Resolution	2 : 1 Interlace : 485 lines
Vertical Effective lines	400 Luxes with F4 (y ON/odB)
Sensitivity	
Minimum Illumination	3 Luxes, F1.4 (without an infrared cut filter)
S/N ratio	50 dB
Power Requirement	DC 12 V
Power Voltage Tolerance	DC 10.5 V ~ 15 V
Power Consumption	2.2 W
Weight	
Camera module	190 g (XC-77)
Tripod attachment	15 g (VCT-37)
Camera cable (2 m)	130 g (CCXC-12P02)
(5 m)	295 g (CCXC-12P05)
(10 m)	560 g (CCXC-12P10)
(25 m)	1.4 Kg (CCXC-12P25)
Junction box	170 g (JB-77)
Storage Temperature	-30°C ~ +60°C
Operating Temperature	0°C ~ 40°C
Shock resistance	70 G
Storage Humidity	Within 90%
Operating Humidity	Within 70%

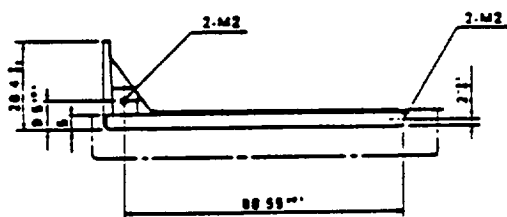
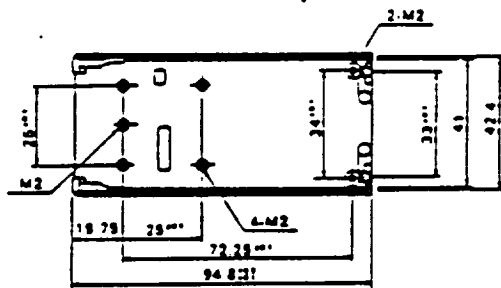
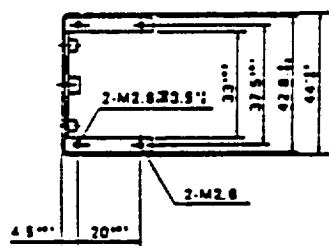
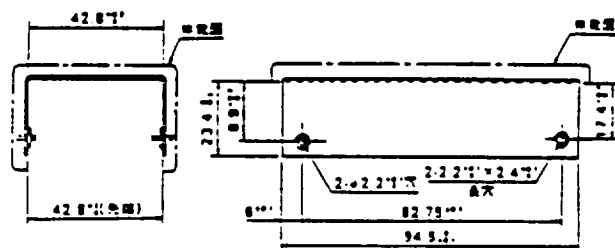
#### <STANDARD LENS VCL-16Y·M>

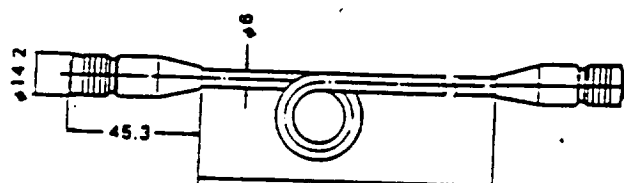
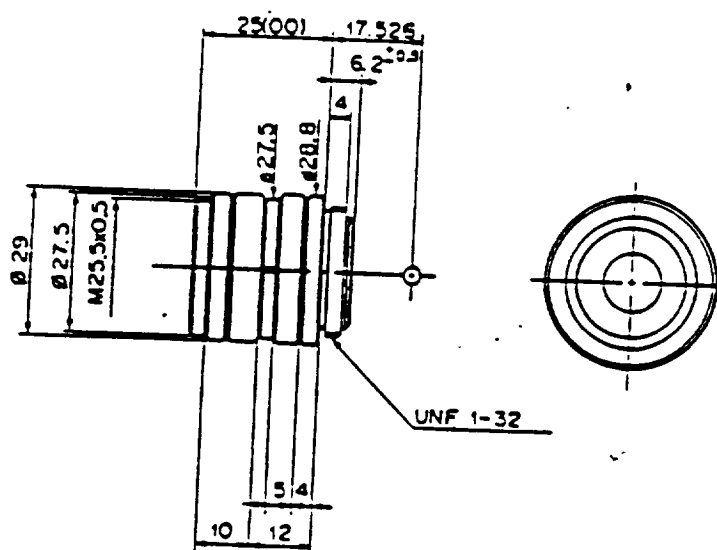
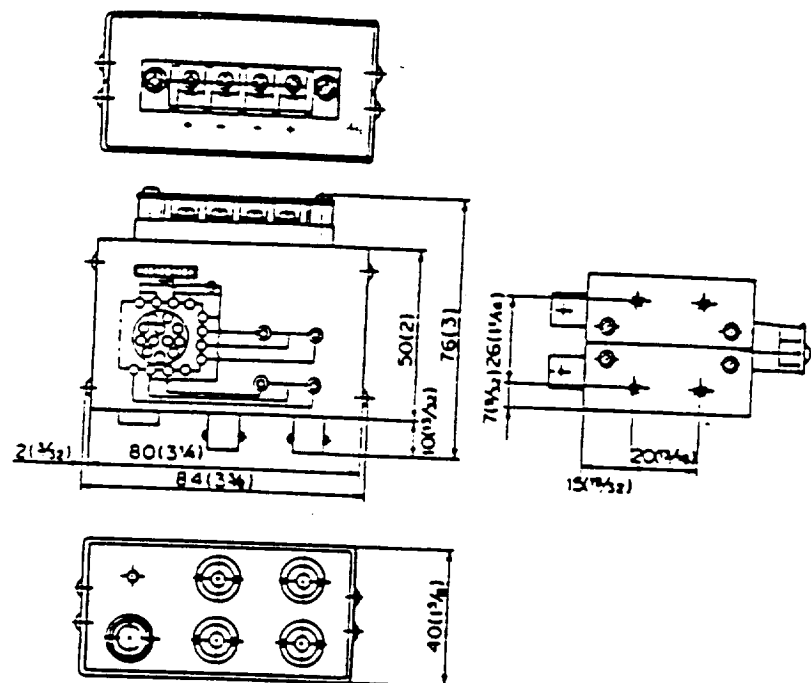
Focal Length	16 mm
Maximum Aperture Ratio	1 : 1.4
Iris Control	F1.4 ~ F16
Filter Thread	M 25.5 mm x P 0.5 mm
Mount	C mount
Weight	50 g

# 2 COMPREHENSIVE SPECIFICATIONS





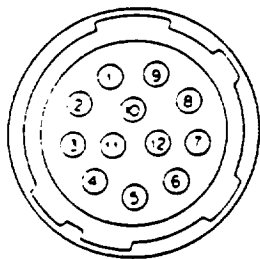




CCXC-12P02: 2 E  
 CCXC-12P05: 5 E  
 CCXC-12P10: 10 E  
 CCXC-12P25: 25 E

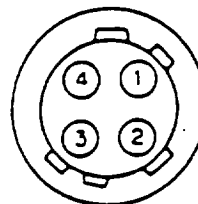
## 2-2. CONNECTORS' PIN FUNCTION

12-P Multiconnector (External view)



PIN NO.	EXTERNAL SYNC MODE			CAMERA SYNCHRONOUS OUTPUT
	HO, VD	VBS/VS	RESTART RESET	
1	GND	GND	GND	GND
2	+12 V	+12 V	+12 V	+12 V
3	VIDEO OUTPUT (GND)	VIDEO OUTPUT (GND)	VIDEO OUTPUT (GND)	VIDEO OUTPUT (GND)
4	VIDEO OUTPUT (SIGNAL)	VIDEO OUTPUT (SIGNAL)	VIDEO OUTPUT (SIGNAL)	VIDEO OUTPUT (SIGNAL)
5	HD INPUT (GND)	—	HD INPUT (GND)	HD OUTPUT (GND)
6	HD INPUT (SIGNAL)	—	HD INPUT (SIGNAL)	HD OUTPUT (SIGNAL)
7	VD INPUT (SIGNAL)	VBS INPUT (SIGNAL)	RESET PULSE (SIGNAL)	FIELD INDEX OUTPUT (SIGNAL)
8	—	—	—	CLOCK OUTPUT (GND)
9	—	—	—	CLOCK OUTPUT (SIGNAL)
10	GND	GND	—	GND
11	+12 V	+12 V	—	+12 V
12	VD INPUT (GND)	VBS INPUT (GND)	RESET PULSE (GND)	FIELD INDEX OUTPUT (GND)

4P Lens Connector (External view)



PIN NO.	SIGNAL	SPECIFICATION
1	+12 V OUT	DC 12 V OUTPUT
2	GND	GND
3	NC	NC
4	VS OUT	VIDEO SIGNAL OUTPUT

## 2-4. External Synchronization

There are three external synchronization modes:

1. VS/VBS mode
2. HD and VD mode
3. RESTART RESET mode

### 2-4-1. VS/VBS mode

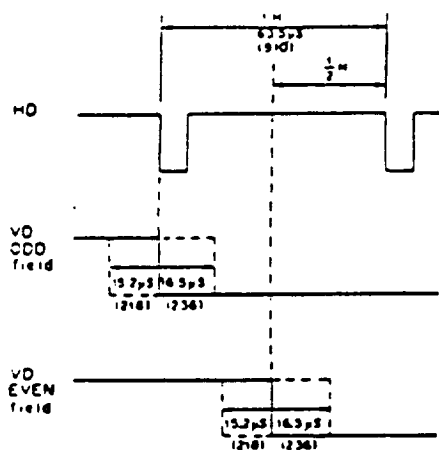
The VS/VBS mode provides external synchronization by supplying a normal composite signal, VS or VBS, to pin 7 of the 12-pin connector.

### 2-4-2. HD and VD mode

The HD and VD mode provides external synchronization by supplying an HD signal to pin 6 and a VD signal to pin 7 of the 12-pin connector.

- Input conditions of HD and VD signals
- Frequency (period)  
HD:  $15.734 \text{ kHz} \pm 1\%$  ( $63.56 \mu\text{s} \pm 1\%$ )  
VD: 244 to 1023  $1/2 \text{ H}$
- The maximum number of vertical effective lines is 486 in the interlace mode.  
In the non-interlace mode, it is 242 for both the ODD field and the EVEN field.

#### • Phase



The figure in parentheses ( ) indicates the number of clock pulses

As shown in the illustration above, the ODD field is provided when the phase shift between the trailing edge of the VD signal and the trailing edge of the HD signal is between a lead of  $15.2 \mu\text{s}$  and a lag of  $16.5 \mu\text{s}$ . The EVEN field is provided when the phase shift between the trailing edge of the VD signal and the point  $1/2\text{H}$  from the trailing edge of the HD signal is between a lead of  $15.2 \mu\text{s}$  and a lag of  $16.5 \mu\text{s}$ .

#### • Interlace and noninterlace

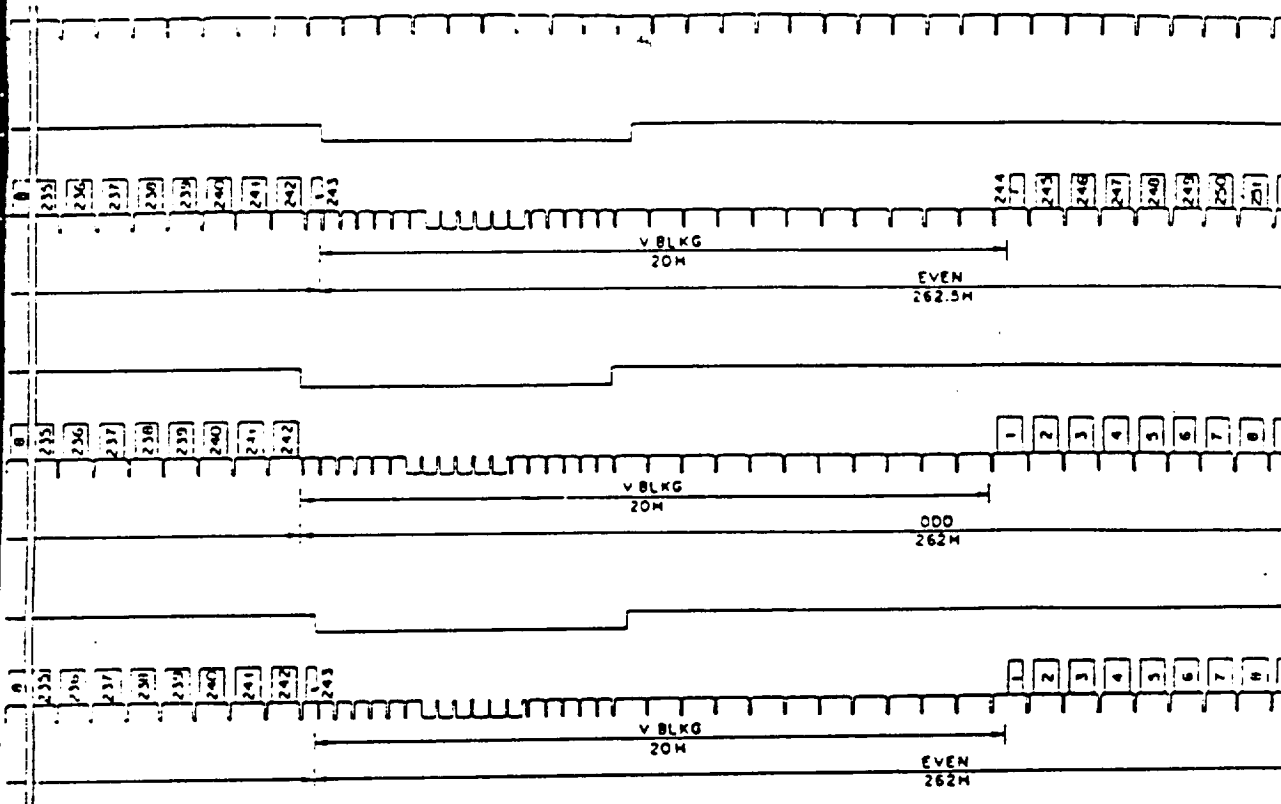
Operation can be performed in either interlace or non-interlace mode by changing the input condition of the VD signal. See Figure 1.

#### • Interlace

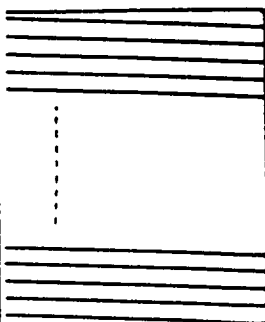
To operate in the interlace mode, set the period of the VD signal to  $(A + 1/2)\text{H}$ . A is an integer, 244 to 1037. In other words, the phase of the leading edge of the VD signal against the leading edge of the HD signal is changed for each VD signal. The field changes from ODD to EVEN and to ODD, repeatedly during operation in the interlace mode. At this time, the number of scanning lines per frame is  $2A + 1$ .

#### • Non-interlace

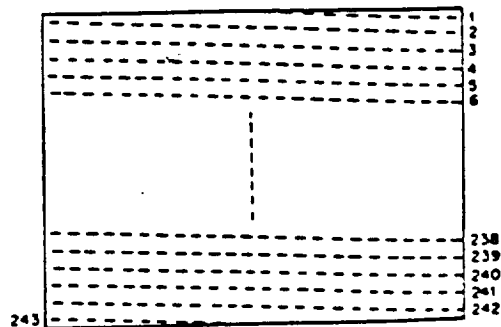
To operate in the non-interlace mode, set the period of the VD signal to  $A \text{ H}$ . A is an integer, 244 to 1037. In other words, the phase of the leading edge of the VD signal against the leading edge of the HD signal is not changed for each VD signal, and the field ODD or EVEN remains unchanged for operation in the non-interlace mode. The number of scanning lines is A; this is half of the number of scanning lines for operation in the interlace mode. The sensitivity is half of the sensitivity provided in the interlace mode, when the frame is stored.



INTERLACE 1

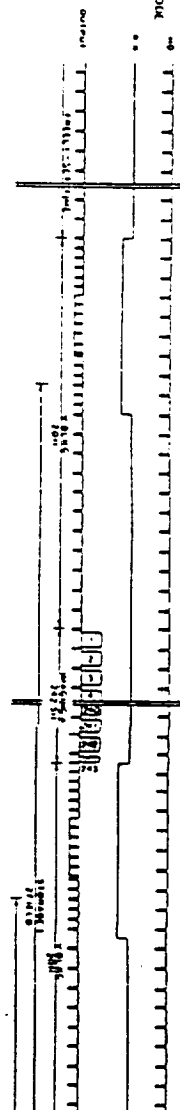


NONINTERLACE 2

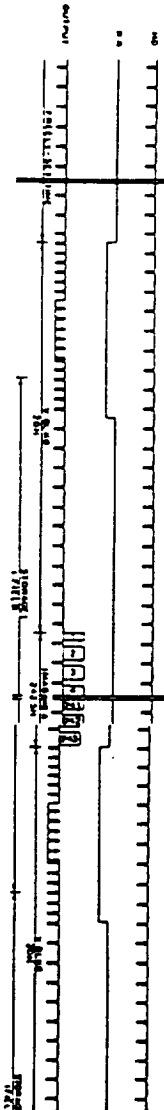




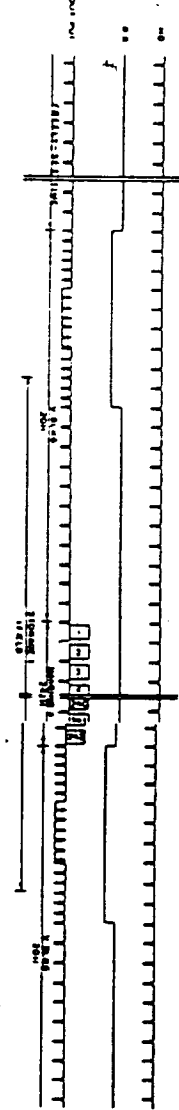
MAIN AMPLIFICATION MODE  
1.0 2.0 3.0 4.0 5.0 6.0 7.0 8.0 9.0 10.0 11.0 12.0 13.0 14.0 15.0 16.0 17.0 18.0 19.0 20.0 21.0 22.0 23.0 24.0 25.0 26.0 27.0 28.0 29.0 30.0 31.0 32.0 33.0 34.0 35.0 36.0 37.0 38.0 39.0 40.0 41.0 42.0 43.0 44.0 45.0 46.0 47.0 48.0 49.0 50.0 51.0 52.0 53.0 54.0 55.0 56.0 57.0 58.0 59.0 60.0 61.0 62.0 63.0 64.0 65.0 66.0 67.0 68.0 69.0 70.0 71.0 72.0 73.0 74.0 75.0 76.0 77.0 78.0 79.0 80.0 81.0 82.0 83.0 84.0 85.0 86.0 87.0 88.0 89.0 90.0 91.0 92.0 93.0 94.0 95.0 96.0 97.0 98.0 99.0 100.0



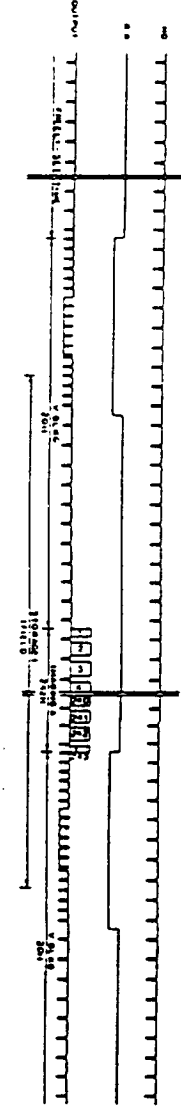
MAIN AMPLIFICATION MODE  
1.0 2.0 3.0 4.0 5.0 6.0 7.0 8.0 9.0 10.0 11.0 12.0 13.0 14.0 15.0 16.0 17.0 18.0 19.0 20.0 21.0 22.0 23.0 24.0 25.0 26.0 27.0 28.0 29.0 30.0 31.0 32.0 33.0 34.0 35.0 36.0 37.0 38.0 39.0 40.0 41.0 42.0 43.0 44.0 45.0 46.0 47.0 48.0 49.0 50.0 51.0 52.0 53.0 54.0 55.0 56.0 57.0 58.0 59.0 60.0 61.0 62.0 63.0 64.0 65.0 66.0 67.0 68.0 69.0 70.0 71.0 72.0 73.0 74.0 75.0 76.0 77.0 78.0 79.0 80.0 81.0 82.0 83.0 84.0 85.0 86.0 87.0 88.0 89.0 90.0 91.0 92.0 93.0 94.0 95.0 96.0 97.0 98.0 99.0 100.0

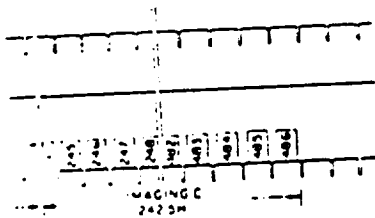
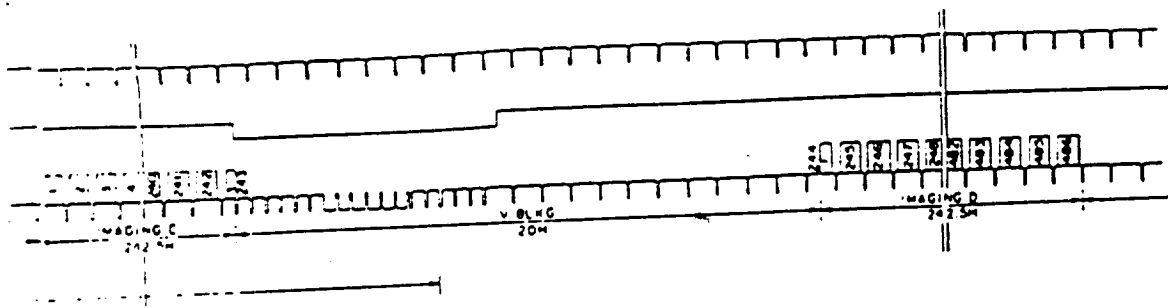


MAIN AMPLIFICATION MODE  
1.0 2.0 3.0 4.0 5.0 6.0 7.0 8.0 9.0 10.0 11.0 12.0 13.0 14.0 15.0 16.0 17.0 18.0 19.0 20.0 21.0 22.0 23.0 24.0 25.0 26.0 27.0 28.0 29.0 30.0 31.0 32.0 33.0 34.0 35.0 36.0 37.0 38.0 39.0 40.0 41.0 42.0 43.0 44.0 45.0 46.0 47.0 48.0 49.0 50.0 51.0 52.0 53.0 54.0 55.0 56.0 57.0 58.0 59.0 60.0 61.0 62.0 63.0 64.0 65.0 66.0 67.0 68.0 69.0 70.0 71.0 72.0 73.0 74.0 75.0 76.0 77.0 78.0 79.0 80.0 81.0 82.0 83.0 84.0 85.0 86.0 87.0 88.0 89.0 90.0 91.0 92.0 93.0 94.0 95.0 96.0 97.0 98.0 99.0 100.0



MAIN AMPLIFICATION MODE  
1.0 2.0 3.0 4.0 5.0 6.0 7.0 8.0 9.0 10.0 11.0 12.0 13.0 14.0 15.0 16.0 17.0 18.0 19.0 20.0 21.0 22.0 23.0 24.0 25.0 26.0 27.0 28.0 29.0 30.0 31.0 32.0 33.0 34.0 35.0 36.0 37.0 38.0 39.0 40.0 41.0 42.0 43.0 44.0 45.0 46.0 47.0 48.0 49.0 50.0 51.0 52.0 53.0 54.0 55.0 56.0 57.0 58.0 59.0 60.0 61.0 62.0 63.0 64.0 65.0 66.0 67.0 68.0 69.0 70.0 71.0 72.0 73.0 74.0 75.0 76.0 77.0 78.0 79.0 80.0 81.0 82.0 83.0 84.0 85.0 86.0 87.0 88.0 89.0 90.0 91.0 92.0 93.0 94.0 95.0 96.0 97.0 98.0 99.0 100.0





## 2-5. Mode Setting

The XC-77 can switch the operation mode, depending on the use.

The modes are set on the PR-89, SG-119, and MB-136 boards.

### PR-89 board

Item	Mode	SHORT	OPEN
AGC	AGC	AGC	FIX
	FIX GAIN	FIX	AGC
$\gamma$	1	$\gamma 1$	$\gamma 2$
	COMPENSATE	$\gamma 2$	$\gamma 1$
WHITE CLIP	$\gamma$	$\gamma 1$	$\gamma 2$
	WHITE CLIP	$\gamma 2$	$\gamma 1$
SUB	FRAME	SUB 1	SUB 2
	FIELD	SUB 2	SUB 1

### SG-119 board

Item	Mode	M't	OPEN
EIA/CCIR	EIA	R 7	R 6
	CCIR	R 6	R 7
FRAME/FIELD	FRAME	R 1	R 2
	FIELD	R 2	R 1
FIELD	NORMAL	R23	R28
	INVERSION	R28	R23
RESTART RESET	NORMAL	R24	R29
	RESET	R29	R24
EIA/CCIR	EIA	R27	R22
	CCIR	R22	R27

\* The value of all resistors is 10 k $\Omega$ .

### MB-136 board

Item	Mode	M't	OPEN
RESTART RESET	NORMAL	R35	
	RESET		R35

\* The value of resistors R35 is 220 k $\Omega$ .

#### • Explanation of all operation modes

##### • VIDEO GAIN mode (AGC/FIX GAIN)

Set the gain of the video output signal with this mode. When it is set to AGC, the automatic gain control functions.

When it is set to FIX GAIN, a fixed gain is obtained.

The setting is performed with the AGC trace on the PR-89 board. To set the gain to AGC, connect the AGC end and disconnect the FIX end. To set the gain to FIX GAIN, connect the FIX end. To set the gain to FIX GAIN, connect the FIX end and disconnect the AGC end.

The factory setting is FIX GAIN.

##### • Gamma compensation mode (1/COMPENSATION)

Set the gamma correction of the video output signal by this mode. When the gamma is set to COMPENSATE, video signals for which gamma correction is performed are output. When it is set to 1, no gamma correction is performed for video signals. This setting provides video signals proportional to the amount of light from the object. The setting is performed with the gamma and white clip traces on the PR-89 board. To set COMPENSATE, connect the gamma 2 ends of both gamma and white clip traces, and disconnect the gamma 1 ends. To set 1, connect the gamma 1 ends of both gamma and white clip patterns, and disconnect the gamma 2 end.

The factory setting is 1.

##### • EIA/CCIR mode (EIA/CCIR)

Set the signal system of the video output signal with this mode.

Always set the signal system to EIA.

##### • Storage mode (FRAME/FIELD)

Set the period in which a signal charge is read from the photosensor in the CCD with this mode.

When it is set to FIELD, a signal charge is read for each field. When it is set to FRAME, a signal charge is read for each frame. Note that if the FRAME mode is set for operation in the non-interlace mode, the sensitivity is half of the sensitivity provided in the interlace mode.

The setting is performed with the SUB trace on the PR-89 board and FRAME/FIELD trace on the SG-119 board.

To set the period to FIELD, connect the SUB1 end of the SUB pattern, and disconnect the SUB2 end. Mount then R1 (10 k $\Omega$ ) on the FRAME/FIELD trace, and demount R2. To set the period to FRAME, connect the SUB2 end, and disconnect the SUB1 end. Mount then R2 (10 k $\Omega$ ) on the FRAME/FIELD trace and demount R1.

The factory setting is FRAME.

## 2-6. THEORY OF OPERATION

### <Operation principle of the CCD>

A CCD (Charge Coupled Device) consists of MOS (Metal-Oxide-Semiconductor) capacitors arranged in a regular array.

It basically performs three functions connected with handling charges.

#### 1. Photoelectric conversion (photosensor)

Incident light generates charges on the MOS capacitors, with the quantity of charge being proportional to the brightness.

#### 2. Accumulation of charges

When a voltage is applied to the electrodes of the MOS capacitors, an electric potential well is formed in the silicon layer. The charge is accumulated in this well.

#### 3. Transmission of charge

When a high voltage is applied to the electrodes, a deeper well is formed; when a low voltage is applied, a shallower well is formed. In the CCD, this property is used to transmit the charge. When a high voltage is applied to the electrodes, a deep electric potential well is formed, and charge flows in from neighboring well. When this is repeated over and over among the regularly arranged electrodes, the charge is transferred from one MOS capacitor to another. This is the principle of CCD charge transmission.

### <Mechanism of CCD charge transfer>

#### 1. Vertical transfer

The vertical shift register transfers charges using a four-phase drive mode. Figure 1 shows an example of the changes which can occur in potential wells in successive time intervals.

At  $t_0$ , the electrode voltages are  $(V_1 = V_2) > (V_3 = V_4)$ , so the potential wells are deeper toward the electrode at the higher voltages  $V_1$  and  $V_2$ . Charges accumulate in these deep wells. At  $t_1$ , the electrode voltages are  $(V_1 = V_2 = V_3) > (V_4)$ , so the charges accumulate in the wells toward the electrode at  $V_1$ ,  $V_2$  and  $V_3$ . At  $t_2$ , the electrode voltages are  $(V_2 = V_3) > (V_4 = V_1)$ , so the charges accumulate in the wells toward the electrode at  $V_2$  and  $V_3$ .

Electrode voltage states at  $t_3$  and after are shown below.

$t_3$   $(V_2 = V_3 = V_4) > (V_1)$

$t_4$   $(V_3 = V_4) > (V_1 = V_2)$

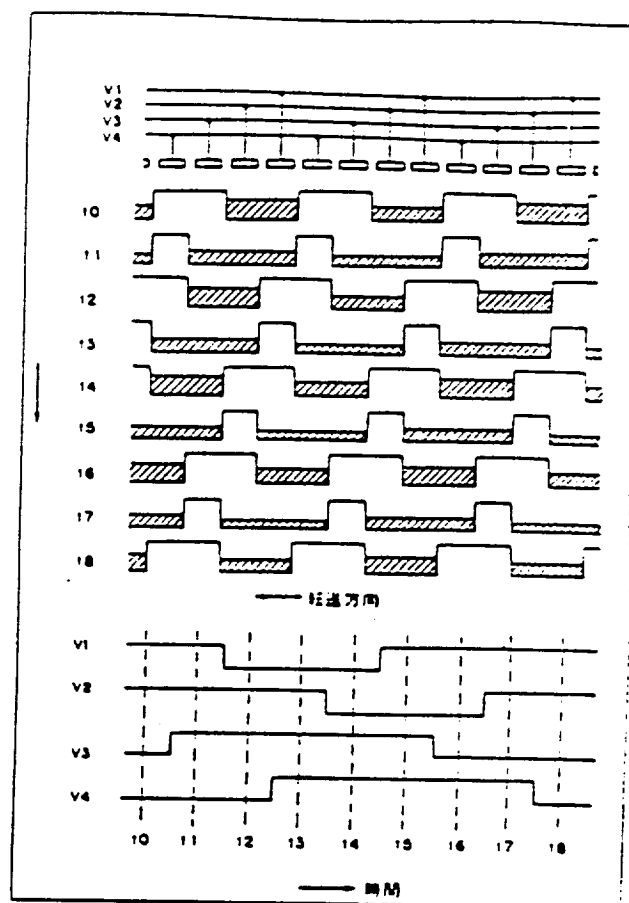
$t_5$   $(V_4) > (V_1 = V_2 = V_3)$

$t_6$   $(V_4 = V_1) > (V_2 = V_3)$

$t_7$   $(V_4 = V_1 = V_2) > (V_3)$

$t_8$   $(V_1 = V_2) > (V_3 = V_4)$  (Initial state)

These operations are repeated to execute the vertical transfer.



#### <SH-27 board>

It contains a sample and hold circuit. CCD output signals sent from the BI-12 board are divided into two. Both signals are sampled and held by a sampling and holding pulses (SHP, SHD). One signal is sampled and held three times by these pulses; in order of the SHP, SHD and SHP pulses. The other signal is sampled and held two times by the SHD pulse and then SHP pulse. The difference of these two signal removes a noise component of CCD output signal to obtain the video signal, using a differential amplifier consisting of Q16 through Q19. The video signal from the differential amplifier is sent to the PR-89 board.

#### <PR-89 board>

It contains a video signal processing circuit, which converts the video signal from the SH-27 board into a video signal of EIA standard. The video signal from the SH-27 board is fed to IC1. IC1 contains an auto-iris circuit and a gain control amplifier for AGC. The signal from the gain control amplifier passes through a low-pass filter FL1 and is then fed to IC2. In IC2, various signal processings such as clamping, gamma correction, white clipping, blanking mixing, setup addition, and sync signal mixing are executed. The resultant signal is then passed through an output driver circuit consisting of Q1 through Q8 and sent from this board.

#### <CN-163 board>

It connects the MB-136 board with each external connector. 12-pin multiconnector (DC IN/SYNC connector), 4-pin connector (LENS connector) and BNC connector (VIDEO OUT connector) are mounted on this board. At 12-pin multiconnector, +12 V power voltage, external synchronizing signals (EXT HD, EXT VD, RESET PULSE, VBS and VS) are input and the video signal (VS) and synchronizing signals (CLOCK, HD, FIELD INDEX) are output. 12-pin multiconnector I/O signals varies according to selection of sync model (internal sync or external sync model). Refer to Section 2-2 in details. +12 V power supply and video signal for auto-iris lens are output from 4-pin connector. The video signal (VS) is output from the BNC connector.

#### <RG-18 board>

It supplies a DC voltage to be applied to CCD driving clock generator and CCD substrate.

#### <MB-136 board>

It contains an external synchronizing signal detection circuit, 1820 fh oscillator, DC-to-DC converter and CCD driving clock generator. When external synchronizing signals are supplied to this board, the camera automatically selects external sync mode and outputs a video signal synchronized with the external synchronizing signal. For external synchronizing, EXT VD and EXT HD, or EXT SYNC, or EXT HD and RESET PULSE can be used. When EXT HD and EXT VD, or EXT HD and RESET PULSE are supplied, the MB-136 board wave-shapes these signals using Q1, Q2, Q3 and IC7 and outputs them to the SG-119 board. When EXT SYNC of VBS or VS is supplied, this board detects only a sync component using Q2, Q3 and IC7, and wave-shapes it. The resultant SYNC signal is output to the SG-119 board.

1820 fh oscillator is subdivided into two, which are for external and internal synchronizing. In the internal sync mode, the oscillator using a crystal oscillator (X1) operates. In the external sync mode, the voltage controlled oscillator VCO which is an LC oscillator operates. The VCO can vary oscillation frequency within  $\pm 1\%$ . A control voltage of VCO are supplied between 0 V and 5 V. When the control voltage is 2.8 V, the oscillation frequency is set to be 28.6363 MHz (= 1820 fh).

The clock signal of 1820 fh is fed to the CCD driving clock generator. The DC-to-DC converter converts the externally-supplied DC (+12 V) into four DC voltages: +15 V, +10 V, +7 V, and +5 V. These voltages are fed to each board.

CCD driving clock generator generates the clock signal necessary to drive the CCD. When the HD and VD signals from the SG-119 board and the clock signal of 1820 fh from the 1820 fh oscillator are fed to IC1.

It outputs the following signals.

- CLOCK: The clock signal of 910 fh (half the clock signal of 1820 fh)
- H1, H2: Two-phase clock signal  
These are used to drive the horizontal shift register and to transfer the signal charges.
- V1 to V4: Four-phase clock signal  
These are used to drive the vertical shift register and to transfer the signal charges.
- PG: Precharge gate control pulse  
A precharge gate is the gate of the output section connected to the horizontal register. This gate is controlled by this pulse to convert a transferred signal charge into the voltage.
- SHP, SHD: These pulses are used to sample the CCD output signal.
- CLP1: This pulse is used to clamp the optical black level of the CCD output signal.

CCD driving clock signals H1, H2, V1 to V4, and PG are output to the CCD after passing through the drive circuit consisting of IC3, IC5 and IC6.

## SECTION 3 ALIGNMENT

### 3-1. PREPARATION

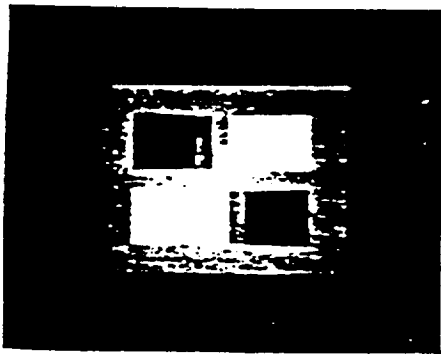
#### Step 1: Jigs and measuring instruments

- Oscilloscope
- Waveform monitor
- B/W monitor
- Digital voltmeter
- Power supply equipment: Junction box JB-77 (sold on the market), regulated power supply unit
- Tripod attachment: VCT-37 (sold on the market)
- Lens: Standard VCL-16Y-M (sold on the market)
- Pattern box: PTB-500 or PTB-100 (SONY part No.: J-6029-140-A)

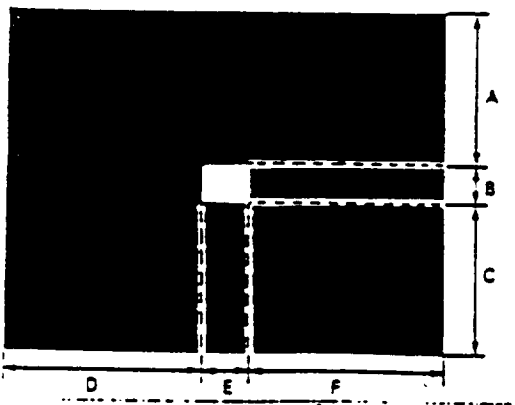
[If the pattern box is unavailable]

- 100-W bulb
- Variable voltage transformer

- Grayscale chart (SONY part No.: J-6026-130-A)



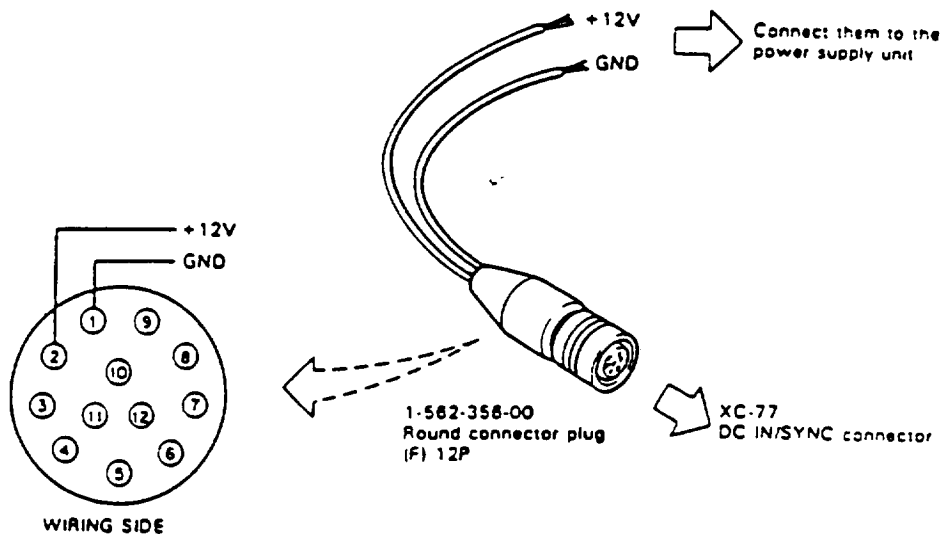
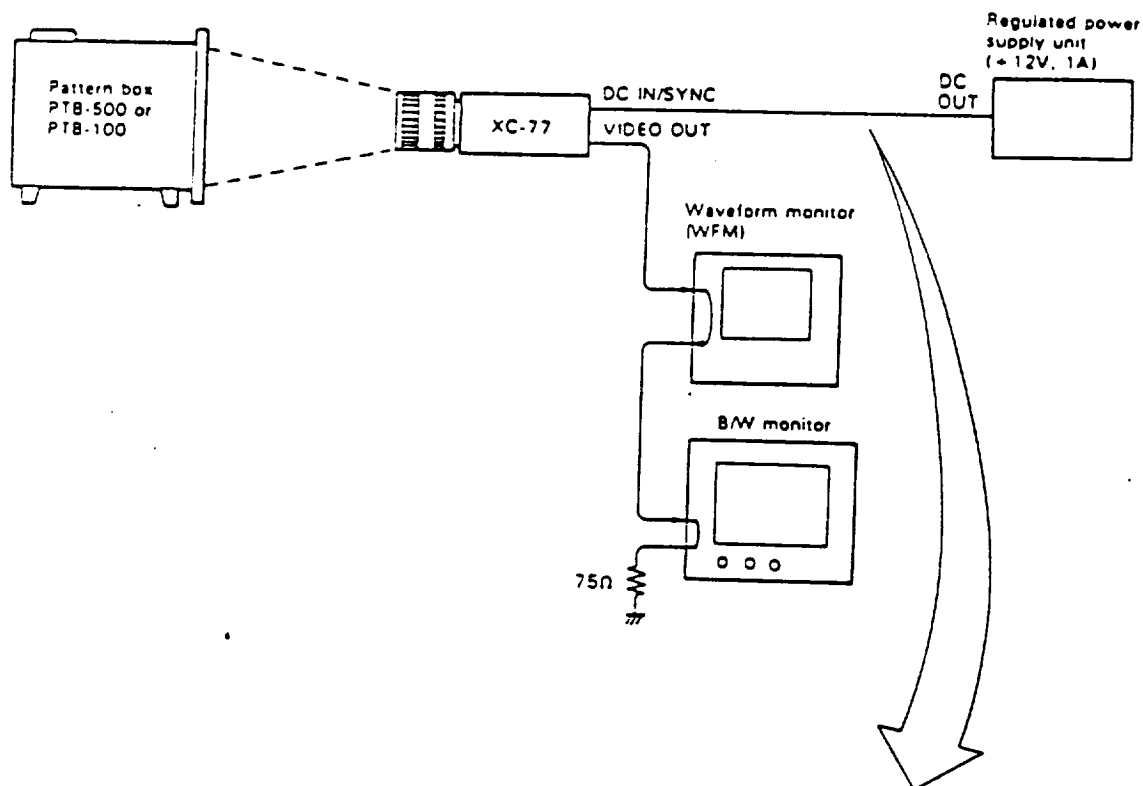
- White window chart  
Make a hole in black paper as shown in the figure.



Vertical A:B:C = 4.5:1:4.5  
Horizontal D:E:F = 4.5:1:4.5

## Step 2: Connection diagram

[Connection method 1]



## 3-2. OVERALL ADJUSTMENT

### Step 1: V SUB (field) adjustment

- Caution

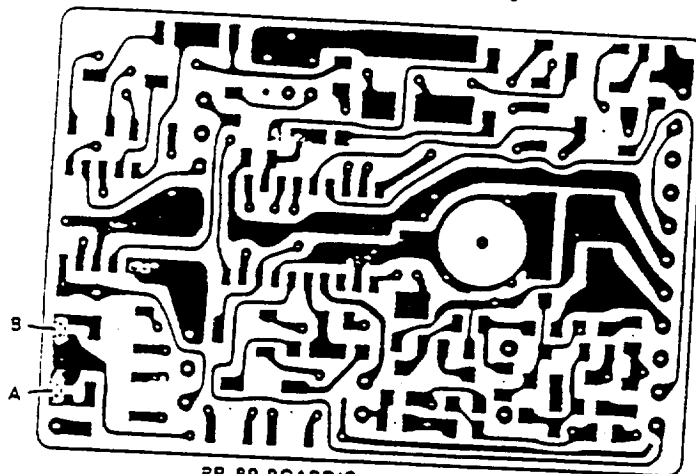
Do not make this adjustment except when the CCD is replaced.

- Setting

Measuring instrument | Digital voltmeter

- Preparation

Solder part A and remove the solder from part B as shown in the figure.



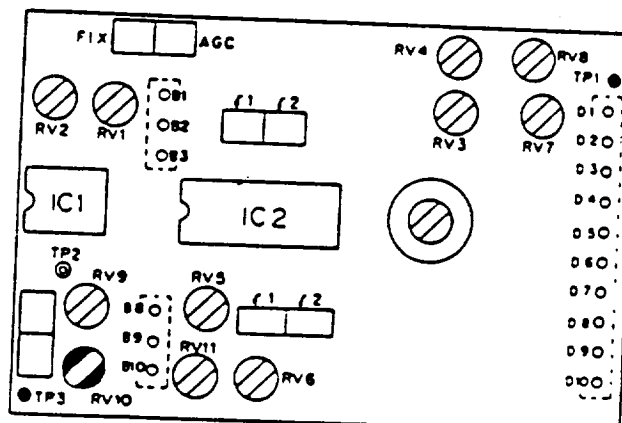
PR-89 BOARD(Component Side)

- Adjustment procedure

#### 1. Test Point; TP3 (GND:TP1)/PR-89 board

Adj. Point: ○ RV10/PR-89 board

Spec.: When using a new CCD, adjust the V SUB voltage so that the specification written in the back of the CCD is satisfied.



PR-89 BOARD (Component Side)



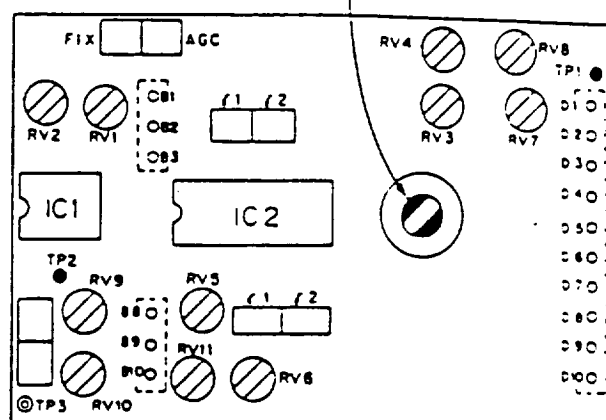
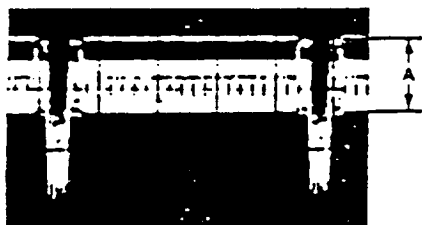
### Step 3: Coupling noise elimination adjustment

#### • Setting

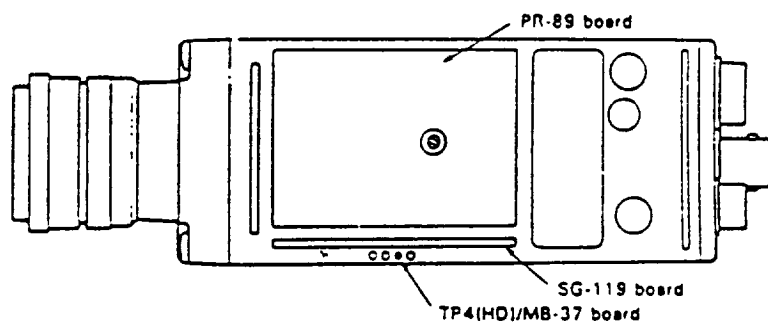
Lens iris	Close it with the lens cap	Trigger	TP4(HD)/MB-136 board
Measuring instrument	Oscilloscope		

#### • Adjustment procedure

Test Point/PR-89 board	Adj. Point	Spec.
TP2(GND:TP1)	CV1/SH-27 board	A shall be minimized.

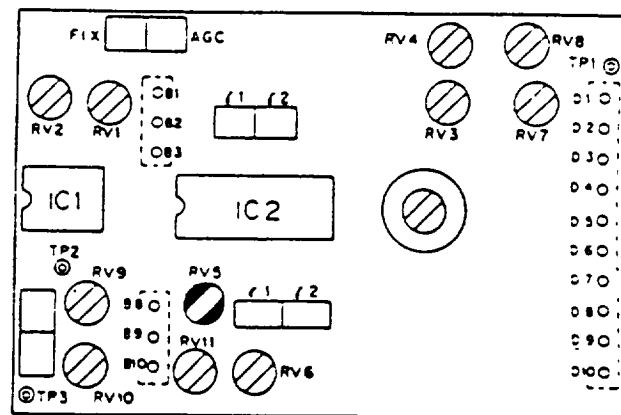
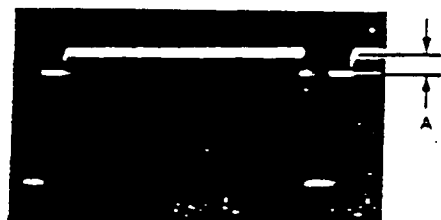


PR-89 BOARD (Component Side)



• Adjustment procedure

Test Point	Adj. Point	Spec.
VIDEO OUT terminal	ORV5/PR-89 board	$A = 8.0 \pm 0.5 \text{ IRE}$



PR-89 BOARD (Component Side)

3 ALIGNMENT

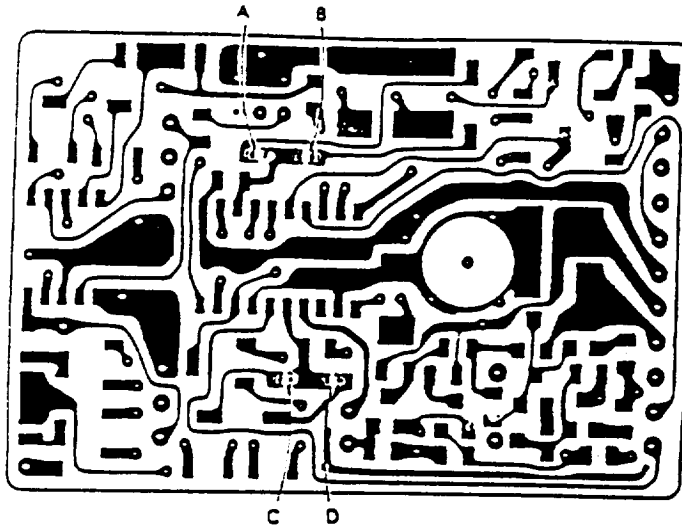
## Step 6: GAIN adjustment

### • Setting

Object	Grayscale chart	Measuring instrument	Oscilloscope and waveform monitor
--------	-----------------	----------------------	-----------------------------------

### • Preparation

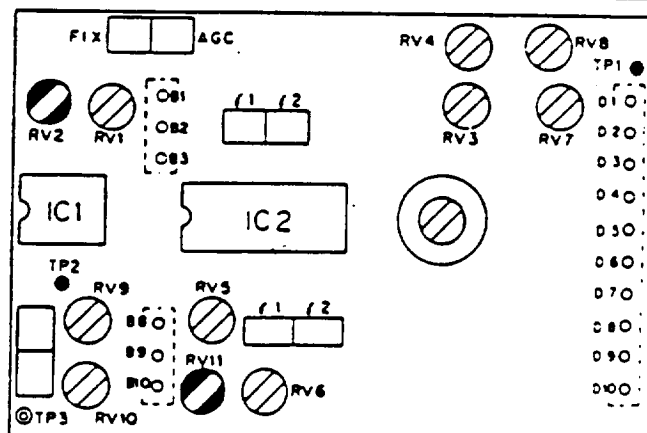
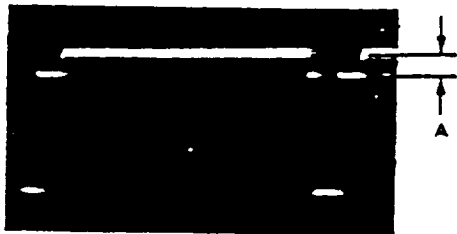
1. Solder parts A and C and remove the solder from parts B and D as shown in the figure.



PR-89 BOARD (Component Side)

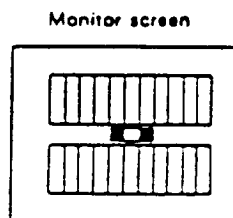
### • Adjustment procedure

1. Lens iris ⇒ Close it with the lens cap
2. Test point: VIDEO OUT terminal  
Adj. Point: RV11/PR89 board  
Spec.: A =  $7.0 \pm 0.5$  IRE



PR-89 BOARD (Component Side)

3. Shoot the grayscale chart, and place the camera so that the chart frame touches the underscanned picture frame on the monitor screen.



(Continued to next page)

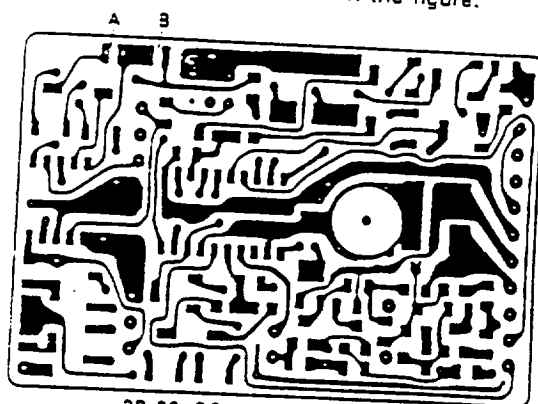
## Step 7: AGC adjustment

### • Setting

Object	Grayscale chart	Measuring instrument	Oscilloscope and waveform monitor
--------	-----------------	----------------------	-----------------------------------

### • Preparation

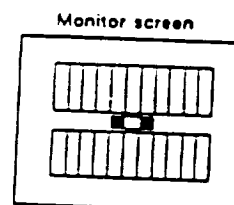
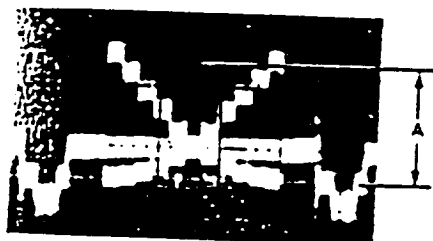
Solder part B and remove the solder from part A as shown in the figure.



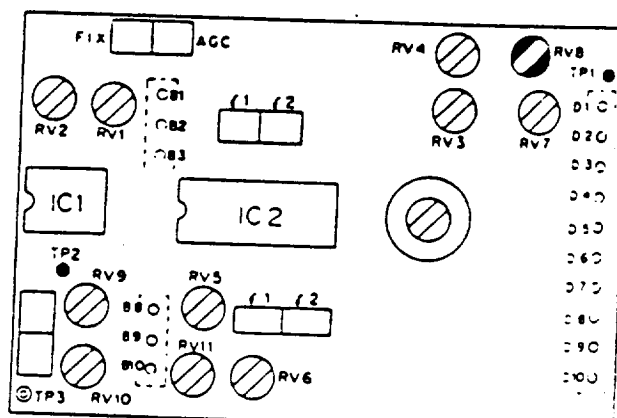
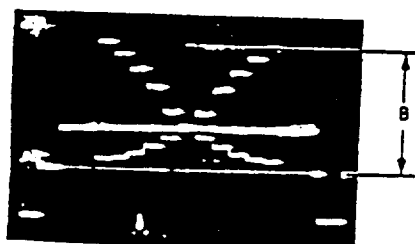
PR-89 BOARD (Component Side)

### • Adjustment procedure

1. Shoot the grayscale chart, and place the camera so that the picture frame of the chart touches the underscanned picture frame on the monitor screen.
2. Test Point: TP2 (GND: TP1)/PR-89 board  
Trigger: TP4 (HD1)/MB-136 board  
Adj. Point: Lens iris  
Spec.:  $A = 350 \pm 10 \text{ mV}$



3. Test Point: VIDEO OUT terminal  
Adj. Point: RV8/PR-89 board  
Spec.:  $B = 100 \pm 5 \text{ IRE}$



PR-89 BOARD (Component Side)

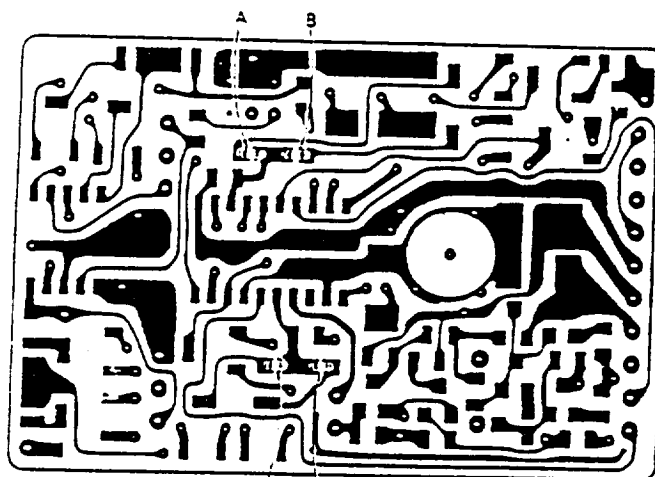
## Step 9: Gamma adjustment

### • Setting

Object	Grayscale chart	Measuring instrument	Oscilloscope and waveform monitor
--------	-----------------	----------------------	-----------------------------------

### • Preparation

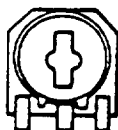
1. Solder parts B and D and remove the solder from parts A and C as shown in the figure.



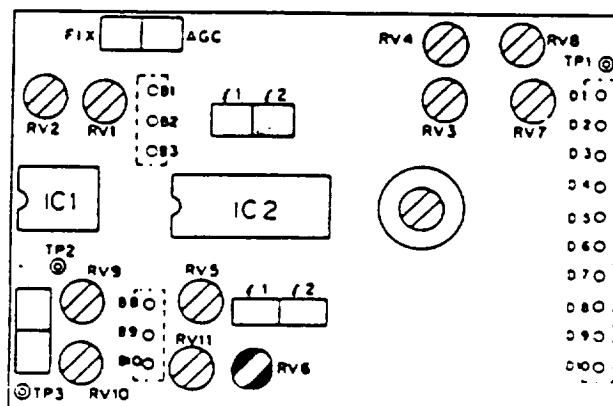
PR-89 BOARD (Component Side)

2. Set RV6/PR-89 on the PR-89 board to the mechanical center.

[Front view]



[Top view]



(Continued to next page)

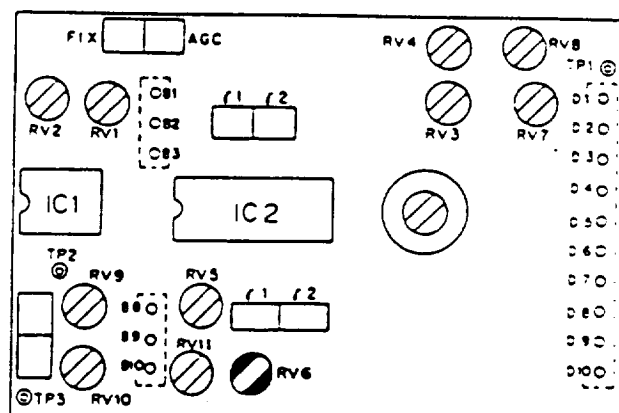
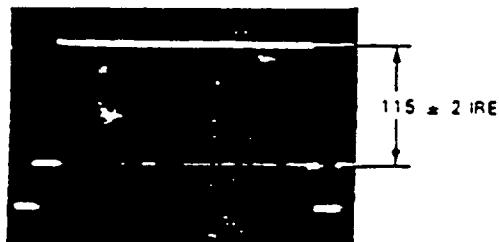
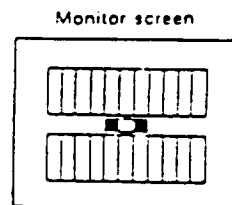
# Step 10: White clip adjustment 2

## • Setting

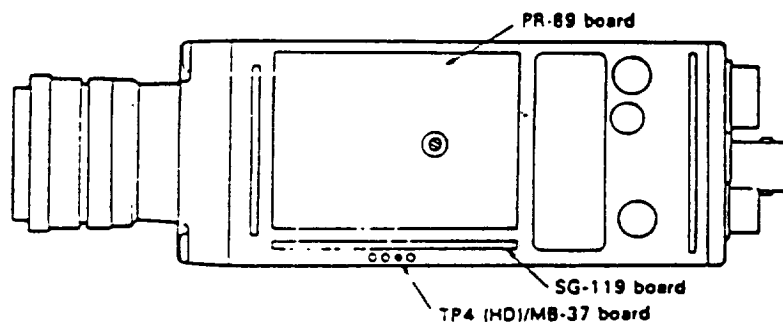
Object	Grayscale chart	Measuring instrument	Waveform monitor (WF4)
--------	-----------------	----------------------	------------------------

## • Adjustment procedure

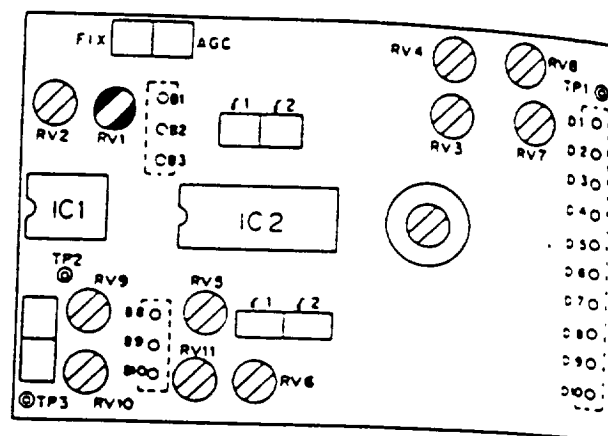
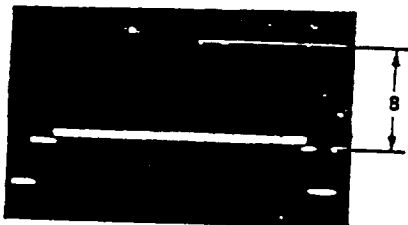
1. Shoot the grayscale chart, and place the camera so that the chart frame touches the underscanned picture frame on the monitor screen.
2. Test Point: VIDEO OUT terminal  
Adj. Point:  $\odot$  RV6/PR-89 board  
Adjustment: Open the lens iris and adjust so that the VIDEO OUT waveform clips at  $115 \pm 2$  IRE.



PR-89 BOARD (Component Side)



3. Test/Point: VIDEO OUT terminal  
 Adj. Point: RV1/PR-89 board  
 Spec.:  $S = 100 \pm 10$  IRE



3 ALIGNMENT